A NEW TRANSMITTING ANTENNA SYSTEM FOR VERY LOW RADIO FREQUENCIES

Thesis by

Willard Van Tuyl Rusch

In Partial Fulfillment of the Requirements

For the Degree of

Doctor of Philosophy

California Institute of Technology

Pasadena, California

1959

ACKNOWLEDGEMENTS

I wish to express my very deep appreciation to Professor Robert S. Macmillan for his guidance and encouragement throughout this program of research, and to Professor Robert V. Langmuir for his valuable suggestions in the propagation experiments and preparation of this thesis.

My appreciation is also extended to numerous others who contributed significantly to this research, among them:

Officials of the Southern California Edison Company, for their permission to use the Dinkey Creek power line as the transmitting antenna, for their technical suggestions in the design of the antenna system, and for their patience with occasional breakdowns we may have caused;

Mr. Harry Aubuchon and the E.D.S. line crew for construction and maintenance of the system;

Mr. Kenneth J. Hebert, for assistance in writing the computer program;

Mrs. Anne Graff, for preparation of the manuscript.

Finally, I would like to express my gratitude to the National Science Foundation for my N.S.F. graduate fellowship, and to the Air Force Office of Scientific Research for their financial support which enabled us to carry on this program of research.

Willard Van Tuyl Rusch

ABSTRACT

Recent widespread interest in very low-frequency radio propagation has increased the importance of developing adequate vlf transmitting systems. After briefly examining conventional vertical vlf antennas, a system is presented which employs resonant loading circuits to convert a section of an existing power line into a horizontal vlf transmitting antenna. The simplicity, low cost, and useful radiation pattern of this horizontal antenna are well suited for many experimental applications.

The theoretical antenna problem is solved using a normal mode expansion of the current distribution. A matrix method is developed to compute the current distribution of a thin, linear antenna loaded with lumped-circuit elements. The series is found to converge relatively fast. A digital computer is used to solve the matrix equations. Results are obtained for a full-wave linear antenna symmetrically loaded with real impedances Z_o, one half-wavelength apart. Current distributions, feedpoint impedances, radiation patterns, etc., are presented as functions of Z_o. Results of the idealized problem are applied to the power-line antenna. The matrix method can also be extended to the general linear antenna with any type of loading or feeding.

System components and performance of the Dinkey Creek power-line antenna are described. The problem of interference with nearby audio-frequency communication systems is examined.

The 8.4 kc propagation experiments using the Dinkey Creek antenna are described. The series of whistler-mode propagations to probe the exosphere has not been completed. However, ionospheric soundings have yielded considerable information about the properties of the ionosphere at vlf. Successful long-distance propagation experiments are also described, and samples of the results are presented.

TABLE OF CONTENTS

I. INTRODUCTION

The early pioneers of radio operated their primitive transmitters in the low-frequency region. In 1905 it was felt that (reference 1):

> "...enormously high frequencies...are not so desirable as they were at first believed to be, but oscillating currents having a periodicity of 100,000 per second...give the best results, since (they) produce longer wavelengths, which are more penetrating..."

Gradually, however, interest was directed to the higher frequencies. The radio frequency spectrum crept upward, until the present day when the highest allocated broadcast frequencies are in the band between 10,000 mc and 10,500 mc. Military transmitters operate still higher. The very low-frequency region (below 30 kc) is consigned to radio navigation stations and long-range transmitters for world-wide communication.

The present decade is witnessing a rebirth of interest in the very low-frequency (vlf) end of the radio frequency spectrum. For example, development of the submarine as a global offensive weapon requires a reliable method of long-range communication to undersea receivers. In typical sea water (conductivity about 4 mhos/meter) the skin depth δ is

$$\delta = \frac{1}{68.8}\sqrt{\lambda_o} \quad \text{meters} \qquad \text{(I-1)}$$

where λ_o is the free-space wavelength in meters. Consequently, only vlf waves are capable of penetrating the ocean to an appreciable depth. A vlf communication system is also more reliable, since fading in the normal sense is not believed to occur at these frequencies (references 2 and 3).

Very low-frequency wave propagation also presents a valuable means for exploration of both the base and extremely distant portions of the ionosphere. Very little is known about the structure of the lowest region of the ionosphere, the D-layer, which exists primarily during the daytime hours. Since very long waves penetrate the ionosphere only slightly, they offer an excellent "probe" for exploring the base of the ionosphere. The lowest frequency at which D-layer information has been obtained is 16 kc, at the GBR station in Rugby, England (reference 4).

Exploration of the outer ionosphere, or exosphere, with vlf waves may be possible by exploiting the "whistler" mode of vlf propagation. Studies of a particular type of atmospheric noise called "whistlers" indicate that some of the energy from lightning discharges is guided far into space by the earth's magnetic field in the presence of sufficient ionization (reference 5). This energy may be guided as far as several earth radii from the earth's surface, eventually returning to earth at the magnetic conjugate point in the form of a dispersed wave train. This phenomenon occurs in the frequency range from 400 cps to 25 kc. Since whistler time delays depend upon the integrated ionization density and magnetic field along the path, they provide a powerful tool for sounding parts of the ionosphere which are virtually inaccessible by conventional radio techniques. Consequently, by reproducing this mode of propagation with a high power vlf transmitter, it is expected that important information can be obtained concerning the nature of the outer ionosphere.

During the past two or three years particular attention has been given to schemes which employ the excellent phase stability of vlf transmissions. Transatlantic study of the 16 kc GBR signal, considered as a standard frequency source, has given evidence that a single source of frequency can be made available on a world-wide basis (reference 6). At a distance of 5,200 kilometers from the transmitter the doppler effects in transmission seldom exceeded $\pm$ 3 parts in 10^9, and measurements have been made to $\pm$ 1 part in 10^9 over an interval of 15 minutes. Accuracies of $\pm$ 1 part in 10^{10} and better were consistently obtained over an interval of several hours. Considerable attention is being given to the possibility of a National Bureau of Standards WWV broadcast at vlf which is expected to improve the stability of the present 10 - 25 mc transmissions by as much as a factor of 100 (reference 7).

The excellent phase stability of vlf transmissions suggests that it might be well suited for extremely accurate navigation systems. As the commercial and military airlanes grow increasingly crowded, it is becoming more and more necessary to develop navigation systems which do not suffer from doppler phase shifts, since these phase shifts would be interpreted as positional errors at the receivers. Very low-frequency transmissions are a possible solution to this problem. It is the prohibitive size of conventional transmitting antenna systems which prevents vlf from being used in modern navigation systems (reference 8).

As the number of potential applications of vlf wave propagation continues to grow, it becomes increasingly important to develop adequate vlf transmitting systems. The few vlf transmitting antennas in existence today are used primarily for military purposes. Sections II, III, and IV of this thesis will describe a new vlf transmitting system with the flexibility and economy needed for experimental projects, yet with a range sufficient for long-distance applications. First, however, several different types of vlf transmitting systems will be described.

A. Conventional Very Low-Frequency Transmitting Antennas

Conventional vlf transmitting antennas are of the grounded, vertical-wire type with varying degrees of toploading (reference 9). Antennas of this type are electrically short, i.e., their physical dimensions are a very small fraction of the operating wavelength. Consequently, at very low frequencies the toploaded, grounded, vertical-wire antenna suffers from two characteristic disadvantages:

1. The antenna radiation resistance is extremely small.

2. The input impedance consists almost entirely of a large capacitive reactance.

The radiation resistance is determined primarily by the length of the vertical conductors and the distribution of current on them (reference 9). For vertical conductors with a uniform cross-section, the current distribution is very nearly sinusoidal. Without toploading, the current at the top is zero and varies sinusoidally from the top.

When toploading is added to the vertical sections, the current at the top is no longer zero, but is proportional to the capacitance of the toploading. In this manner the electrical length of the antenna is increased. (The electrical length or effective height of a grounded vertical-wire antenna is the height that a vertical wire would be required to have to radiate the same field horizontally as is actually present if the wire carried a current that is constant along its entire length and of the same value as at the base of the actual antenna, reference 10). For practical vlf antennas, the radiation resistance is proportional to the second power of the effective height.

While the radiated power is proportional to the radiation resistance, the losses of vlf antennas are determined by several factors, all of which require special engineering attention:

1. Since the antenna current flows to ground through the top-loading capacitance, considerable power is lost in the ground itself, and the effective resistance of the best engineered ground systems is often larger than the radiation resistance.

2. In order to meet the conditions of maximum power transfer, a series tuning inductor is connected in series with the antenna feed to resonate the antenna capacitance. Consequently power is lost in coil dissipation.

3. The high operating potentials, due to the small resistance and large reactance of the antenna, cause considerable dielectric loss.

4. The great length of the antenna conductors themselves gives rise to appreciable conductor loss, since relatively poorly-conducting high-strength alloy conductors must be used.

All of the above-mentioned losses contribute greatly to a reduction in the efficiencies of vlf antennas. Considerable expense and engineering must be devoted to minimizing them.

Ground systems used for antennas below 500 kc (reference 9) differ markedly from those used at standard broadcast frequencies and above since, (a) it is impractical to bury electrically long ground wires at these extremely long wavelengths, and (b) at very low frequencies the skin depth of the underlying earth becomes very large and the ground currents extend far deeper than at higher frequencies. Consequently, three general types of ground systems are used to reduce the power lost in ground heating:

1. Radial buried-wire system, consisting of 15 to 150 radial wires buried in the soil and centered at the base of the antenna (figure 1A). This system is similar to ground systems used at standard broadcast frequencies. However, since these radials are electrically short, several methods are used at vlf to reduce ground current densities:

   (a). Vertical ground rods are sometimes attached to the ends of the radials to intercept current at the periphery of the system.

   (b). The radials are brought above the ground at an appreciable distance from the base of the antenna, preventing excessive current densities in the ground at the collecting point at the base of the antenna. This above-ground system also forms an electrostatic shield at the base of the antenna, thereby reducing

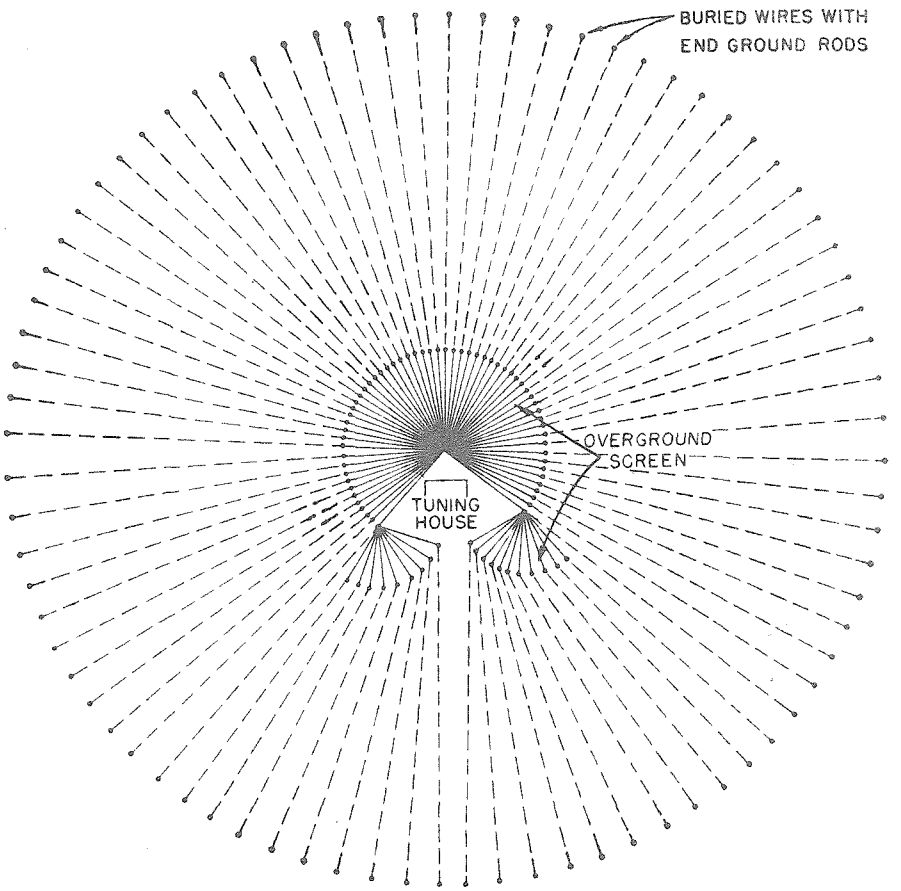

FIGURE 1A. RADIAL BURIED-WIRE GROUND SYSTEM.
By permission from Radio Antenna Engineering, by E. A. Laport.

dielectric losses in the ground caused by the intense potential gradients near the base of the antenna.

(c). No closed paths exist in the ground system since they would allow large circulating currents to increase the copper loss.

(d). Conductor sizes are as large as economically possible, and are proportional to the current densities at that point in the ground system.

2. Multiple-star ground system, consisting of a number of short buried-wire radial systems, uniformly spaced around the base of the antenna and connected to the base of the antenna by overground buses (figure 1B). In practice two or more concentric circles of stars are used, with series inductors in the connecting buses of the inner stars to prevent excessive concentration of current in the inner stars. It is generally more efficient to use more stars of shorter radial length than a few stars of long radials.

3. Counterpoise, or large insulated network of radial conductors supported above the ground (figure 1C). The effect of the counterpoise is to distribute the ground currents uniformly over its area. The capacitance between the counterpoise and ground is as large as possible to reduce the potential from counterpoise to ground, which may still cause considerable hazard to personnel. However, if the cost and danger of the counterpoise system can be tolerated, it is generally preferable to the multiple-star and buried-wire systems. All three systems possess above-ground conductors at the antenna base.

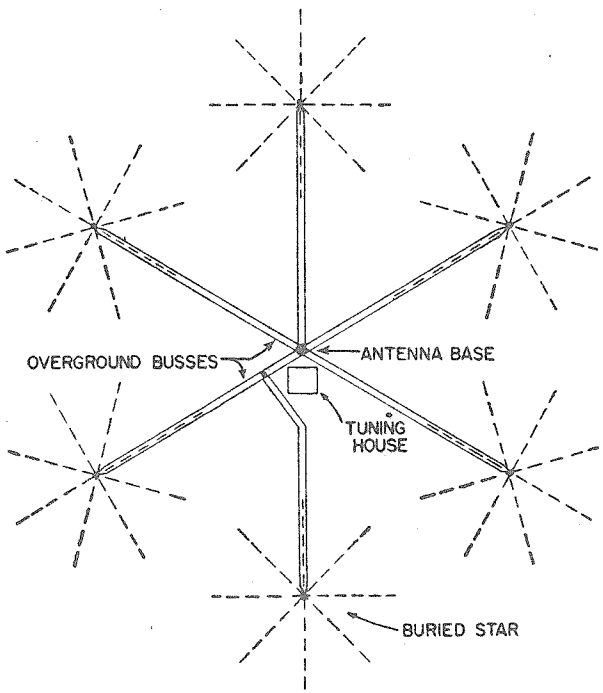

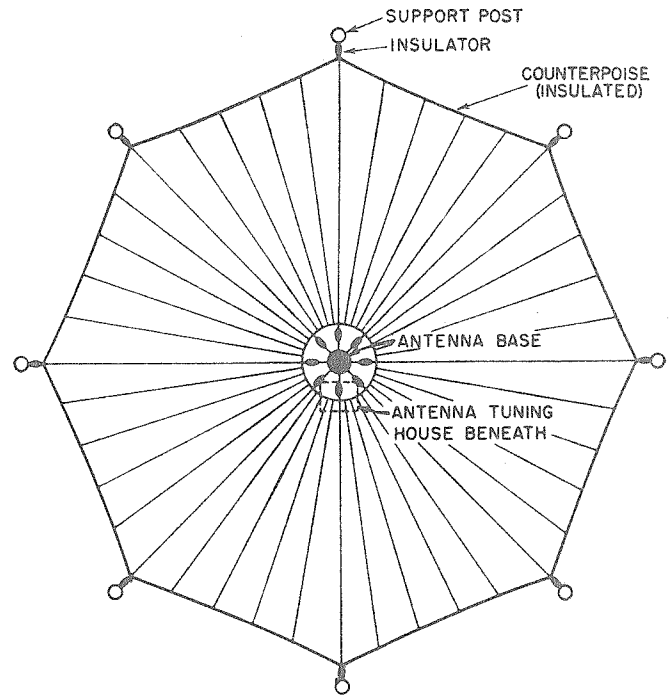

FIGURE 1B. MULTIPLE-STAR GROUND SYSTEM.

FIGURE 1C. COUNTERPOISE.

The tuning inductor in series with the antenna feed must be designed to have very little dissipation at the operating frequency. Consequently, the quality factor, Q , of the coil must be as large as possible. In order to accomplish this, the coil is as large in diameter as is mechanically practical; the conductor size is also large. Frequently large Litz cable is used.

The high antenna potentials not only cause appreciable dielectric loss due to the high potential gradients in parts of the system, but also introduce serious problems with flashover and arcing. Eventually, the power input of a vlf antenna is limited by the maximum potential that the system can withstand. Since the antenna potential is proportional to the antenna reactance, careful design must be given to reducing the antenna reactance. In order to reduce gradients, conductors of sufficient diameter must be used. Corona shields are also used to reduce gradients at sharp points.

The second aspect of the high potential problem is the proper selection of solid insulators to isolate the antenna conductors from ground and supporting members. Aerial insulators must have both electrical and mechanical strength. They are generally of two basic types: special cylindrical porcelain tubular insulators with cemented end fittings, and the oil-filled safety-core type. These insulators may be as large as six ft long and six in. in diameter. They may have a mechanical strength as high as 1,000,000 lb and an electrical strength of several hundred kilovolts (wet).

The physical size of vlf antennas gives rise to extremely serious mechanical problems. In addition to the tons of conductor and dielectric in the antenna itself, climatic conditions must also be considered. For example, the Jim Creek vlf antenna at Arlington, Washington, was designed to withstand 1/2 in. radial ice in a 65 mph gale. It is frequently necessary to provide means for removing the ice from the antenna by circulating a 60 cps current in the structure without disturbing the radio frequency performance of the antenna. Some antenna systems possess means to release an antenna wire which has become overloaded, in order to prevent loss of a tower from overloading or an unbalanced pull.

The largest vlf antenna in operation today is the U. S. Navy's one megawatt Jim Creek antenna (references 11 and 12). The top-loading for this antenna consists of ten catenary spans suspended in a zig-zag pattern from 200 ft support towers which are erected on the crests of twin mountain ranges (figure 2). All spans are 500 ft apart at their mid-points except for the fifth and sixth spans which are 1,000 ft apart and divide the antenna into two sections. The conducting element of each span is 1.01 in. cable made from 37 strands of No. 7 extra-high-strength copperweld. Because the valley tapers, the spans vary in length from 8,700 ft to 5,600 ft. To provide a proper safety factor for wind and ice loadings, the sags in each span vary from 495 ft for the shortest to 1,063 ft for the longest. The area between the twelve support towers covers 725 acres, 435 of which are covered by active elements of the antenna.

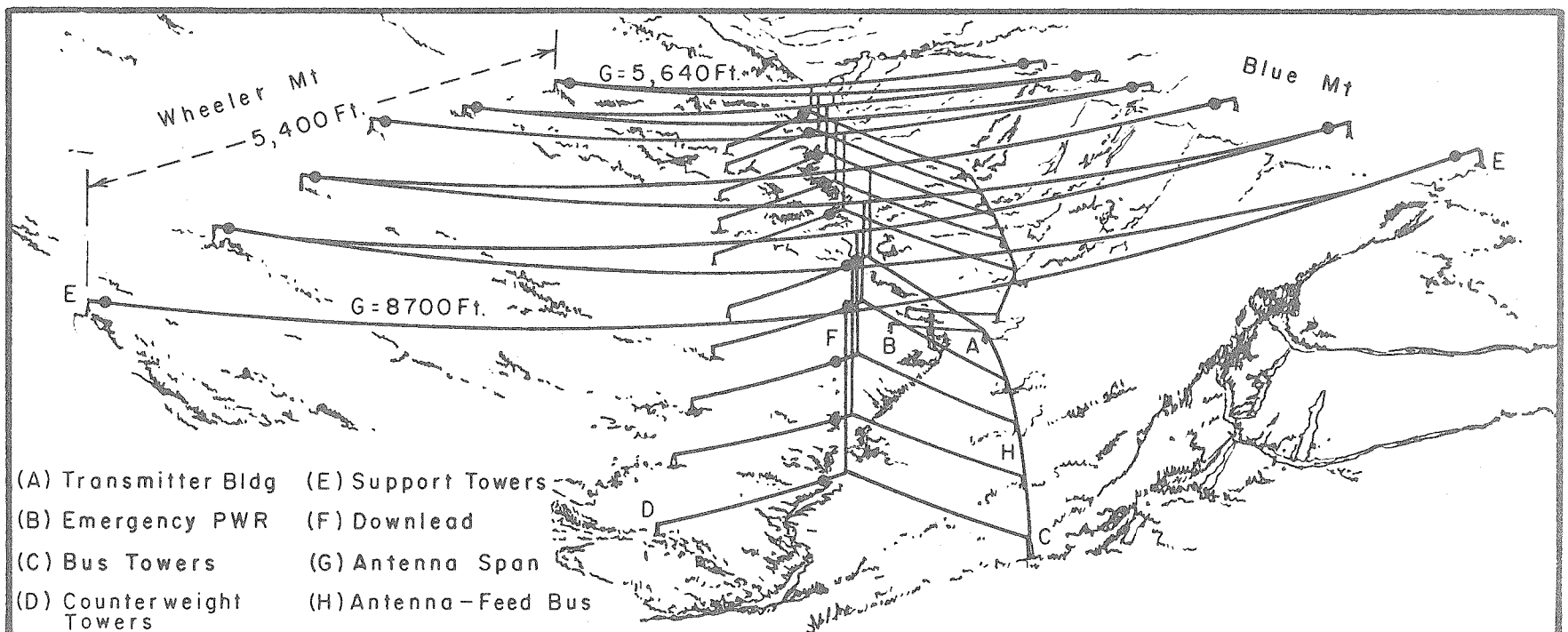

FIGURE 2. JIM CREEK VLF TRANSMITTING ANTENNA (AFTER HOBART).

A downlead of 0.92 in. hollow copper tubing is connected to the center of each span and terminates in two spans which are connected to towers at opposite ends of the valley. The downleads are held in tension by concrete counterweight-and-pulley systems. Each half of the antenna is fed by half of the transmitter. Antenna-feed buses run along the south slope of the valley supported on 125 ft towers and connected to the downlead by means of feed spans. The total antenna current is approximately 2, 100 amp and the insulator voltage is 240 kv.

An antenna similar to the Jim Creek Station is used by the Navy at Haiku, Oahu, T. H. (reference 13). It consists of four spans about 4, 500 ft long, each with a downlead of about 1, 450 ft. It is also supported by two mountain tops, but no towers are used.

At Annapolis, Maryland, the Navy's NSS station uses a triatic type antenna. This consists of a large topload supported by nine 600 ft towers. The towers are arranged in two rows of four each with the ninth tower forming a point at one end. Spacing between rows is about 850 ft and spacing between towers in a row is about 1, 000 ft. Average topload height is 472 ft. Two downleads are used, with a spacing of about 2, 000 ft between downleads. Each downlead has a tuning helix, but only one downlead is fed at a time.

A Navy antenna at Lualualei, Oahu, T. H. is very similar to the one at Annapolis. However, it has only seven 600 ft towers supporting the topload. Spacing between the two rows is 1, 000 ft and the spacing between towers in a row is 1, 250 ft. It also uses two tuned downleads, with only one downlead being fed. Its average topload height is about 440 ft.

Some of the electrical characteristics of the four Navy vlf antennas are exhibited in the following table:

Station	Jim Creek	Annapolis	Lualualei	Haiku
Nominal transmitter power (kw)	1,000	500	500	200
Estimated effective height (meters)	140	105	97	151
Operating frequency (kc)	18.6	15.5	19.8	16.6
Efficiency at operating frequency (percent)	29.6	17.0	27.4	12.2
Radiation resistance (ohms)	0.121	0.047	0.065	0.111
Antenna capacitance (mfd)	0.081	0.044	0.0406	0.0248
Antenna Reactance (ohms)	68	212	185	360

TABLE 1. ELECTRICAL CHARACTERISTICS OF NAVY VLF TRANSMITTING ANTENNAS

Another high power vlf transmitter is the 500 kw Rugby radio station of the British Post Office (references 14 and 15). The antenna for the Rugby station (figure 3A) consists of two separate antennas of different capacities which may be used separately or in combination to form a larger antenna. Two 820 ft masts are spaced symmetrically about the transmitter, 1,320 ft apart, and are common to both antenna systems. The larger antenna is supported on eight masts, arranged in the form of an elongated octagonal shape with 1,320 ft sides. The

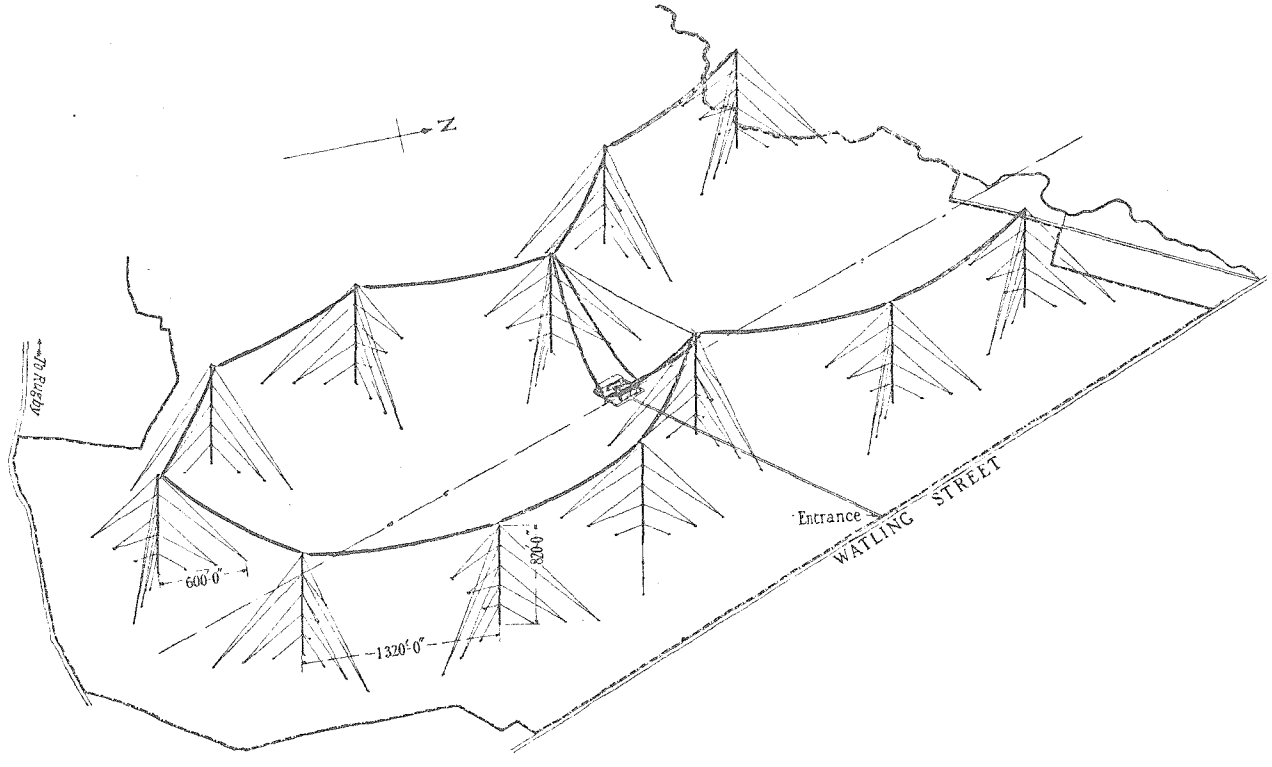

FIGURE 3A. RUGBY GBR TRANSMITTING ANTENNA.
By permission from "The Rugby Radio Station of the British Post Office", by E. H. Shaughnessy.
Proceedings of the Institution of Electrical Engineers, Vol. 64, June, 1926.

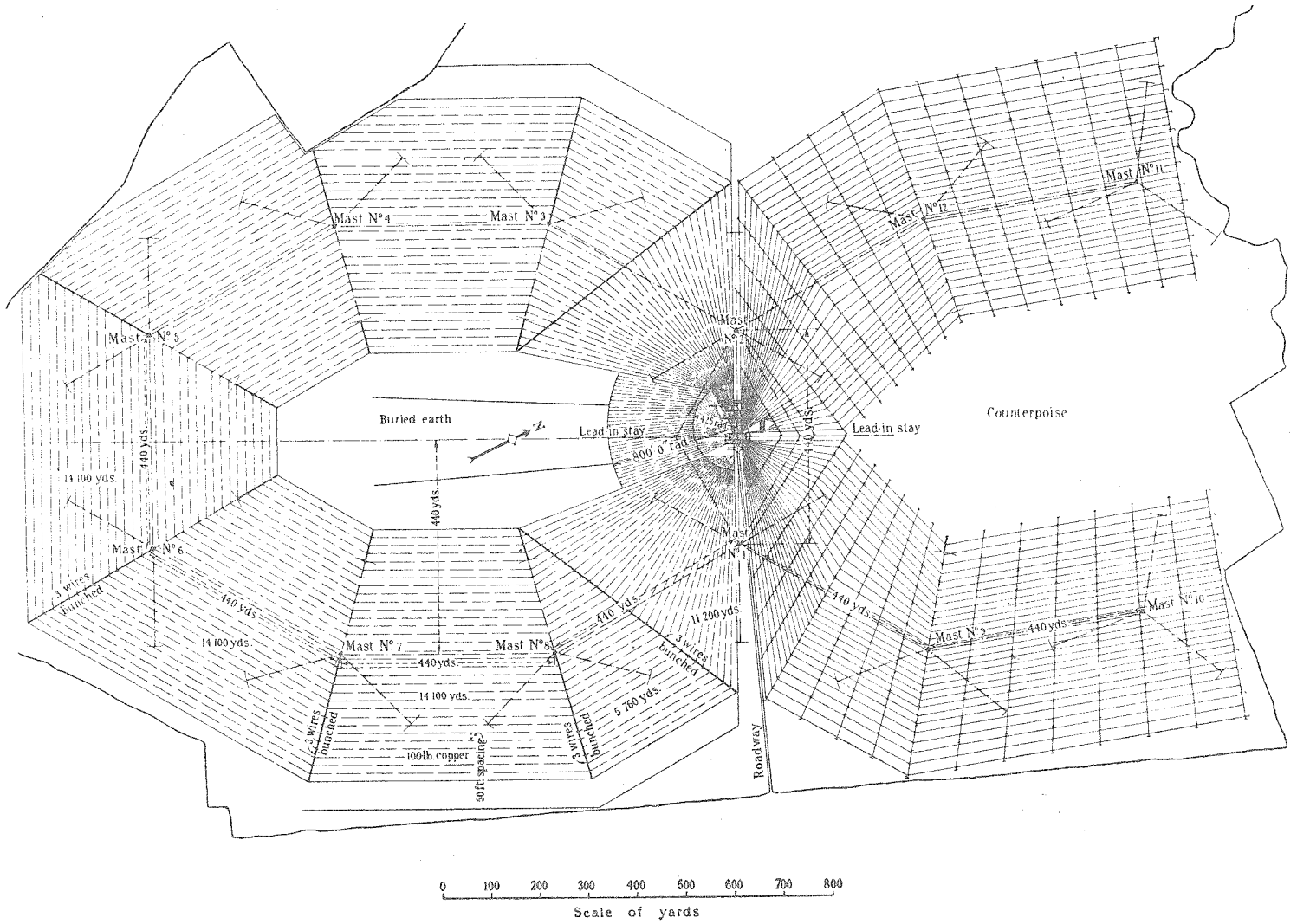

FIGURE 3B. RUGBY GBR TRANSMITTING ANTENNA GROUND SYSTEM.
By permission from "The Rugby Radio Station of the British Post Office", by E. H. Shaughnessy.
Proceedings of the Institution of Electrical Engineers, Vol. 64, June, 1926.

smaller antenna is supported on six masts with the same spacing, but with two open arms.

The combined antenna system has a capacity of 0.045 microfarad, and a total resistance of approximately 1 ohm, including losses. The operating frequency of the combined system is 16 kc. The effective height is 607 ft. The larger antenna has a capacitance of 0.0334 microfarad and a resistance of 0.8 ohm at 38 kc. The necessary tuning inductance at this frequency is 530 microhenries. The smaller antenna has a capacitance of 0.0164 microfarad at 62 kc, the tuning inductance being 394 microhenries.

The ground system (figure 3B) beneath the larger antenna consists of No. 12 copper wire, buried a few inches underground. The ground follows the shape of the antenna but extends 800 ft beyond the masts. Near the feedpoint the wires leave the ground and converge on the transmitter building. The ground system beneath the smaller antenna is an insulated counterpoise, averaging 16 ft above the ground. The counterpoise follows the general shape of the antenna. The spacing between individual wires varies from 40 ft (near the transmitter) to 80 ft (at the edges).

B. The Horizontal Half-Wave Very Low-Frequency Transmitting Antenna

In 1952 a new type of vlf transmitting antenna was developed which eliminated many of the disadvantages of conventional toploaded, vertical vlf antennas (reference 16). In order to avoid costly mechanical construction, the antenna was mounted horizontally on poles, a very

small electrical distance above the earth. The long antenna was half-wave resonant at the operating frequency, thus not requiring tuning elements. Construction of a conventional ground system was unnecessary. The prototype was constructed near Randsburg, California, in the Mojave Desert. Very satisfactory vertical incidence ionospheric sounding data were obtained with the antenna (reference 17).

The radiation fields of the half-wave, horizontal, linear antenna, located at the surface of an imperfect earth, have been calculated by this author for an assumed cosinusoidal current distribution (reference 18). (The problem of solving for the exact current distribution is discussed in Section II-E.) These fields are:

1. A horizontally-polarized field radiated in the plane normal to the antenna at its center.

2. A vertically-polarized field radiated along the axis of the antenna. This vertically-polarized field is zero in the plane normal to the antenna at its center.

The horizontal radiation field in the plane normal to the antenna is:

$$E_{horiz} = \frac{j I_o}{2\pi} \sqrt{\frac{\mu_v}{\varepsilon_v}} \frac{2 \cos\theta}{\sqrt{1/u^2 - \sin^2\theta} + \cos\theta} \frac{e^{-j(kR - \omega t)}}{R} \qquad (I\text{-}2)$$

where θ is the colatitude angle, R is the distance from the center of the antenna, I_o is the magnitude of the current at the feedpoint, $k^2 = \omega^2 \mu_v \varepsilon_v$, $u^2 = k^2/(\omega^2 \mu\varepsilon - j\omega\mu\sigma)$, and μ, ε, σ are measured in the earth.

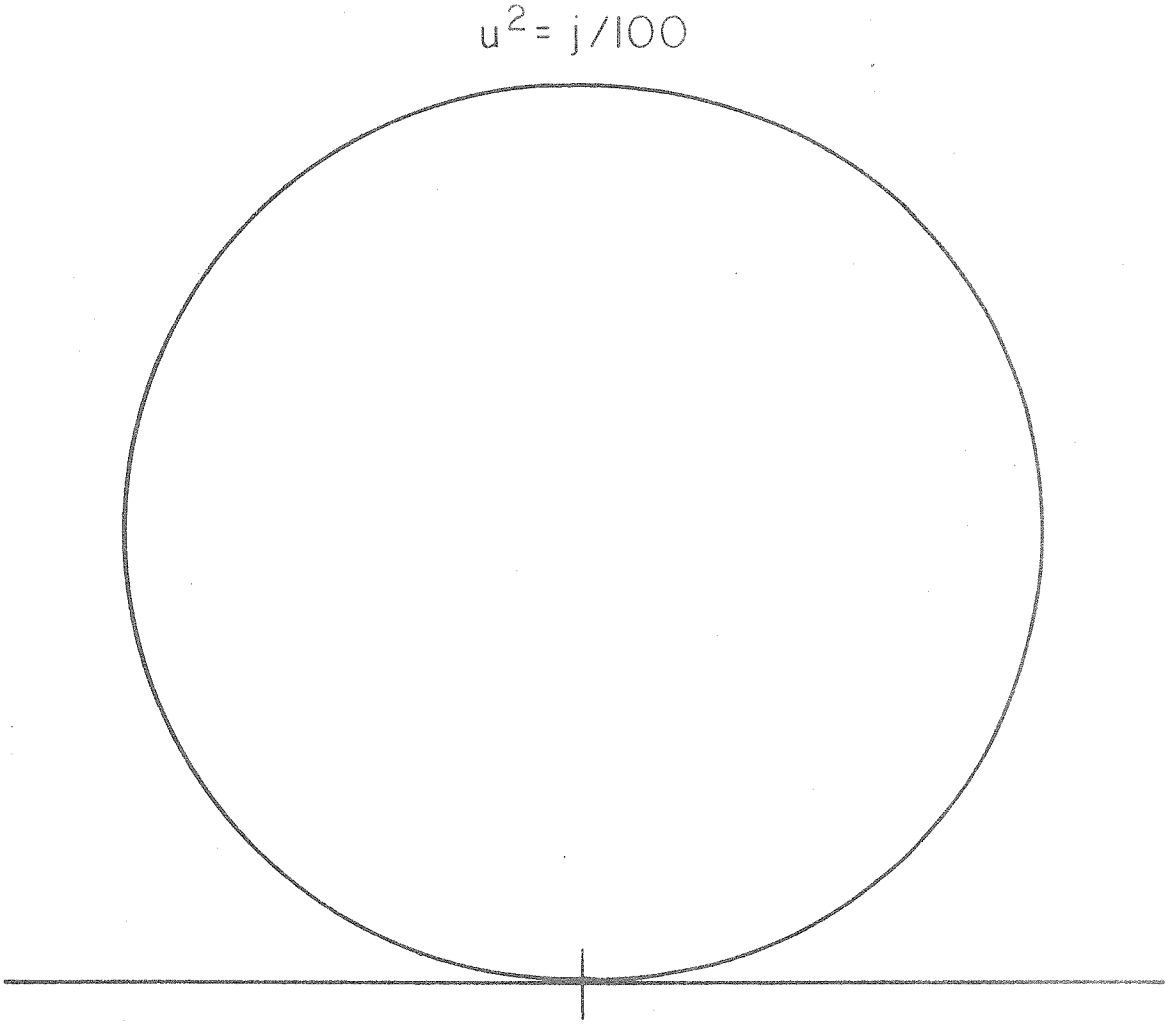

FIGURE 4. RADIATION PATTERN OF THE HORIZONTALLY-POLARIZED FIELD IN THE PLANE NORMAL TO THE ANTENNA AT ITS CENTER FOR A HALF-WAVE ANTENNA LOCATED ABOVE A PLANE CONDUCTING EARTH.

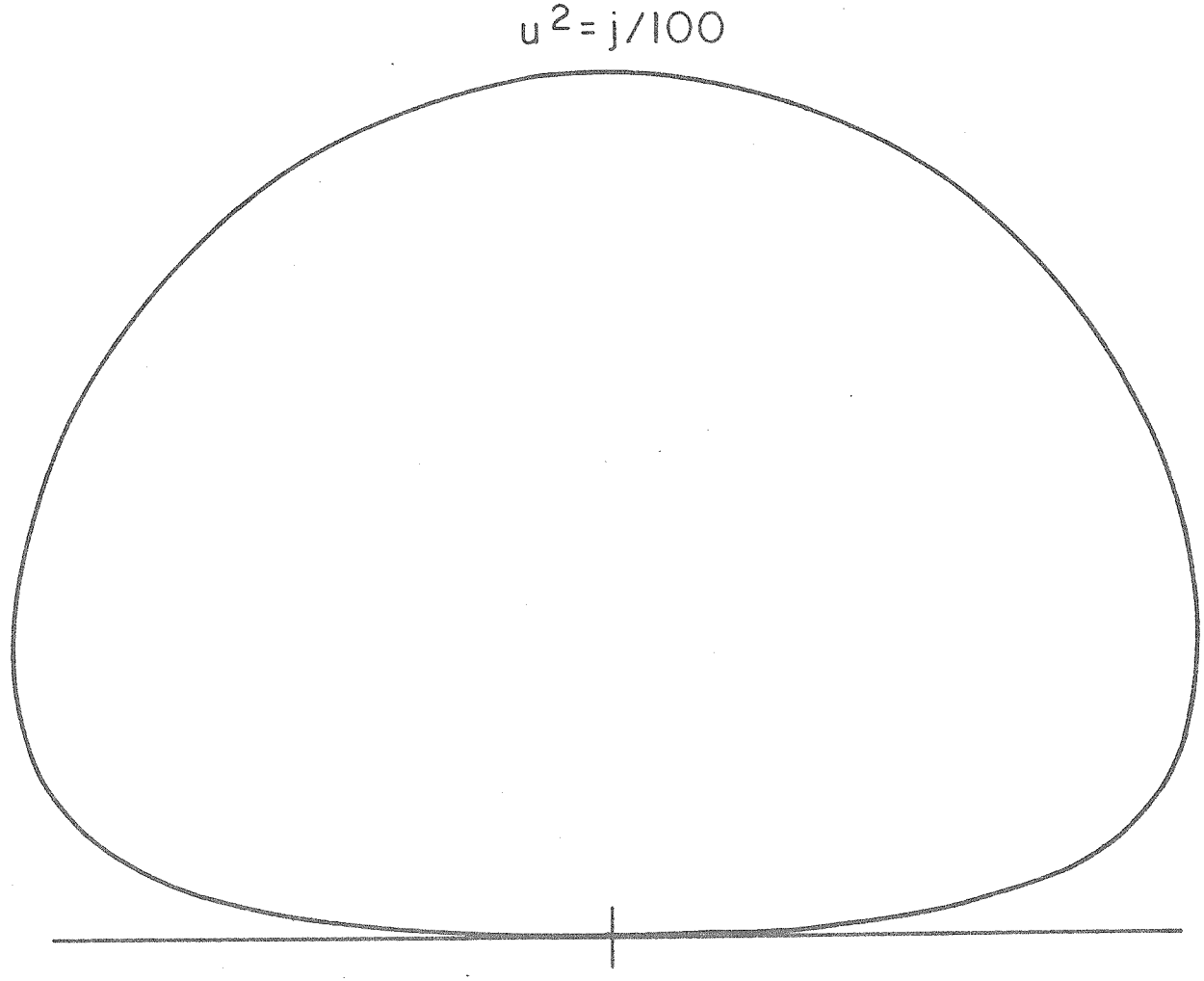

FIGURE 5. RADIATION PATTERN IN THE VERTICAL PLANE ALONG THE ANTENNA FOR A HALF-WAVE ANTENNA LOCATED ABOVE A PLANE CONDUCTING EARTH.

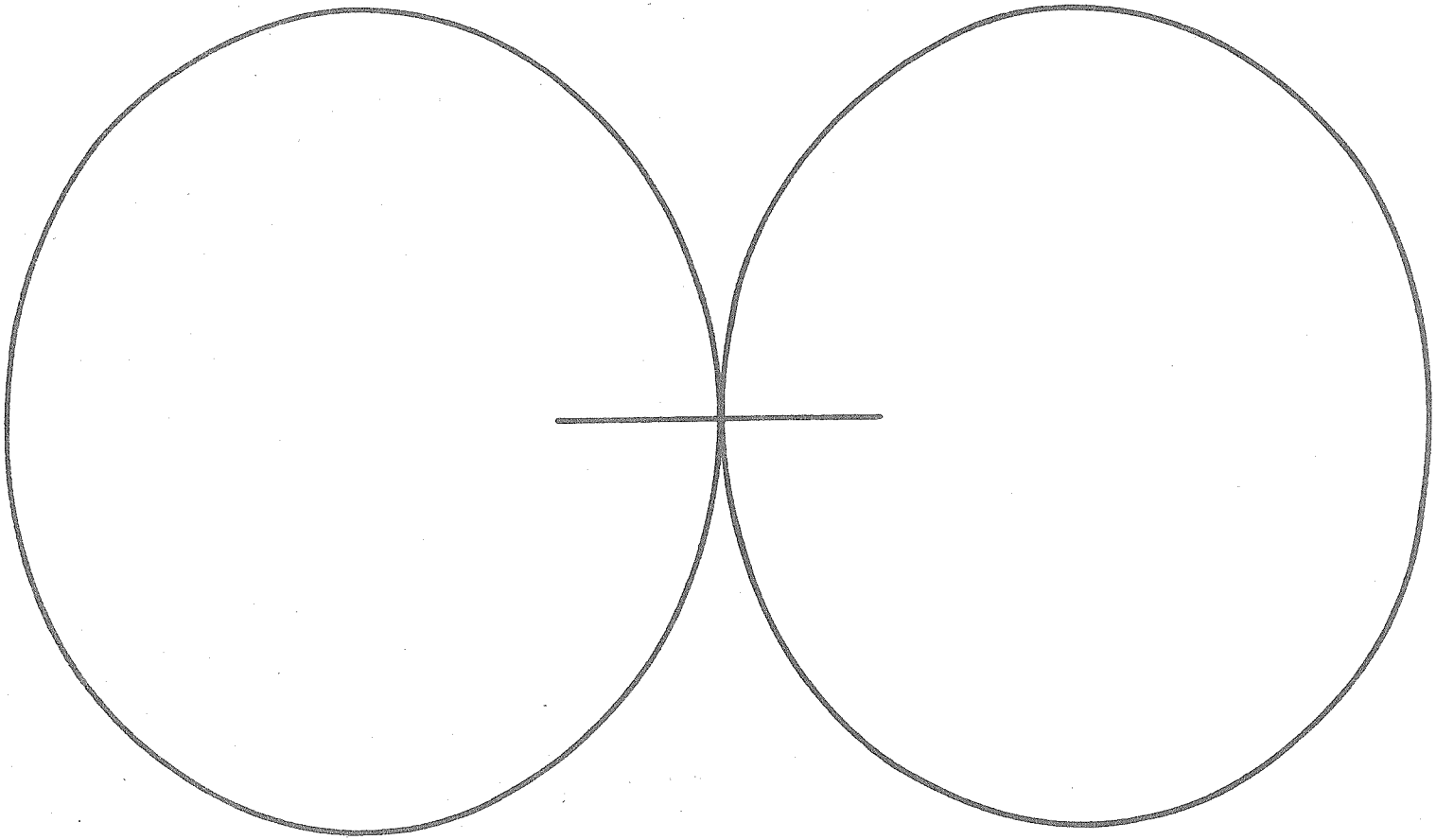

FIGURE 6. RADIATION PATTERN OF THE VERTICALLY-POLARIZED GROUND WAVE AT THE SURFACE OF THE EARTH FOR A HALF-WAVE ANTENNA LOCATED ABOVE A PLANE CONDUCTING EARTH.

The radiation field in the vertical plane of the antenna is:

$$E_\theta = \frac{jI_o}{\pi}\sqrt{\frac{\mu_v}{\varepsilon_v}}\ \frac{u\sqrt{1-u^2\sin^2\theta}}{\cos\theta + u\sqrt{1-u^2\sin^2\theta}}\ \frac{\cos\left(\frac{\pi}{2}\sin\theta\right)}{\cos\theta}\ \frac{e^{-j(kR-\omega t)}}{R} \qquad \text{(I-3)}$$

The vertically-polarized ground wave field is:

$$E_{vert} = \frac{juI_o}{2\pi}\sqrt{\frac{\mu_v}{\varepsilon_v}}\ \frac{2\cos\phi\cos\left(\frac{\pi}{2}\cos\phi\right)}{\sin^2\phi}\ \frac{e^{-j(kR-\omega t)}}{R}\ \cdot$$

$$\cdot\left\{1 - j\sqrt{\pi w}\ e^{-w} + \text{higher order terms}\right\} \qquad \text{(I-4)}$$

where ϕ is measured from the axis of the antenna and $w = -j2kRu^2(1-u^2)$. The radiation patterns in the three mutually perpendicular planes are plotted in figures 4, 5, and 6. These fields have been verified experimentally.

The radiation fields of this antenna are considerably smaller than the fields of an identical antenna located in free space, because of the lossy ground below the antenna. The ratio of the actual field directly above the antenna to the free-space field is plotted in figure 7 as a function of the frequency-resistivity product. Clearly, when operating at very low frequencies, the ground conductivity must be as low as possible for relatively high antenna efficiencies (unlike vertical vlf antennas which require high ground conductivities). Consequently, an extensive study of the relationship of ground conductivity to geology was made over most of Central and Southern California by this author and others (reference 18). The results of this study revealed that

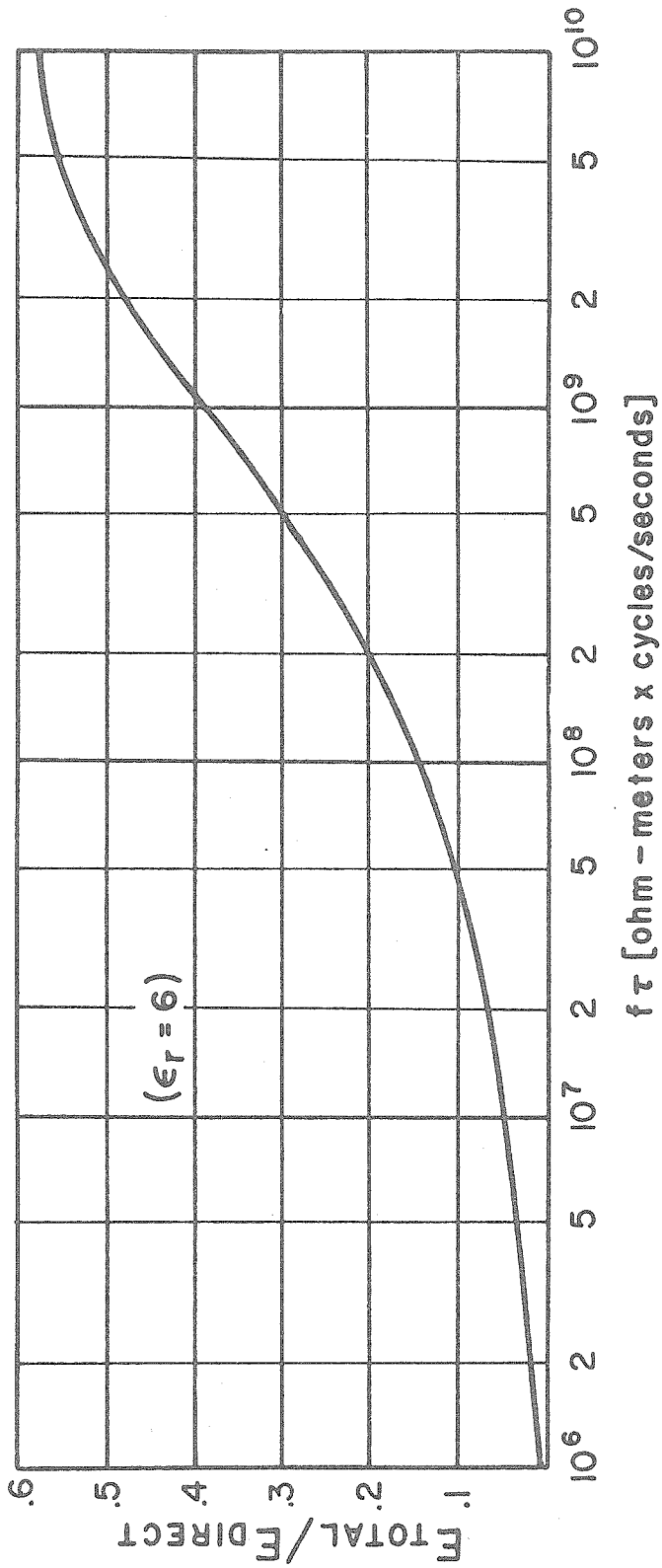

FIGURE 7. MAGNITUDE OF THE RATIO OF THE FIELD DIRECTLY ABOVE THE ANTENNA TO THE FREE-SPACE FIELD VS. THE FREQUENCY-RESISTIVITY PRODUCT FOR A HALF-WAVE ANTENNA LOCATED ABOVE A PLANE CONDUCTING EARTH.

high values of resistivity are found in areas where the underlying substructure is relatively unfractured. The amount of annual rainfall and other climatic conditions are of little significance. The highest values of resistivity were measured in the Sierra Nevada Mountains (2, 100 to 5, 120 ohm-meters). The underlying rock in the Sierra Nevada consists primarily of solid granite. However, in the Mojave Desert, where there is as little as 0.5 to 2.0 in. of rainfall annually, and where the water table is as low as 2, 300 ft below the surface, the measured values of resistivity only ranged from 68 to 330 ohm-meters. These relatively low values were attributed to the high degree of faulting in the rocks below the surface of the Mojave.

Therefore the low efficiencies of the horizontal vlf antenna may be increased by locating the antenna over proper rock structure. Furthermore, the simplicity, flexibility, and inexpensiveness of this antenna make it well suited for many experimental purposes. Because of its unique radiation pattern, the horizontal, half-wave antenna is ideal for ionospheric experiments. Radiation is maximum in the vertical direction. In addition, a receiver located in the ground-wave null does not receive any directly radiated fields, but only those reflected from the ionosphere. Consequently, unlike vertical transmitting systems, it is unnecessary to separate the direct signal from the reflected signal at the receiver.

C. Research Under the Air Force Office of Scientific Research

In 1955 a program of research was initiated by the California Institute of Technology under the sponsorship of the Office of Scientific Research of the Air Research and Development Command. The purpose of this research was to investigate the whistler mode of vlf propagation by constructing a transmitting antenna to generate whistler-mode echoes. In the progress of this research several other aspects of vlf propagation were also investigated.

Initially, it was intended to construct a horizontal, half-wave antenna, similar to the Randsburg antenna. It was subsequently proposed, however, that a commercial power line might be used as the transmitting antenna. This proposal led to the analysis, design, and construction of a unique vlf antenna system. This system employed a single-phase, medium voltage, commercial power line. The antenna section was isolated from the rest of the distribution system by parallel resonant circuits, or line traps (figures 8 and 9). These isolation networks were similar to the line traps employed in carrier current communication systems now in extensive use by many power companies (reference 19).

Two of these traps were located at each end of the half-wavelength antenna section, and two at the center of the antenna. The end traps served principally to prevent the radio frequency energy from coupling past the antenna section into the remainder of the power distribution system. The center traps isolated the antenna section into two halves so that it could be fed as a balanced, center-fed antenna. The radio

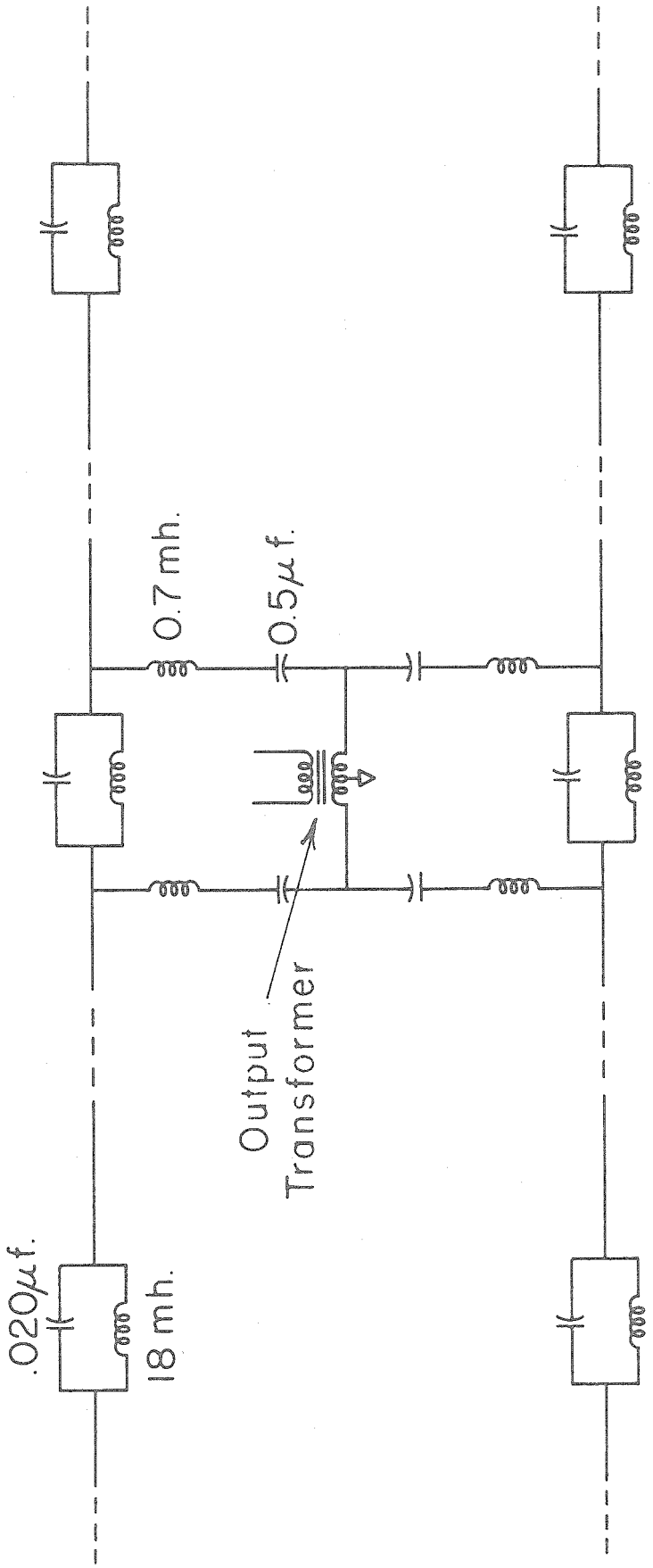

FIGURE 8. SCHEMATIC DIAGRAM OF THE POWER-LINE ANTENNA SYSTEM.

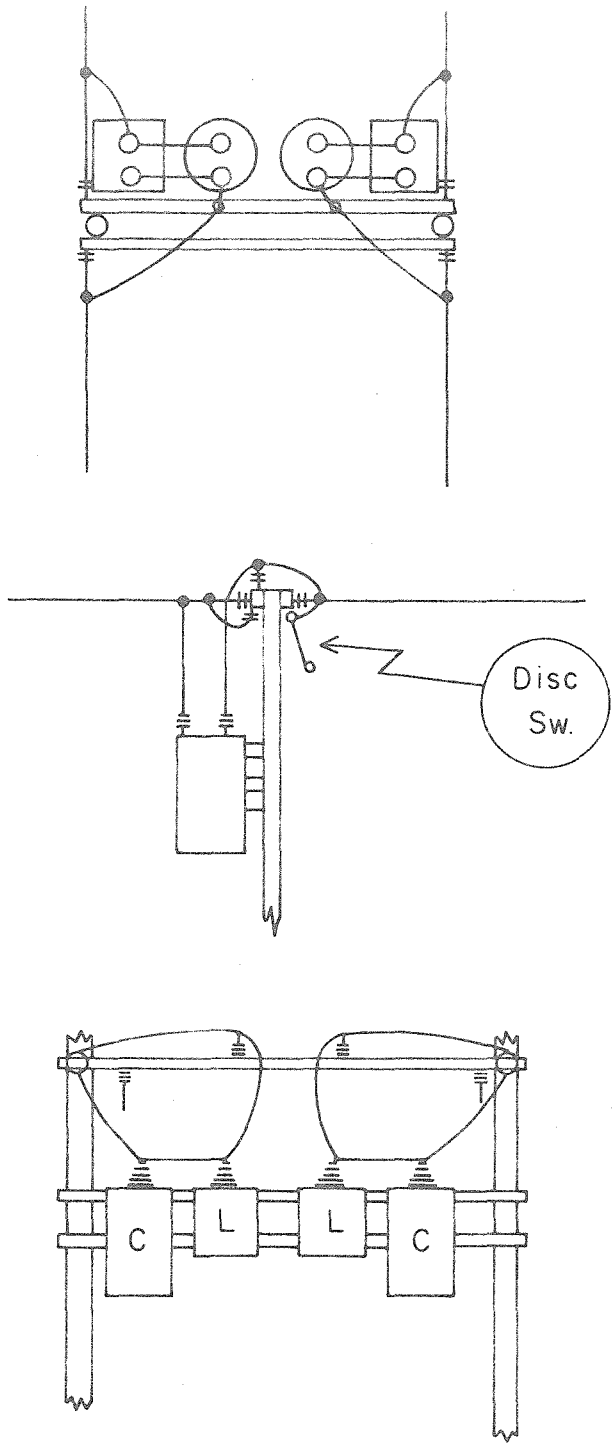

FIGURE 9. LINE TRAP INSTALLATION FOR THE POWER-LINE ANTENNA SYSTEM.

frequency traps were designed to present a negligible impedance to the flow of 60 cps power and a maximum impedance to the radio frequency power. In this manner it was possible to draw 50 kw of 60 cps power from the center of the antenna section to drive the transmitter while simultaneously radiating vlf energy from the same section of line.

Section II of this thesis contains a theoretical analysis of the antenna loading problem developed by this author. Section III describes the design, construction, and performance of the power-line antenna system itself. In Section IV, the vlf propagation experiments for which the antenna was used are described, and some of the experimental data are presented.

II. ANALYSIS OF THE LINEAR ANTENNA WITH LOADING

A. Review of Previous Solutions of Linear Antennas Without Loading

In 1938 a linearized integral equation was formulated by Hallén (reference 20) for the solution of linear antennas with a cross-sectional dimension which was very small relative to the length of the antenna and also very small relative to a wavelength. Referring to the geometry of figure 10, Hallén's theory is briefly outlined below. For a harmonic time-dependence of $e^{j\omega t}$:

$$\overline{E} = -\nabla\phi - j\omega\overline{A} \qquad \text{(II-1a)}$$

and

$$\phi = \frac{j}{\omega\mu\varepsilon}\nabla\cdot\overline{A} \qquad \text{(II-1b)}$$

where $\overline{E}$ is the electric field, $\overline{A}$ is the vector potential, and ϕ is the scalar potential (reference 21). The z-component of the electric field is then

$$E_z = -\frac{j\omega}{\beta_o^2}\left(\frac{\partial}{\partial z}\nabla\cdot\overline{A} + \beta_o^2 A_z\right) \qquad \text{(II-2)}$$

where $\beta_o = \frac{\omega}{c}$, the free-space propagation constant. For the idealized linear antenna of figure 10, both A_x and A_y are zero everywhere in space, so equation II-2 becomes:

$$E_z = -\frac{j\omega}{\beta_o^2}\left(\frac{d^2 A_z}{dz^2} + \beta_o^2 A_z\right) \qquad \text{(II-3)}$$

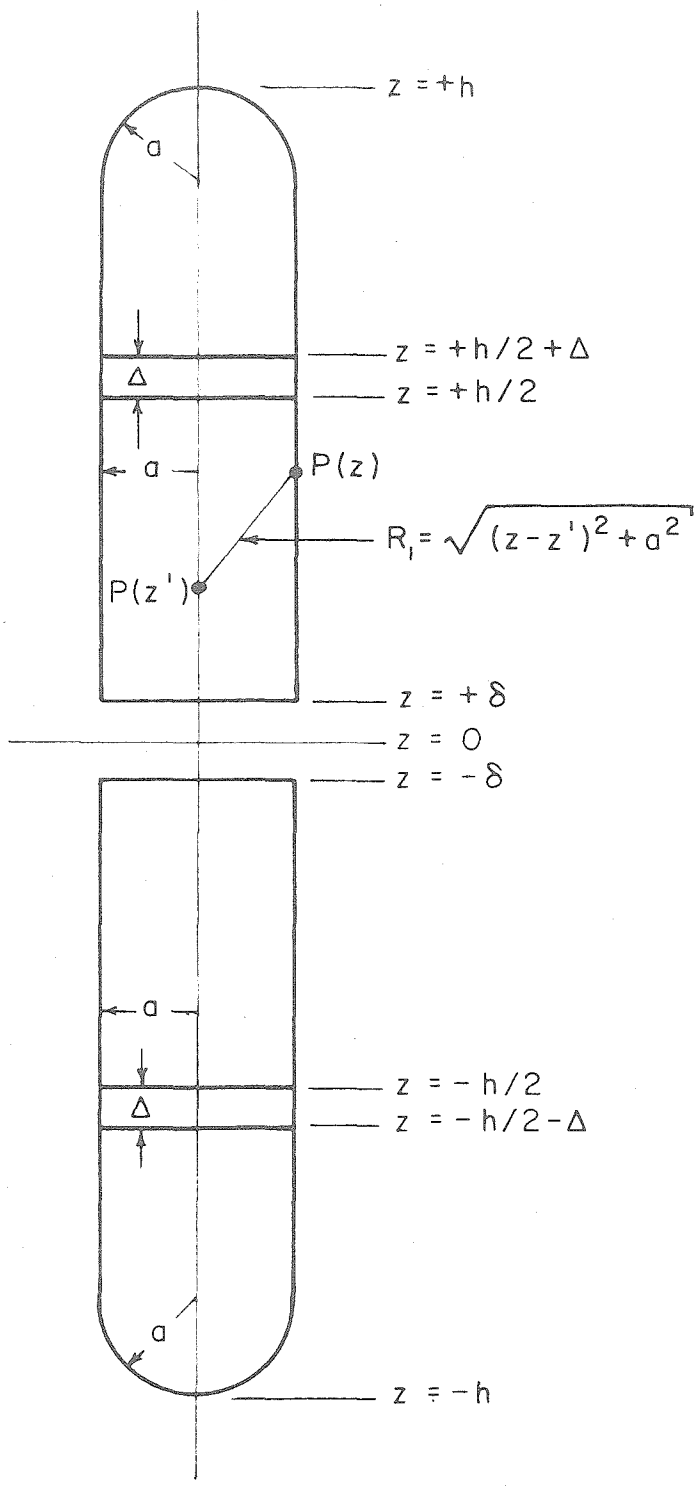

FIGURE 10. GEOMETRY OF THE IDEALIZED LINEAR ANTENNA.

The total axial current I_z in the antenna is related to the axial component of the electric field E_z at the surface of the antenna by the formula defining the internal impedance per unit length of the conductor Z^i:

$$(E_z)_{r=a} \triangleq Z^i I_z \qquad \text{(II-4)}$$

Equating equations II-3 and II-4 at the surface of the antenna:

$$\frac{d^2 A_z}{dz^2} + \beta_o^2 A_z = \frac{j\beta_o^2}{\omega} Z^i I_z \qquad \text{(II-5)}$$

Solution of equation II-5 yields the Hallén integral equation:

$$\frac{\mu}{4\pi}\left[\int_{-h}^{-\delta} + \int_{\delta}^{h}\right] \frac{I_z(z')\, e^{-j\beta_o R_1}}{R_1}\, dz' = A_o \cos\beta_o z - \frac{jV_o}{2c}\sin\beta_o|z|$$

$$+\frac{jZ^i}{c}\int_{\delta}^{z} I_z(s)\sin\beta_o(z-s)ds \qquad \text{(II-6)}$$

where

$$R_1 = \sqrt{a^2 + (z'-z)^2}$$

A_o = an unknown complex constant

V_o = potential difference applied at the antenna feed

Solution of equation II-6 for the current distribution $I_z(z)$ will yield all of the properties of the linear antenna, e.g., the feedpoint

impedance, radiation pattern, etc. However an exact general solution has never been found for the integral equation II-6. It is frequently assumed that the antenna is highly conducting so that the term in Z^i can be neglected; then a solution is obtained by iteration or successive approximations. Since Hallén's original work, others have developed and improved the iteration method with increasing degrees of accuracy. The improved theory of King (reference 22) has given results which best agree with experiment. However, even the improved theories are cumbersome because of the difficulty in solution of the integral equation. Only two terms of the successive approximation series have been evaluated. The accuracy of this two-term approximation is undetermined. As additional terms are computed, the mathematical functions rapidly become extremely difficult to evaluate. Use of the Hallén-King method to solve a linear antenna with loading leads to prohibitive mathematical difficulties. Nevertheless, the Hallén-King solution of the unloaded linear antenna problem gives results which are in good agreement with experimental data.

In 1952 Storm (reference 23) obtained an approximate solution to equation II-6 by expanding the current distribution in a Fourier series of the normal current modes of the antenna. Using symmetry and the boundary conditions that $I_z(\pm h) = 0$, the current distribution becomes:

$$I(z) = A \sin \beta_o(h - |z|) + \sum_n A_n \cos k_n z \qquad \text{(II-7)}$$

where A and A_n are undetermined complex coefficients, $k_n = \frac{n\pi}{2h}$, $n = 1, 3, 5, 7, \cdots$. The leading term is the zero-order approximation

of King. Substitution of II-7 into II-6 leads to the evaluation of three types of integrals:

$$\int_{-h}^{+h} \sin(\beta_o(h - |z'|)) \frac{e^{-j\beta_o R_1}}{R_1} dz' \qquad \text{(II-8a)}$$

$$\text{Re} \int_{-h}^{+h} \cos(k_n z') \frac{e^{-j\beta_o R_1}}{R_1} dz' \qquad \text{(II-8b)}$$

$$\text{Im} \int_{-h}^{+h} \cos(k_n z') \frac{e^{-j\beta_o R_1}}{R_1} dz' \qquad \text{(II-8c)}$$

Equation II-8a can be evaluated in terms of tabulated Si(z) and Ci(z) functions. Equations II-8b and II-8c can be solved only approximately but with considerable accuracy. When the integrals of II-6 have been expressed as a sum of integrated terms, m independent equations may be obtained by evaluating the modified form of II-6 at m values of z from 0 to h. From these m equations, A and m - 1 of the coefficients A_n can be determined. When these coefficients are known, the current distribution can be determined from II-7. Although it becomes difficult to solve the set of m equations when m becomes large, no new mathematical difficulties are introduced beyond evaluating

the integrals II-8. Only the labor required to solve the set of m algebraic equations limits the accuracy of the solution. Consequently this method is well-suited for problems for which the series II-7 converges rapidly. Although this method has given excellent agreement with experimental data for only five terms of the series, considerable doubt has been raised concerning the uniqueness of the solution, since any m points along the antenna can be used to evaluate equation II-6.

A second method employing Fourier expansions to solve the unloaded linear antenna problem was introduced by Nomura and Hatta (reference 24). However, in this case an approach is used which is entirely different from the Hallén-King method. Both the current distribution and the field intensity at the surface of the antenna are expanded in a Fourier series. An impedance matrix is introduced which relates the expansion coefficients. The current may then be computed after inverting the impedance matrix. The number of terms in the series expansion is limited only by the means available to invert the impedance matrix. Therefore, unless a large impedance matrix can be inverted, the accuracy of the solution using a smaller matrix may be rather poor. Nomura and Hatta used approximation methods to invert the impedance matrix, thereby limiting the accuracy of their solution.

B. Matrix Solution of a Linear Antenna With Loading

The following section contains a description of the matrix method solution of the loaded, linear antenna problem developed by this author. In order to carry out the analysis on a one-dimensional basis, it was first necessary for the author to make several standard linearizing assumptions. These assumptions are presented below, and will be discussed more completely in Section II-E.

1. The radius a of the circular-cylindrical antenna wire must be extremely small compared to the length of the antenna (figure 10).

$$a \ll 2h \tag{II-9}$$

If II-9 is valid, it can be shown (reference 22) that the vector potential at a point P directly outside the antenna wire is independent of the cross-sectional distribution of the axial current, as long as P is more than a distance of $5a$ from the end of the antenna. Since the current in the regions within a distance of $5a$ from the ends of the antenna is nearly zero for thin antennas, this approximation for the vector potential will be made over the entire length of the antenna. The analysis will then consider the axially-directed current to be confined to the axis of the cylindrical antenna. It will only be necessary to solve for the axial distribution of the current $I_z(z)$.

2. The current at the ends of the antenna is assumed to be zero.

$$I_z(\pm h) = 0 \tag{II-10}$$

If the antenna had flat ends, or the open ends of a tube, equation II-10 would not be valid since charge would flow onto the flat ends or around the sharp edge and into the tube. For the hemispherical ends of the idealized antenna shown in figure 10, equation II-10 is valid. However, the rounded ends introduce a small radial component of the current near the ends of the antenna. The analysis will neglect the effect of these radial currents.

3. The excitation of the antenna will be provided by an idealized generator which maintains a scalar potential difference $V_o e^{j\omega t}$ across the edges of the cylindrical envelope between $z = \pm \delta$ as $\delta \rightarrow 0$. The excitation is maintained symmetrically so that there is no ϕ-dependence of any field quantities. The effects of the antenna feed conductors are not taken into account in this analysis.

Having made the linearizing assumptions, the author has expanded the axially-directed current in a Fourier series in a manner similar to Nomura and Hatta:

$$I(z)\, e^{j\omega t} = e^{j\omega t} \sum_{n=1}^{\infty} I_n \sin(k_n z + \alpha_n) \qquad \text{(II-11)}$$

where $k_n = \frac{n\pi}{2h}$ and $\alpha_n = \frac{n\pi}{2}$ to satisfy condition II-10. For convenience, the subscript z will be dropped from the current notation. Because of the symmetry about $z = 0$, it is easily shown that n must be odd. However, the general form of equation II-11 will be retained throughout in order to be valid for antennas with asymmetrical feed or asymmetrical loading.

The z-component of the electric field on the surface of the antenna wire can also be expanded in a Fourier series:

$$E_z(a, z)\, e^{j\omega t} = - \frac{e^{j\omega t}}{h} \sum_{n=1}^{\infty} E_n \sin(k_n z + \alpha_n) \qquad \text{(II-12a)}$$

and

$$E_n = - \int_{-h}^{h} \sin(k_n z + \alpha_n)\, E_z(a, z)\, dz \qquad \text{(II-12b)}$$

where k_n and α_n are the same as in equation II-11.

For an antenna with a potential difference V_o at $z = 0$ and with an internal impedance per unit length of the antenna wire $Z^i(z)$, the axial electric field at the surface of the antenna is:

$$E_z(a, z) = - V_o \delta(z) + Z^i(z)\, I(z) \qquad \text{(II-13)}$$

where

$$\delta(z) = 0 \quad \text{when} \quad z \neq 0 \qquad \text{(II-14a)}$$

and

$$\int_{-h}^{+h} f(z)\, \delta(z)\, dz = f(0) \qquad \text{(II-14b)}$$

The antenna is perfectly conducting except for the symmetrical loading impedances at $z = \pm h/2$:

$$Z^i(z) = \begin{cases} 0, & -h \leqslant z \leqslant -\frac{h}{2} - \Delta \\ \frac{Z_o}{\Delta}, & -\frac{h}{2} - \Delta \leqslant z \leqslant -\frac{h}{2} \\ 0, & -\frac{h}{2} \leqslant z \leqslant \frac{h}{2} \\ \frac{Z_o}{\Delta}, & \frac{h}{2} \leqslant z \leqslant \frac{h}{2} + \Delta \\ 0, & \frac{h}{2} + \Delta \leqslant z \leqslant h \end{cases} \qquad \text{(II-15)}$$

Actually the impedance per unit length of the antenna is given by the formula (reference 25):

$$\frac{E_z(a, z)}{I_z} = Z^i(z) \cong \frac{1 + j}{2\pi a} \sqrt{\frac{\omega\mu}{2\sigma}} \qquad \text{(II-16)}$$

However, over most of the antenna, the conductivity σ is sufficiently large to validate the approximation that in this range $Z^i(z) = 0$. In the segments at $z = \pm \frac{h}{2}$, this approximation is no longer made. These segments represent the presence in the antenna wire of lumped-circuit loading elements of purely real impedance Z_o. (Z_o has been taken real to simplify the analysis. Complex Z_o could also have been considered.)

Substitution of equations II-11 and II-13 into equation II-12 yields:

$$E_n = V_o \sin\alpha_n - \frac{Z_o}{\Delta} \sum_{m=1}^{\infty} I_m \left[\int_{-\frac{h}{2}-\Delta}^{-\frac{h}{2}} + \int_{\frac{h}{2}}^{\frac{h}{2}+\Delta} \right] \sin(k_n z + \alpha_n) \cdot \sin(k_m z + \alpha_m) \, dz \qquad \text{(II-17)}$$

When $k_n \Delta \ll 1$, equation II-17 becomes:

$$E_n = V_o \sin\alpha_n - \sum_{m=1}^{\infty} F_{nm} I_m \qquad \text{(II-18a)}$$

where

$$F_{nm} = Z_o \left(\sin\frac{n\pi}{4} \sin\frac{m\pi}{4} + \sin\frac{3n\pi}{4} \sin\frac{3m\pi}{4} \right) \qquad \text{(II-18b)}$$

Outside the antenna conductor

$$\overline{E} = -\frac{j\omega}{\beta_o^2} \left(\nabla \nabla \cdot \overline{A} + \beta_o^2 \overline{A} \right) \qquad \text{(II-19)}$$

and*

$$\overline{A} = A_z \overline{e}_z = \frac{\mu \overline{e}_z}{4\pi} \int_{-h}^{+h} I(z') \frac{e^{-j\beta_o R_1}}{R_1} dz' \qquad \text{(II-20)}$$

---

* Here the integration is taken through the potential discontinuity between $z = \pm \delta$, which is generally done in the literature. The error introduced can be neglected if $\beta_o \delta \ll 1$.

where $\bar{e}_z$ is the unit vector in the z-direction, $\beta_o = \omega/c$, and $R_1 = \sqrt{(z - z')^2 + a^2}$. The electric field is therefore linearly related to the current and can be expanded into a sum of partial fields:

$$E_z(\rho, z)\, e^{j\omega t} = e^{j\omega t} \sum_{m=1}^{\infty} G_m(\rho, z)\, I_m \triangleq e^{j\omega t} \sum_{m=1}^{\infty} \mathcal{E}_m(\rho, z) \qquad \text{(II-21)}$$

where the function $G_m(\rho, z)$ will be determined below.

From equation II-21 in the limit as $\rho \to a$,

$$E_z(a, z) = \sum_{m=1}^{\infty} G_m(a, z)\, I_m \qquad \text{(II-22)}$$

which, when substituted in II-12b, yields:

$$E_n = \sum_{m=1}^{\infty} \left[-\int_{-h}^{+h} \sin(k_n z + \alpha_n)\, G_m(a, z)\, dz \right] I_m \qquad \text{(II-23)}$$

and finally

$$E_n = \sum_{m=1}^{\infty} Z_{nm}\, I_m \qquad \text{(II-24a)}$$

where

$$Z_{nm} = -\int_{-h}^{h} \sin(k_n z + \alpha_n)\, G_m(a, z)\, dz \qquad \text{(II-24b)}$$

Evaluation of the impedance Z_{nm} is accomplished by expanding the vector potential into a sum of partial potentials, each caused by the corresponding partial current. Thus:

$$A_m(\rho, z) = \frac{\mu}{4\pi} \int_{-h}^{h} I_m \sin(k_m z' + a_m) \frac{e^{-j\beta_o \sqrt{(z - z')^2 + \rho^2}}}{\sqrt{(z - z')^2 + \rho^2}} dz' \quad \text{(II-25)}$$

From equations II-19 and II-21, the mth partial field $\mathcal{E}_m$ due to the mth current element is:

$$\mathcal{E}_m(\rho, z) = G_m(\rho, z) I_m = \frac{(-j\omega)}{\beta_o^2} \left(\frac{d^2 A_m}{dz^2} + \beta_o^2 A_m \right) \quad \text{(II-26)}$$

Then, using equations II-24b, II-25, and II-26, it can be shown that:

$$Z_{nm} = -\frac{(\beta_o^2 - k_n^2)}{I_m} \int_{-h}^{h} \sin(k_n z + a_n) \frac{(-j\omega)}{\beta_o^2} A_m(a, z) dz$$

$$+ \frac{k_n}{I_m} (-1)^n \frac{(-j\omega)}{\beta_o^2} A_m(a, h) - \frac{k_n}{I_m} \frac{(-j\omega)}{\beta_o^2} A_m(a, -h) \quad \text{(II-27)}$$

Complete evaluation of equation II-27 is carried out in Appendix I.

It is then possible to equate equations II-24a and II-18a, producing the fundamental current equation:

$$\sum_{m=1}^{\infty} Z_{nm} I_m + \sum_{m=1}^{\infty} F_{nm} I_m = V_o \sin \frac{n\pi}{2} \quad \text{(II-28)}$$

Equation II-28 has been obtained for a symmetrical feedpoint and a specific pure-real loading impedance. However, the above method is valid for any general number and location of feedpoints and any arbitrary nature and distribution of loading elements. The generality of the method is discussed in Section II-D. The usefulness of equation II-28 breaks down only when the series expansion II-11 does not

converge fast enough to produce an accurate solution with a reasonably small number of terms.

Since both Z_{nm} and F_{nm} are known, it is possible to solve equation II-28 for I_m. Substitution of I_m into II-11 directly produces the antenna current distribution, from which the feedpoint impedance can be obtained. However, since II-28 represents an independent set of algebraic equations, the solution is obtained most readily by matrix methods. In addition, both Z_{nm} and I_m are complex quantities. Thus the following matrix definitions:

$$\left[Z_{nm}\right] \triangleq \left[R_{nm}\right] + j\left[X_{nm}\right] \triangleq \begin{bmatrix} Z_{11} & Z_{12} & Z_{13} & \cdots & Z_{1m} \\ Z_{21} & Z_{22} & Z_{23} & \cdots & Z_{2m} \\ Z_{31} & Z_{32} & Z_{33} & \cdots & Z_{3m} \\ \vdots & & & & \\ Z_{n1} & Z_{n2} & Z_{n3} & \cdots & Z_{nm} \end{bmatrix} \tag{II-29a}$$

$$\left[R_{nm}\right] \triangleq \begin{bmatrix} \mathrm{Re}(Z_{11}) & \mathrm{Re}(Z_{12}) & \mathrm{Re}(Z_{13}) & \cdots & \mathrm{Re}(Z_{1m}) \\ \mathrm{Re}(Z_{21}) & \mathrm{Re}(Z_{22}) & \mathrm{Re}(Z_{23}) & \cdots & \mathrm{Re}(Z_{2m}) \\ \mathrm{Re}(Z_{31}) & \mathrm{Re}(Z_{32}) & \mathrm{Re}(Z_{33}) & \cdots & \mathrm{Re}(Z_{3m}) \\ \vdots & & & & \\ \mathrm{Re}(Z_{n1}) & \mathrm{Re}(Z_{n2}) & \mathrm{Re}(Z_{n3}) & \cdots & \mathrm{Re}(Z_{nm}) \end{bmatrix} \tag{II-29b}$$

$$[X_{nm}] \triangleq \begin{bmatrix} \mathrm{Im}(Z_{11}) & \mathrm{Im}(Z_{12}) & \mathrm{Im}(Z_{13}) & \cdots & \mathrm{Im}(Z_{1m}) \\ \mathrm{Im}(Z_{21}) & \mathrm{Im}(Z_{22}) & \mathrm{Im}(Z_{23}) & \cdots & \mathrm{Im}(Z_{2m}) \\ \mathrm{Im}(Z_{31}) & \mathrm{Im}(Z_{32}) & \mathrm{Im}(Z_{33}) & \cdots & \mathrm{Im}(Z_{3m}) \\ \vdots & & & & \\ \mathrm{Im}(Z_{n1}) & \mathrm{Im}(Z_{n2}) & \mathrm{Im}(Z_{n3}) & \cdots & \mathrm{Im}(Z_{nm}) \end{bmatrix} \tag{II-29c}$$

$$[F_{nm}] \triangleq \begin{bmatrix} F_{11} & F_{12} & F_{13} & \cdots & F_{1m} \\ F_{21} & F_{22} & F_{23} & \cdots & F_{2m} \\ F_{31} & F_{32} & F_{33} & \cdots & F_{3m} \\ \vdots & & & & \\ F_{n1} & F_{n2} & F_{n3} & \cdots & F_{nm} \end{bmatrix} \tag{II-29d}$$

$$[I_m] \triangleq [I_m^r] + j[I_m^i] \triangleq \begin{bmatrix} I_1 \\ I_2 \\ I_3 \\ \vdots \\ I_m \end{bmatrix} \tag{II-29e}$$

$$\left[I_m^r\right] \triangleq \begin{bmatrix} \mathrm{Re}(I_1) \\ \mathrm{Re}(I_2) \\ \mathrm{Re}(I_3) \\ \vdots \\ \mathrm{Re}(I_m) \end{bmatrix} \qquad \left[I_m^i\right] \triangleq \begin{bmatrix} \mathrm{Im}(I_1) \\ \mathrm{Im}(I_2) \\ \mathrm{Im}(I_3) \\ \vdots \\ \mathrm{Im}(I_m) \end{bmatrix} \tag{II-29f}$$

$$\left[V_n\right] \triangleq V_o \begin{bmatrix} +1 \\ 0 \\ -1 \\ 0 \\ \vdots \\ \sin\left(\frac{n\pi}{2}\right) \end{bmatrix} \tag{II-29g}$$

Equation II-28 then becomes, in matrix notation:

$$\left(\left[R_{nm}\right] + j\left[X_{nm}\right]\right)\left(\left[I_m^r\right] + j\left[I_m^i\right]\right) + \left[F_{nm}\right]\left(\left[I_m^r\right] + j\left[I_m^i\right]\right) = \left[V_n\right] \tag{II-30}$$

Equating the real and imaginary parts, equation II-30 becomes:

$$\left(\left[R_{nm}\right] + \left[F_{nm}\right]\right)\left[I_m^r\right] - \left[X_{nm}\right]\left[I_m^i\right] = \left[V_n\right] \tag{II-31a}$$

$$\left[X_{nm}\right]\left[I_m^r\right] + \left(\left[R_{nm}\right] + \left[F_{nm}\right]\right)\left[I_m^i\right] = 0 \tag{II-31b}$$

Solution of these two matrix equations yields, finally:

$$\left[I_m^i\right] = \left(\left(\left[R_{nm}\right] + \left[F_{nm}\right]\right)\left[X_{nm}\right]^{-1}\left(\left[R_{nm}\right] + \left[F_{nm}\right]\right) + \left[X_{nm}\right]\right)^{-1} \left[V_n\right] \tag{II-32a}$$

and

$$\left[I_m^r\right] = - \left[X_{nm}\right]\left(\left[R_{nm}\right] + \left[F_{nm}\right]\right)\left[I_m^i\right] \tag{II-32b}$$

Solution of equations II-32a and II-32b yields I_m which is then substituted into equation II-11. Since the current distribution is then known, all the electrical properties of the antenna can be simply calculated. (cf. Section II-C). Hence, the matrix method outlined above has completely solved the problem of a linear antenna with loading.

However, since the accuracy of the solution depends upon the convergence of the series expansion of the current distribution II-11, it is necessary to investigate the convergence properties of the series.

1. Convergence of Series II-11 when $Z_o = 0$: This special case will be examined first because it gives the convergence of the current expansion in the matrix method solution of the unloaded antenna problem, a class of problem which is also of considerable interest. It also reveals properties of the convergence when $Z_o \neq 0$. In order to investigate the convergence, an approximate expression for the coefficients in the current series will be derived. From Appendix I, equation A-23:

$$X_{nn} \cong 15 \frac{(n^2 - s^2)}{s} \pi \log \frac{a^2 \pi^2 \left|n^2 - s^2\right|}{16h^2} \tag{II-33}$$

where s is the length of the antenna in half-wavelengths and $s \neq n$. Evaluation of the other matrix elements reveals that, for very thin antennas, $X_{nn} \gg X_{nm}$, $X_{nn} \gg R_{nm}$, and $X_{nn} \gg R_{nn}$. Consequently equation II-32a becomes:

$$\left[I_n^i\right] \cong \left[X_{nn}\right]^{-1} \left[V_n\right] \tag{II-34}$$

where $\left[X_{nn}\right]$ is a diagonal matrix. But when $\left[X_{nn}\right]$ is diagonal, the nth term of $\left[X_{nn}\right]^{-1}$ is $1/X_{nn}$. Then the matrix equation II-34 reduces to the algebraic equation which will be used to examine the convergence of the reactive terms of the current series:

$$I_n^i \cong \frac{sV_n}{15(n^2 - s^2)\pi \log \frac{a^2\pi^2\left|n^2 - s^2\right|}{16h^2}} \qquad n \neq s \tag{II-35}$$

Table 2 provides a comparison of the actual value of I_n^i computed from equation II-32a and the approximate value of I_n^i computed from equation II-35.

n	I_n^i (calculated from equation II-32a)	I_n^i (calculated from equation II-35)
3	$+ 3.516 \times 10^{-4}$	$+ 3.348 \times 10^{-4}$
5	$- 0.796 \times 10^{-4}$	$- 0.845 \times 10^{-4}$
7	$+ 0.432 \times 10^{-4}$	$+ 0.407 \times 10^{-4}$
9	$- 0.229 \times 10^{-4}$	$- 0.244 \times 10^{-4}$
11	$+ 0.174 \times 10^{-4}$	$+ 0.163 \times 10^{-4}$
13	$- 0.101 \times 10^{-4}$	$- 0.118 \times 10^{-4}$
15	$+ 0.095 \times 10^{-4}$	$+ 0.089 \times 10^{-4}$
17	$- 0.065 \times 10^{-4}$	$- 0.070 \times 10^{-4}$
19	$+ 0.060 \times 10^{-4}$	$+ 0.056 \times 10^{-4}$

TABLE 2. EVALUATION OF EQUATION II-35 AS A CONVERGENCE APPROXIMATION, FOR THE CURRENT COEFFICIENTS

It is apparent that equation II-35 provides a good approximation to the actual current terms and hence is a good indication of the convergence. Except for the logarithmic factor, I_n^i converges as $1/(n^2 - s^2)$ or $1/n^2$ for the higher-order terms when $s^2 \ll n^2$. For thin antennas, the logarithmic factor in equation II-35 has a diverging effect on the convergence when n is of the order of 1,000,000. However, for such large values of n, the approximations made at the beginning of Section II-B are no longer valid. The divergence, then, has no physical significance.

From equation II-32b it can be shown that

$$I_n^r \cong - \frac{sR_{n1} I_1^i}{15(n^2 - s^2)\pi \log \frac{a^2\pi^2|n^2 - s^2|}{16h^2}} \qquad n \neq s \qquad \text{(II-36)}$$

which converges even faster than I_n^i since R_{n1} decreases continuously as n increases. These properties of the convergence of the current series for the unloaded antenna can be verified by inspection of the values of I_n^r and I_n^i tabulated in Appendix III for $Z_o = 0$ and $s = 2$.

2. Convergence of Series II-11 when $Z_o \neq 0$: X_{nn} becomes arbitrarily large as n increases, and eventually becomes much larger than Z_o. It is therefore evident from equations II-32a and II-32b that as n becomes large (but $n << 1,000,000$) both I_n^i and I_n^r eventually converge in the same fashion as equations II-35 and II-36, respectively, for the unloaded antenna.

Convergence of the initial coefficients of the current expansion depends greatly upon the size and distribution of the loading elements and the distribution of the feedpoints. In the case of the full-wave, center-fed antenna considered in this thesis, the absolute convergence of I_n^r is examined in figure 11 for different values of Z_o. The magnitude of the real coefficients, normalized to I_1^r, is plotted against n. The resulting points follow a $1/n^2$-dependence almost exactly. For comparison, a curve of K/n is also plotted, the limiting value of absolute convergence. K was chosen to make the two curves match at $n = 7$.

The imaginary current coefficients, however, could not be examined so simply, since they neither followed a smooth curve, nor

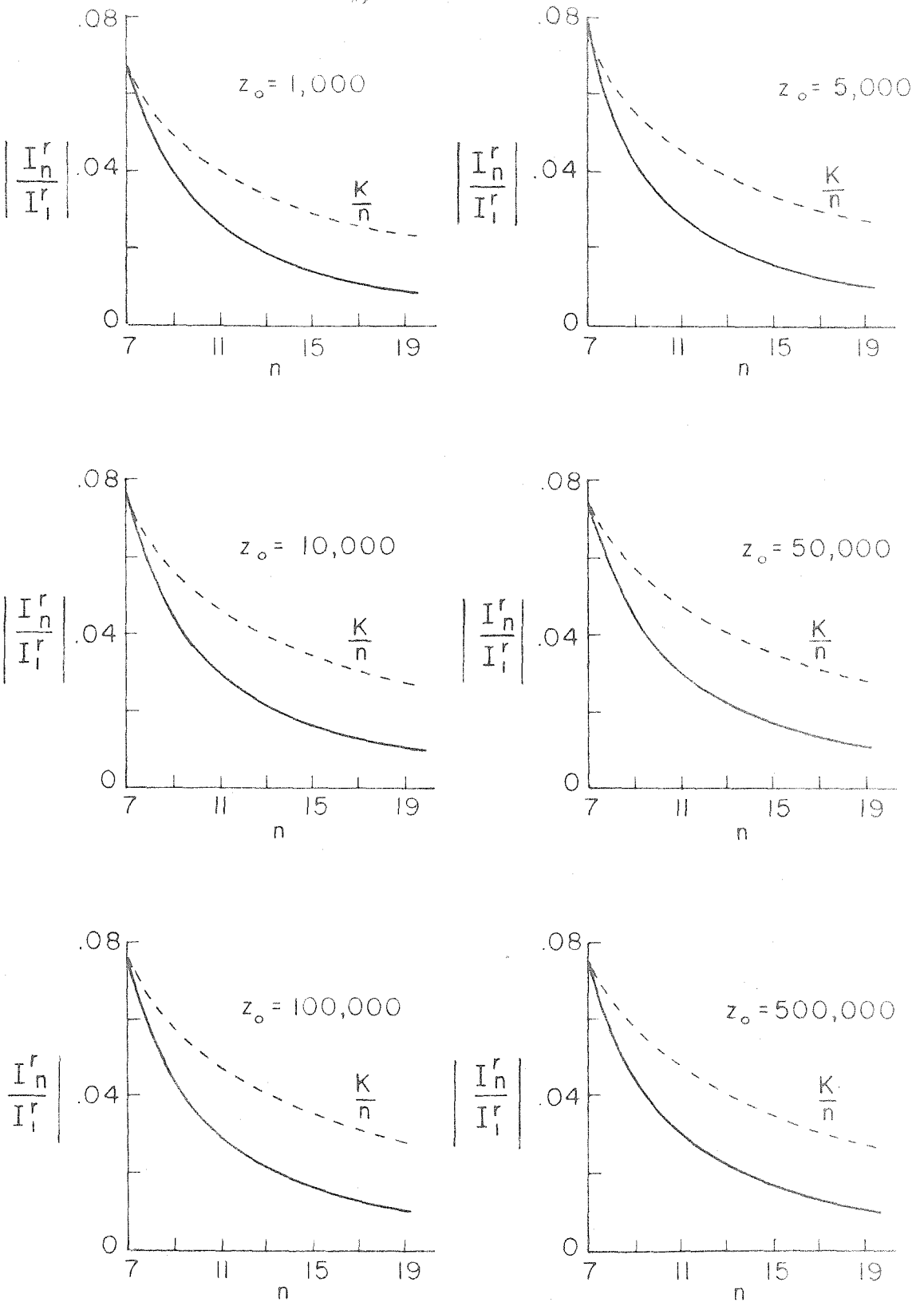

FIGURE 11. CONVERGENCE OF THE REAL CURRENT COEFFICIENTS IN EQUATION II-11 FOR DIFFERENT VALUES OF Z_o.

was $\left|I_n^i\right|$ always larger than $\left|I_{n+2}^i\right|$ for the range of n considered ($1 \leqslant n \leqslant 19$). Consequently, it was not possible to examine the actual convergence of the I_n^i without increasing the number of terms. It could be seen, however, that the fluctuations of the coefficients from the $1/n^2$-dependence were decreasing, and the series would ultimately converge as n became larger (see above). The first few leading terms were also several hundred times larger than the remaining terms.

C. Description of Results of the Matrix Solution

Solution of equations II-32a and II-32b was accomplished with the Burroughs Datatron 205 digital computer, manufactured by the Electro-Data Division of the Burroughs Corporation. Solution of the two matrix equations was greatly facilitated by the semi-automatic coding scheme for matrix operations (references 26 and 27). This scheme is ideally suited for the solution of many thin linear antenna problems by the matrix method developed by this author. A large number of terms in the current distribution expansion can be handled with extreme simplicity, resulting in increased accuracy of the solution. The computer program is found in Appendix II. For the full-wave (i.e., $s = 2$), loaded antenna considered in this section, ten terms were used in the expansion.

For the antenna of figure 10 and $s = 2$, equation II-28 was solved for $\left[I_m\right]$. The coefficients I_m were then substituted into equation II-11, directly producing the current distribution. The real and imaginary current distributions are plotted in figures 12 to 21 for different values of the loading impedance Z_o. As Z_o becomes very large, both

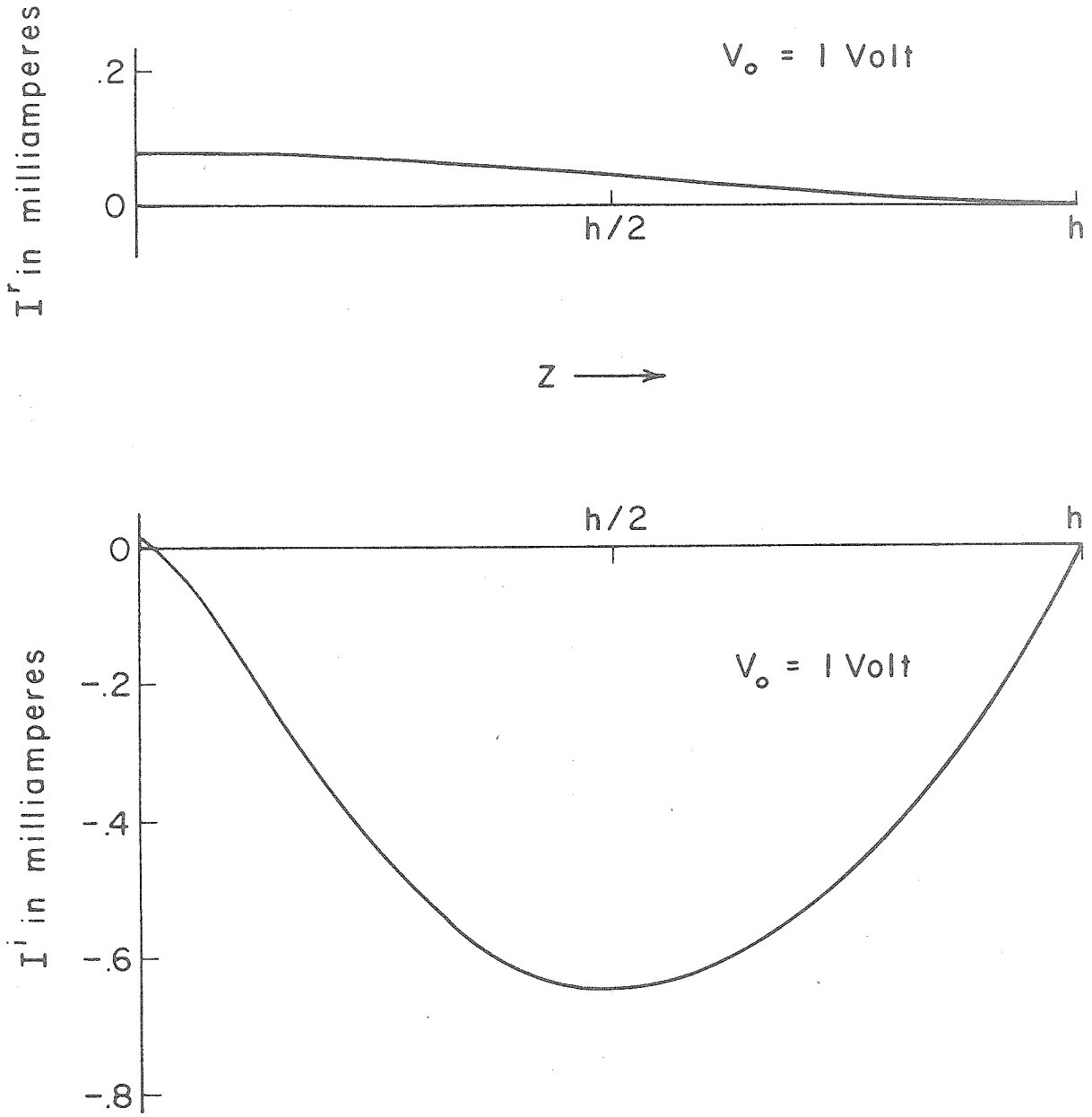

FIGURE 12. REAL AND IMAGINARY CURRENT DISTRIBUTIONS ON FULL-WAVE ANTENNA WITHOUT LOADING IMPEDANCES.

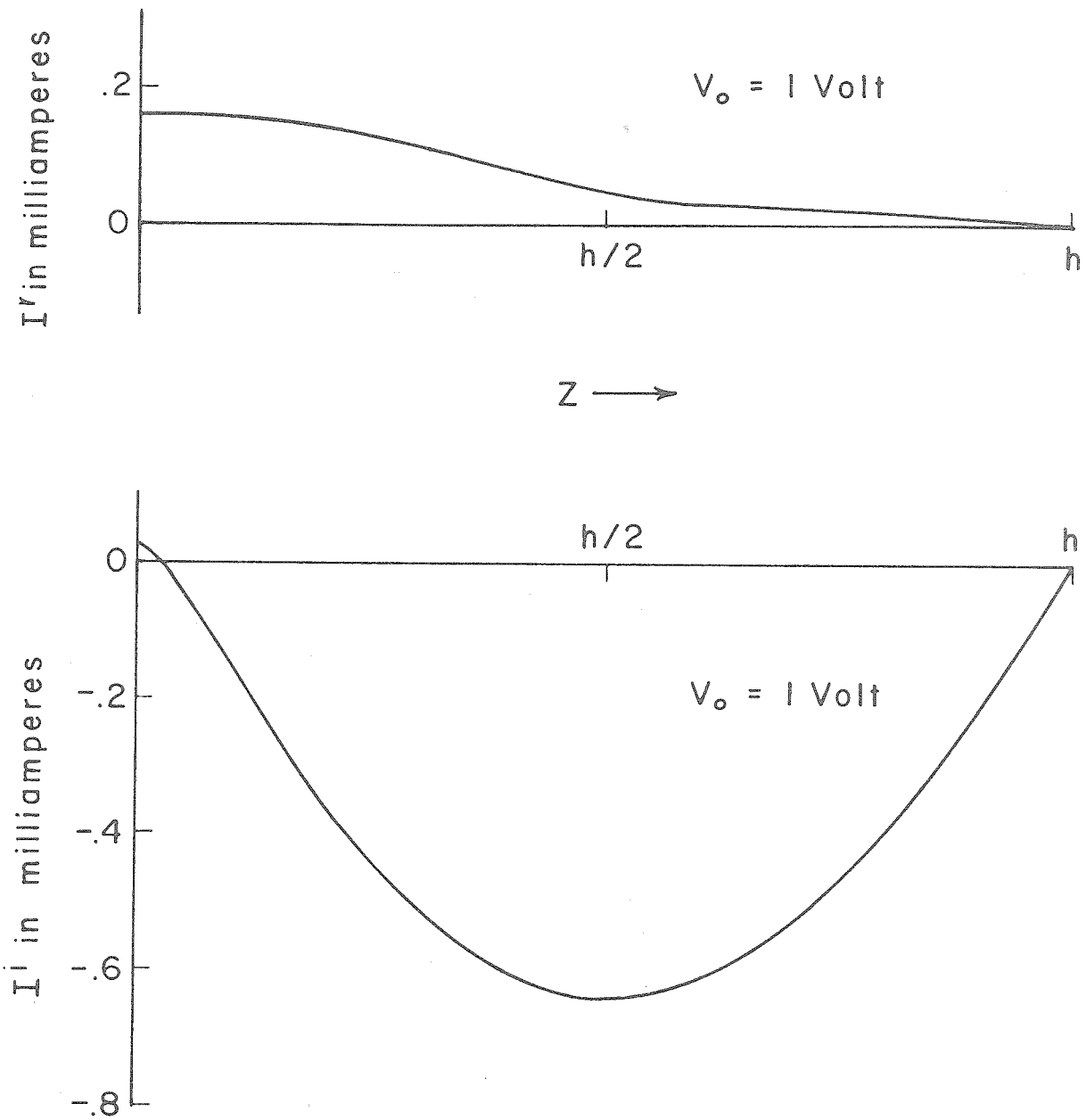

FIGURE 13. REAL AND IMAGINARY CURRENT DISTRIBUTIONS ON FULL-WAVE ANTENNA WITH LOADING IMPEDANCES Z_o = 100 OHMS LOCATED AT $\pm$ H/2 .

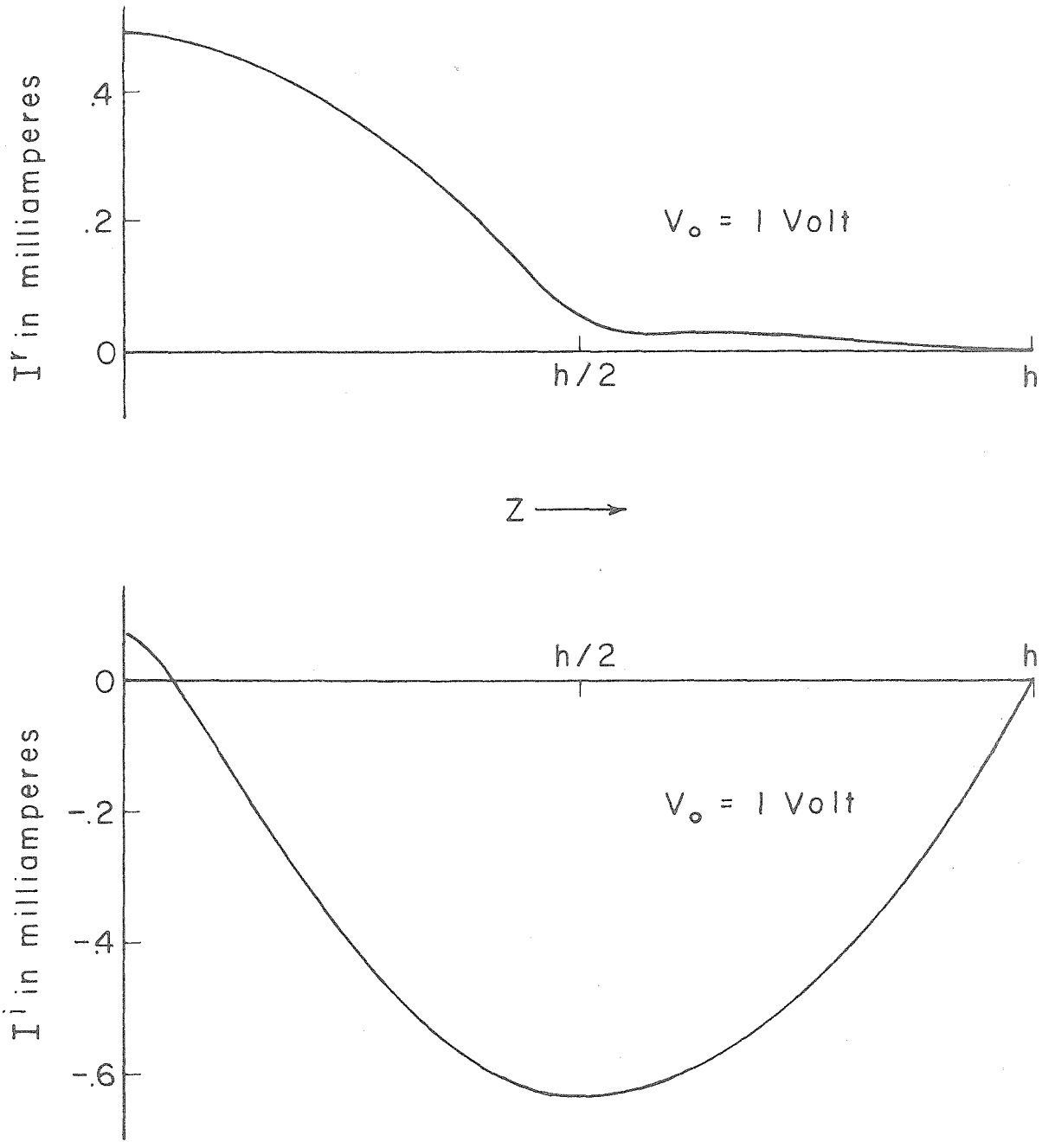

FIGURE 14. REAL AND IMAGINARY CURRENT DISTRIBUTIONS ON FULL-WAVE ANTENNA WITH LOADING IMPEDANCES Z_o = 500 OHMS LOCATED AT $\pm$ H/2 .

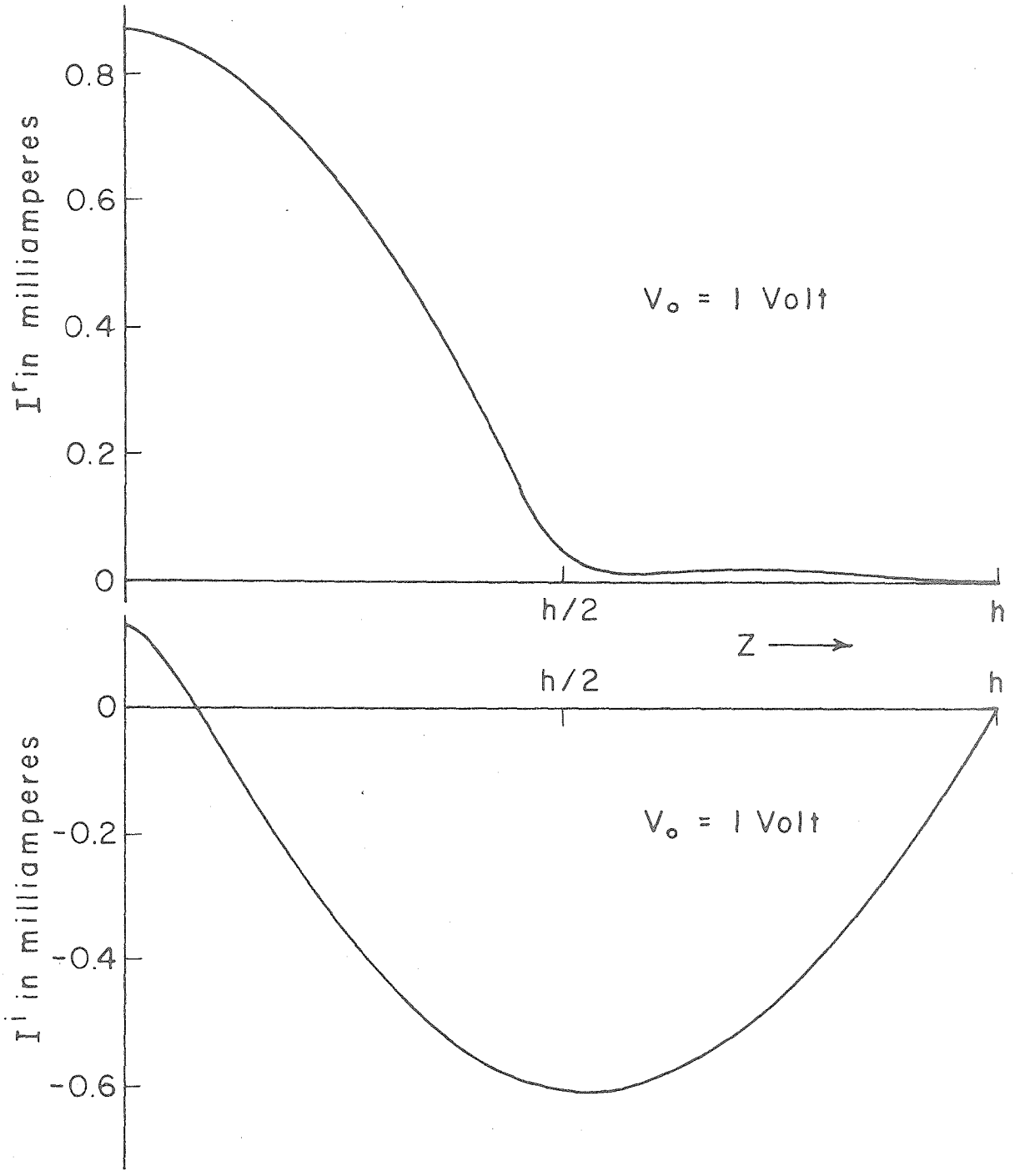

FIGURE 15. REAL AND IMAGINARY CURRENT DISTRIBUTIONS ON FULL-WAVE ANTENNA WITH LOADING IMPEDANCES Z_o = 1,000 OHMS LOCATED AT $\pm$ H/2 .

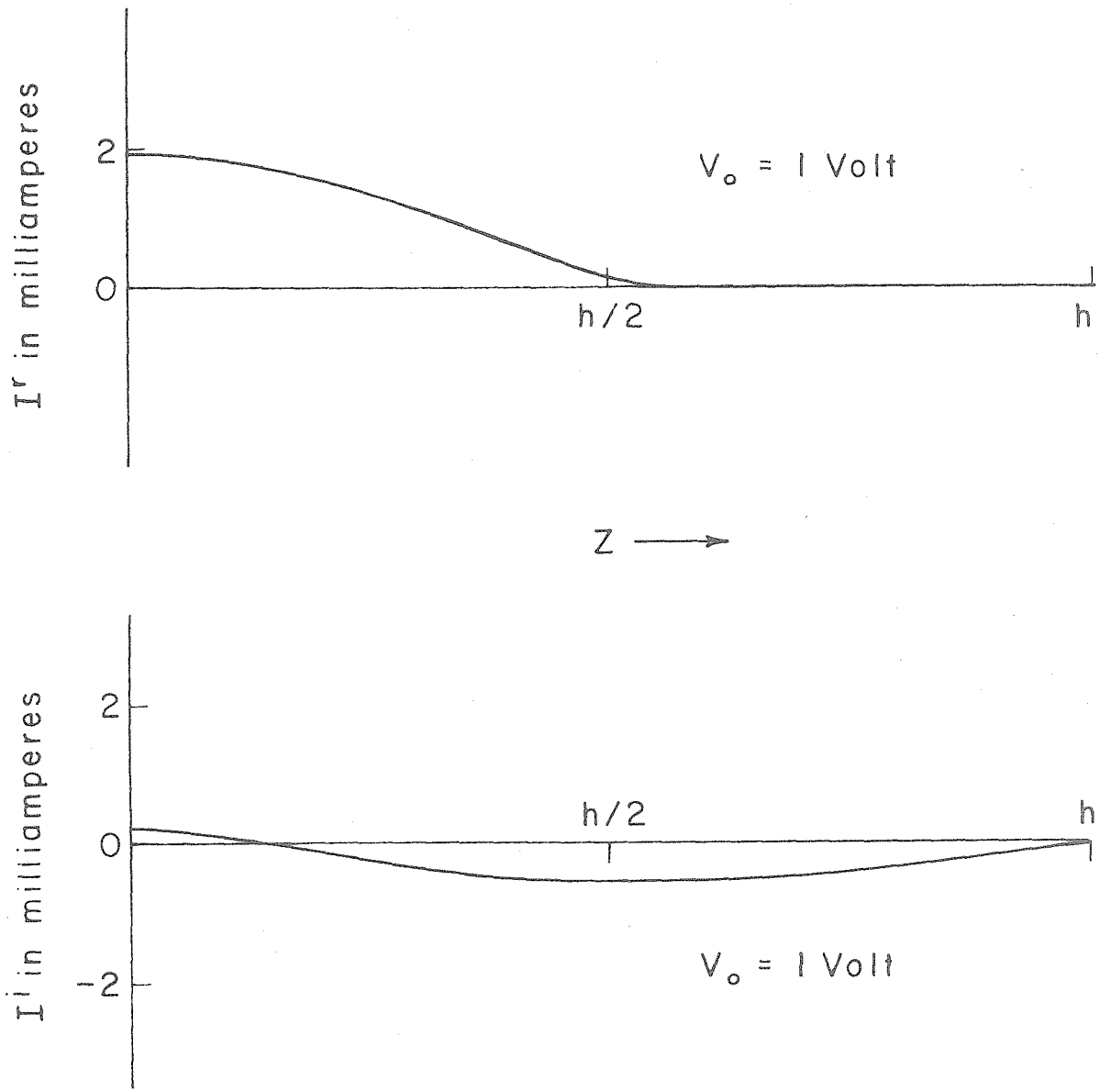

FIGURE 16. REAL AND IMAGINARY CURRENT DISTRIBUTIONS ON FULL-WAVE ANTENNA WITH LOADING IMPEDANCES Z_o = 2,500 OHMS LOCATED AT $\pm$ H/2 .

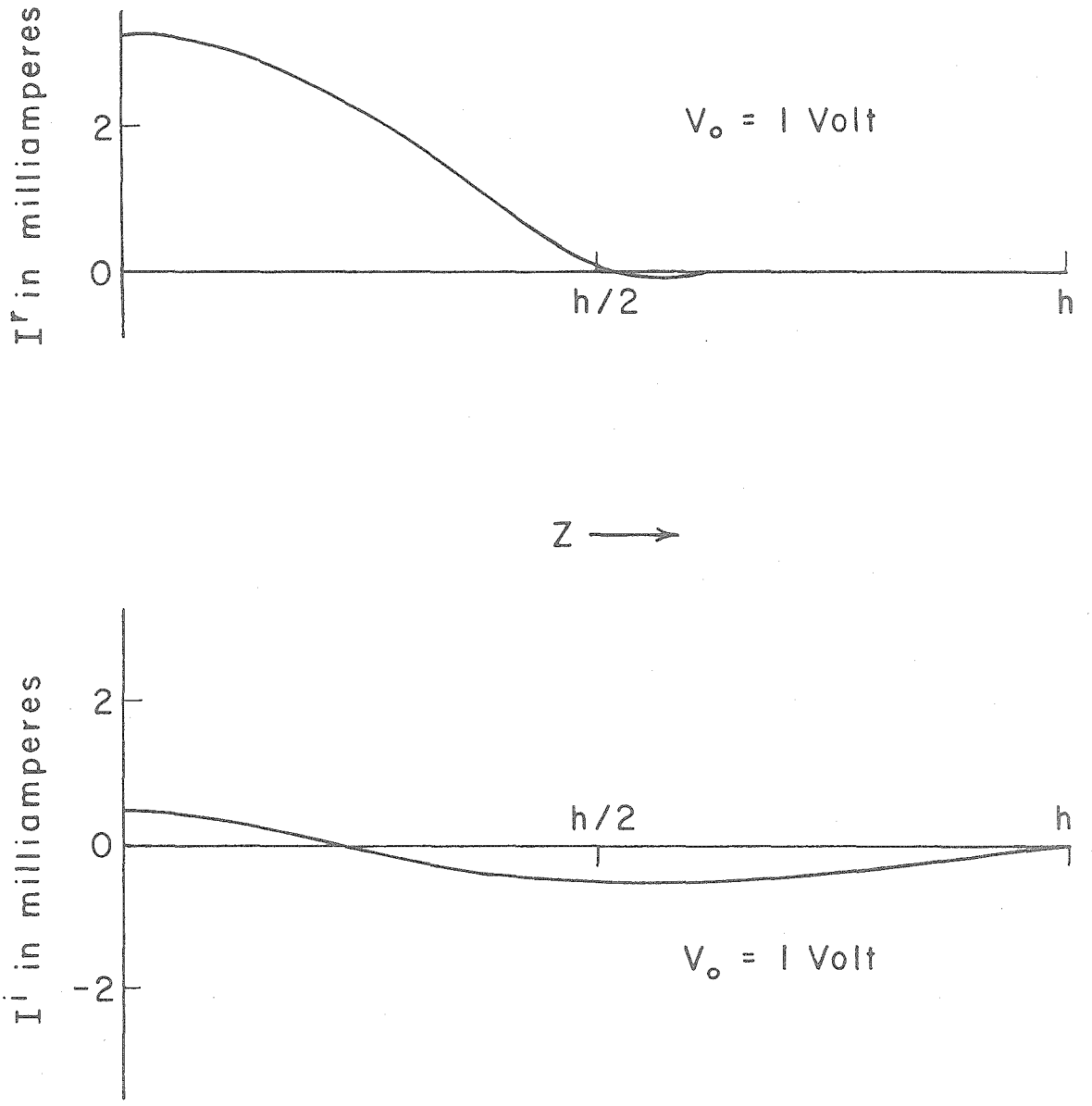

FIGURE 17. REAL AND IMAGINARY CURRENT DISTRIBUTIONS ON FULL-WAVE ANTENNA WITH LOADING IMPEDANCES Z_o = 5,000 OHMS LOCATED AT $\pm$ H/2 .

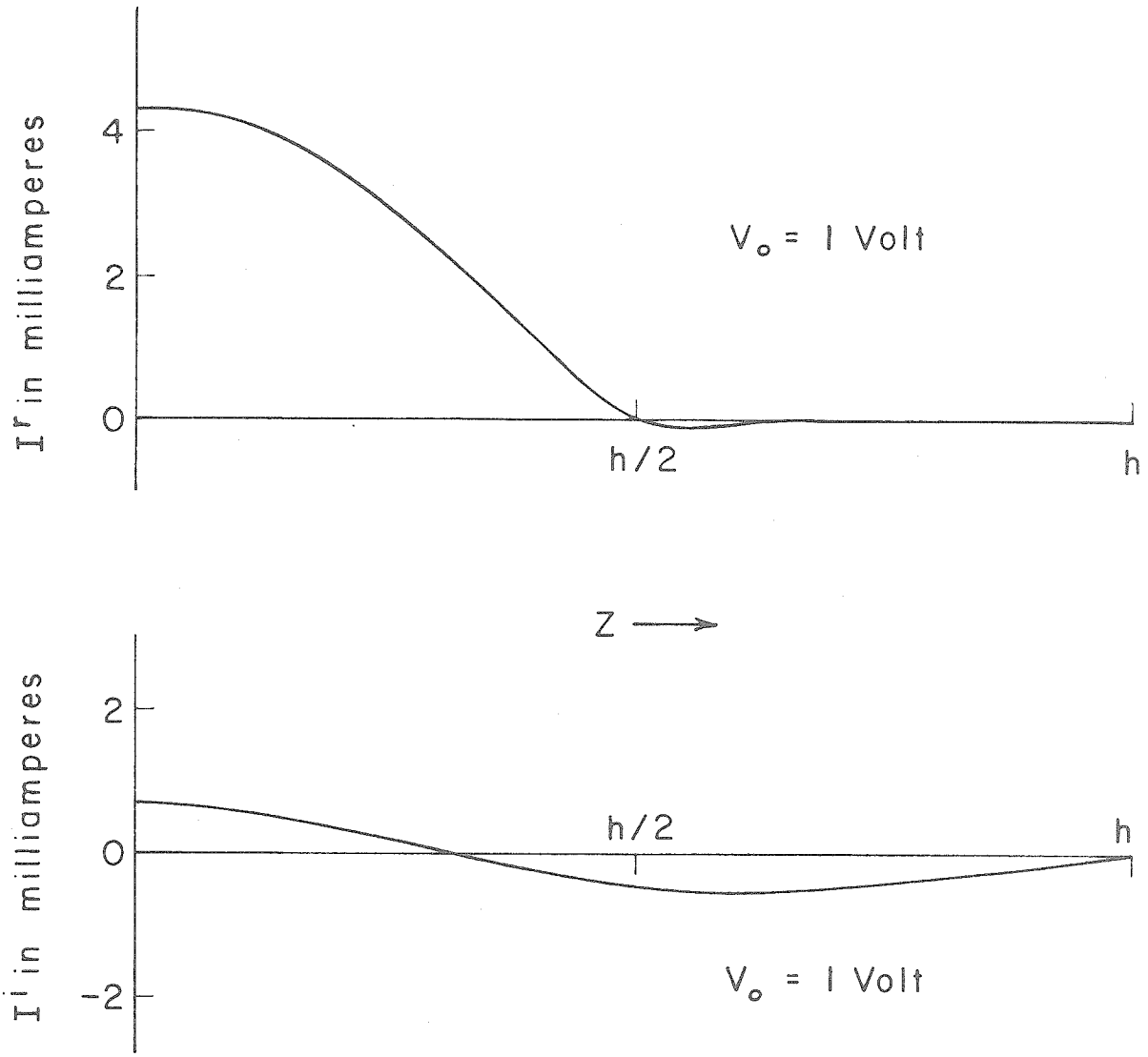

FIGURE 18. REAL AND IMAGINARY CURRENT DISTRIBUTIONS ON FULL-WAVE ANTENNA WITH LOADING IMPEDANCES Z_o = 7,500 OHMS LOCATED AT $\pm$ H/2 .

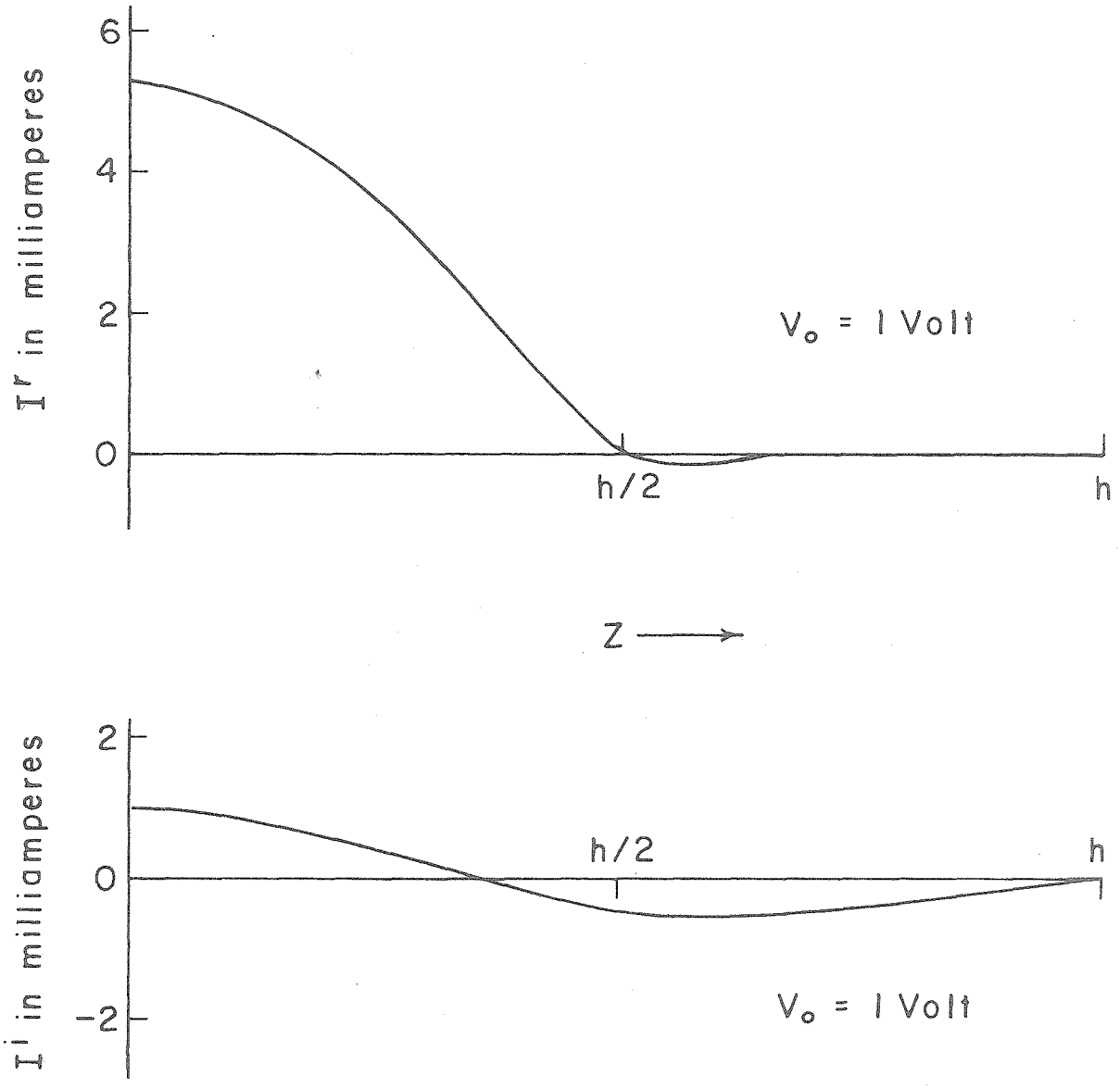

FIGURE 19. REAL AND IMAGINARY CURRENT DISTRIBUTIONS ON FULL-WAVE ANTENNA WITH LOADING IMPEDANCES Z_o = 10,000 OHMS LOCATED AT $\pm$ H/2 .

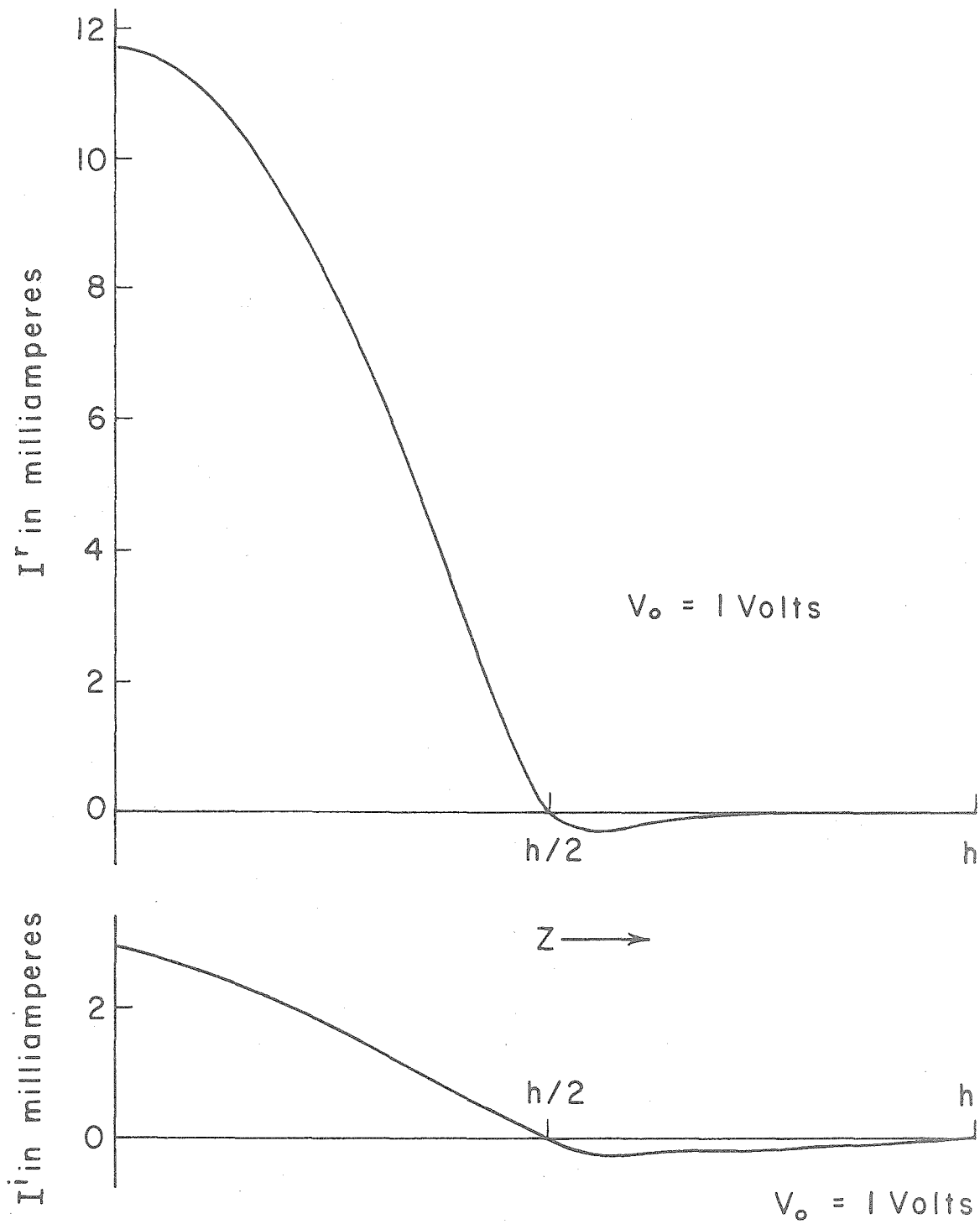

FIGURE 20. REAL AND IMAGINARY CURRENT DISTRIBUTIONS ON FULL-WAVE ANTENNA WITH LOADING IMPEDANCES Z_o = 100,000 OHMS LOCATED AT $\pm$ H/2 .

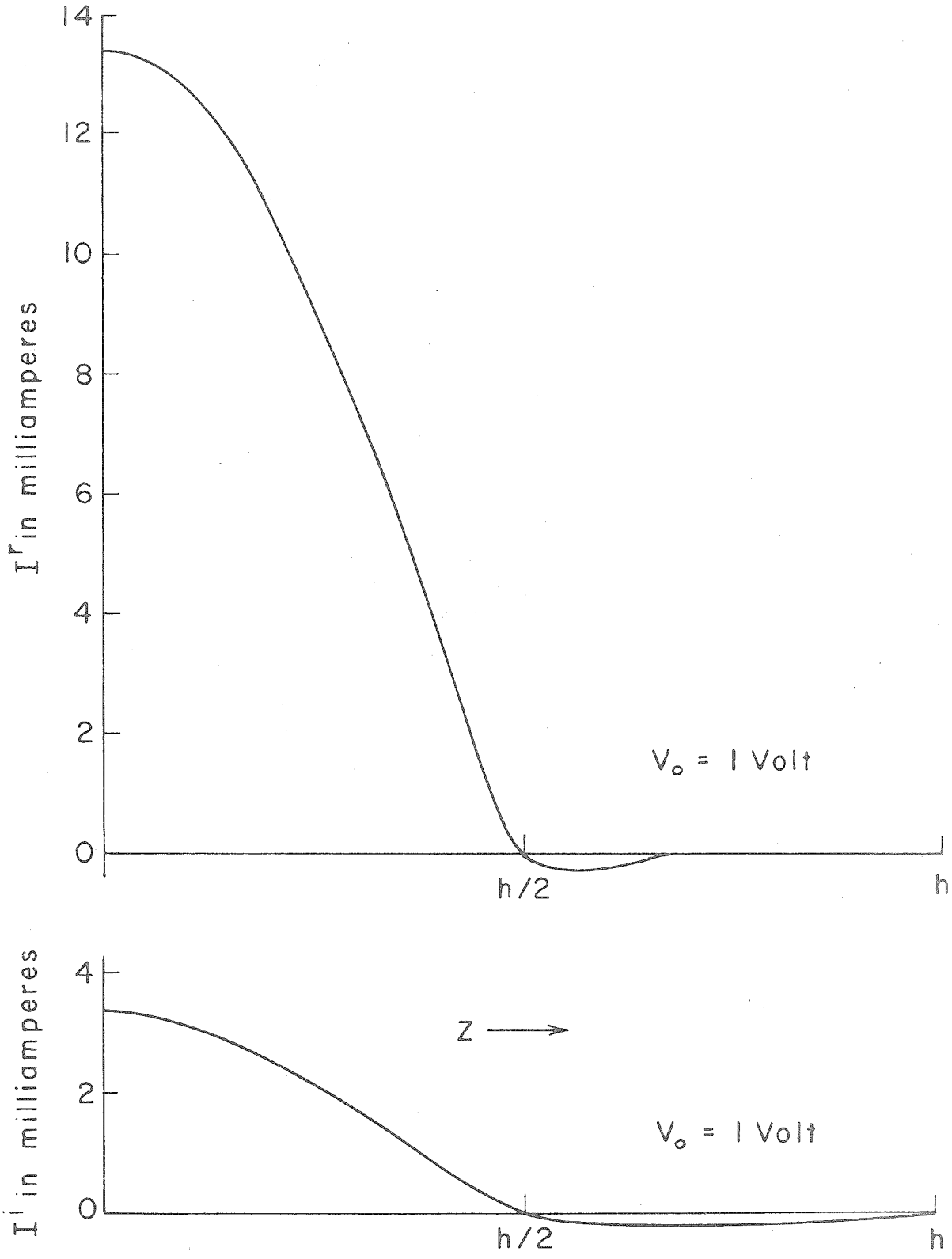

FIGURE 21. REAL AND IMAGINARY CURRENT DISTRIBUTIONS ON FULL-WAVE ANTENNA WITH LOADING IMPEDANCES Z_o = 1,000,000 OHMS LOCATED AT $\pm$ H/2 .

components of the current are forced into the half-wave section between the loading elements, and less of the current flows in the sections beyond the loading elements. Gradually, with increasing Z_o, the full-wave antenna takes on the appearance of a half-wave antenna, and for very large Z_o, there is negligible current beyond the loading elements.

The feedpoint impedance Z_{fp} is

$$Z_{fp} = \frac{V_o}{I(0)} = R_{fp} + j X_{fp} \qquad \text{(II-37)}$$

R_{fp} and X_{fp} are plotted in figure 22 as a function of Z_o. For $Z_o = 0$, Z_{fp} is the feedpoint impedance of a very thin, unloaded, full-wave antenna which is nearly antiresonant, and the current distribution in this case (figure 12) is the corresponding current distribution of an unloaded full-wave antenna. As Z_o becomes large, the effect of the sections beyond the loading elements diminishes. The asymptotic value of the magnitude of Z_{fp} for large Z_o approaches the magnitude of the feedpoint impedance for an unloaded half-wave antenna. However, the sign of the reactance is opposite to that of the half-wave antenna. (This sign change will be discussed below.)

Since the scalar potential difference across the loading elements $V(\pm h/2)$ is of considerable interest in the design of components for a power-line antenna, this voltage is plotted in figure 23 as a function of Z_o for $V_o = 1$ volt.

$$V(\pm h/2) = Z_o I(\pm h/2) \qquad \text{(II-38)}$$

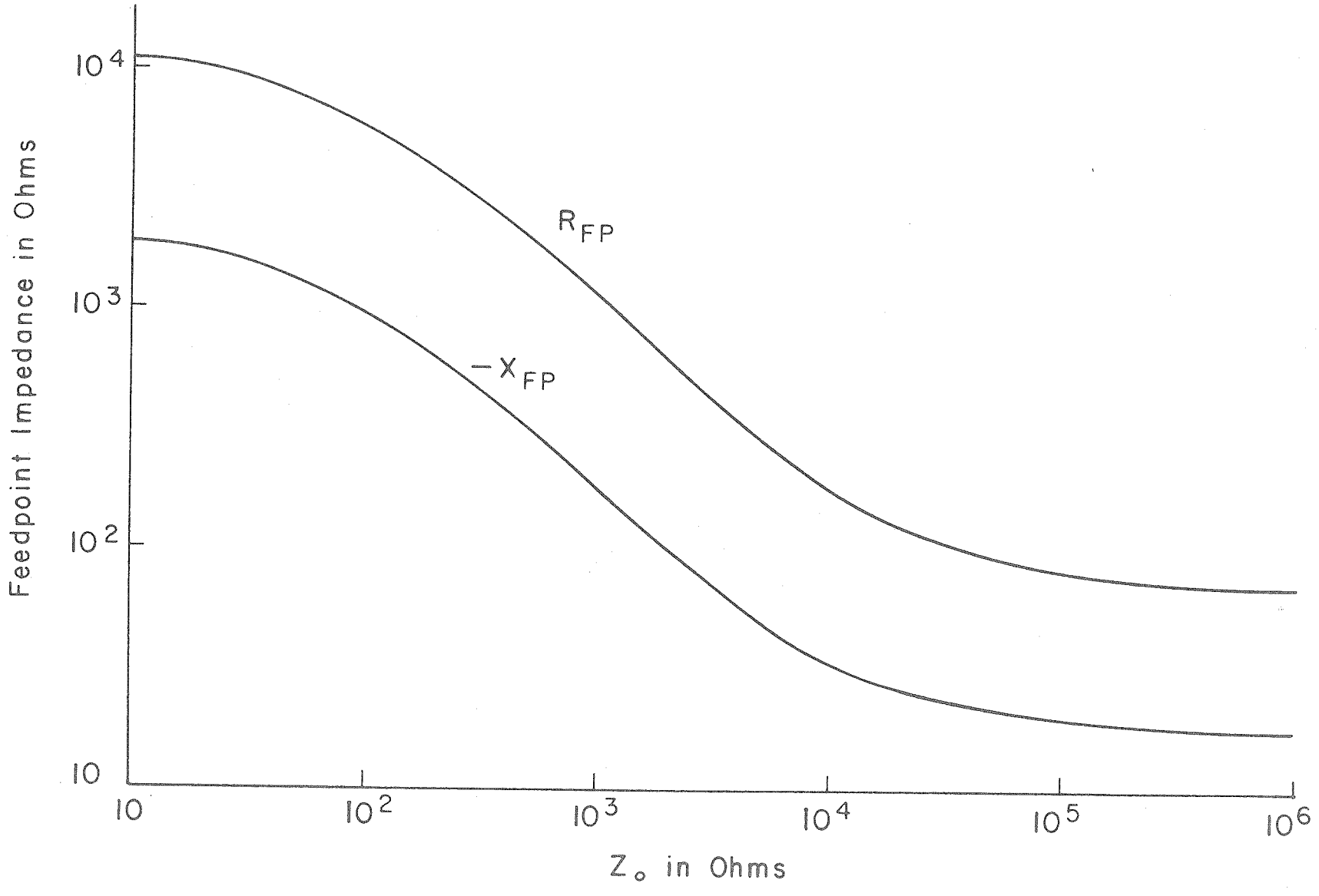

FIGURE 22. FEEDPOINT IMPEDANCE OF FULL-WAVE ANTENNA VS. LOADING IMPEDANCE Z_o.

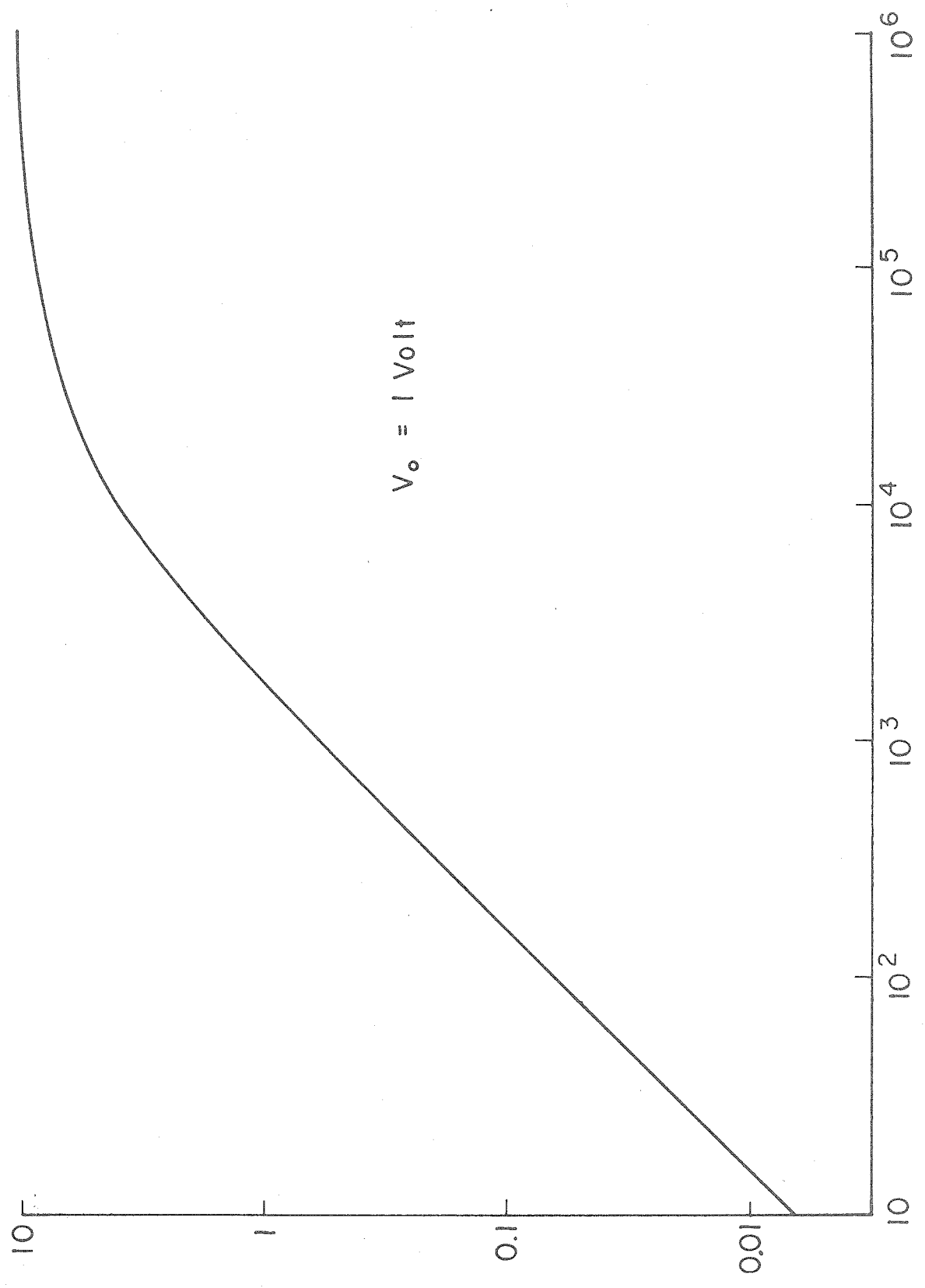

FIGURE 23. VOLTAGE ACROSS LOADING ELEMENTS OF FULL-WAVE ANTENNA VS. LOADING IMPEDANCE Z_o.

This voltage is linearly related to Z_o for small Z_o, and approaches a constant asymptotic value as Z_o becomes large.

An approximate measure of the fraction of the total energy which is coupled beyond the loading elements is plotted in figure 24 as a function of Z_o. This quantity is of considerable interest for power-line antennas since the radio frequency energy which is coupled beyond the line traps must be extremely small. This approximate fraction has been obtained from equation II-20 by assuming that the fields at a point z_o on the surface of the antenna are almost entirely caused by the current $I(z_o)$ because of the factor $1/R_1$ in the integrand. This approximation is valid unless $I(z_o)$ is very small. However, for a first-order approximation

$$E(z_o) = K\left|I(z_o)\right|^2 dz \qquad \text{(II-39)}$$

where $E(z_o)$ is the average energy radiated per second from length dz located at z_o, and K is a constant. Using equation II-39, the ratio of the energy radiated from the sections beyond the loading elements to the total radiated energy can be computed. This fraction is plotted in figure 24.

The amount of power which is dissipated in each loading element is:

$$P(\pm h/2) = Z_o\left|I(\pm h/2)\right|^2 \qquad \text{(II-40)}$$

This power is of considerable interest in the design of the antenna system, since it contributes to a decrease in the efficiency of the antenna. The efficiency of the antenna of figure 10 in free space is

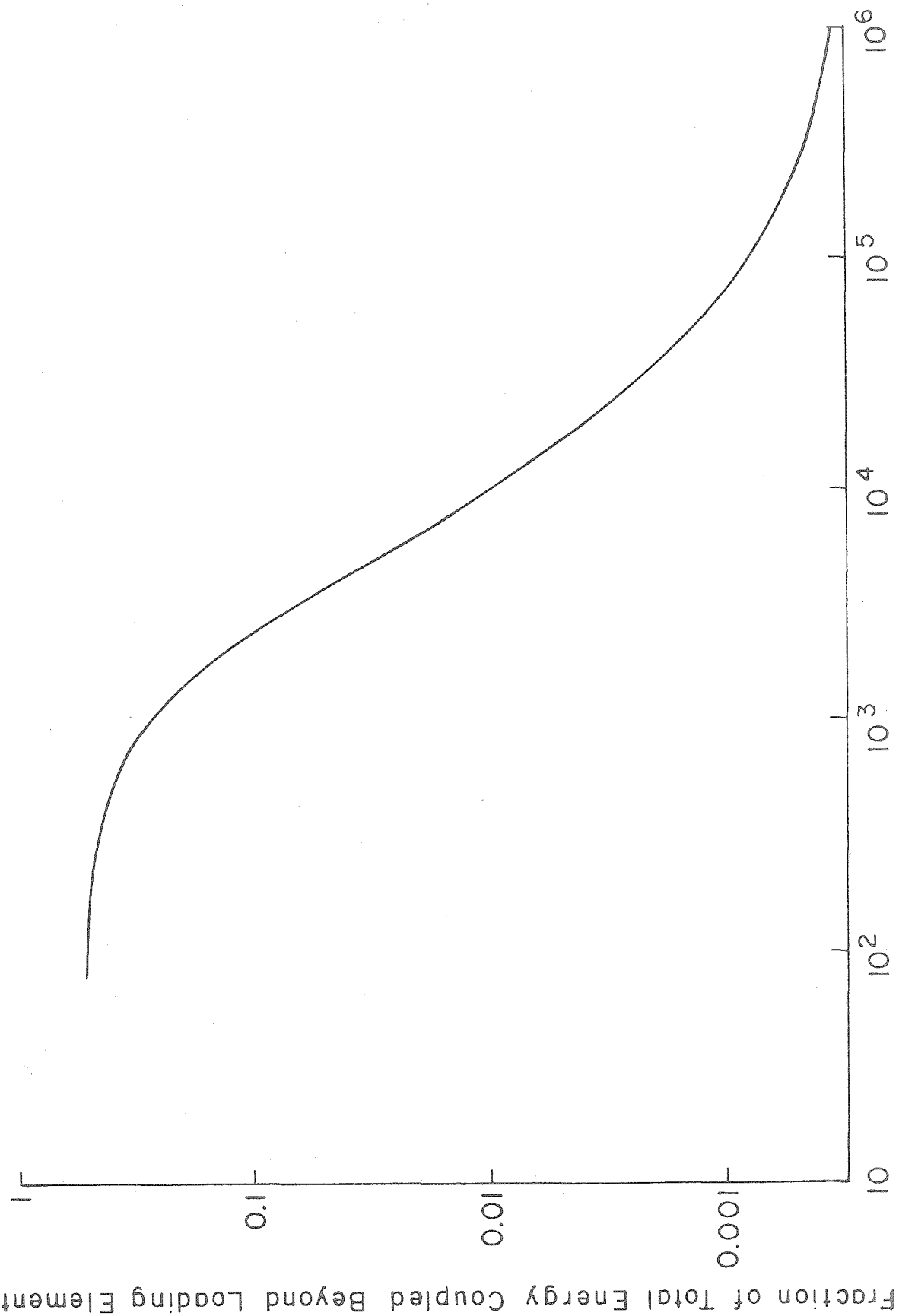

FIGURE 24. FRACTION OF TOTAL ENERGY COUPLED BEYOND LOADING ELEMENTS OF FULL-WAVE ANTENNA VS. Z_o.

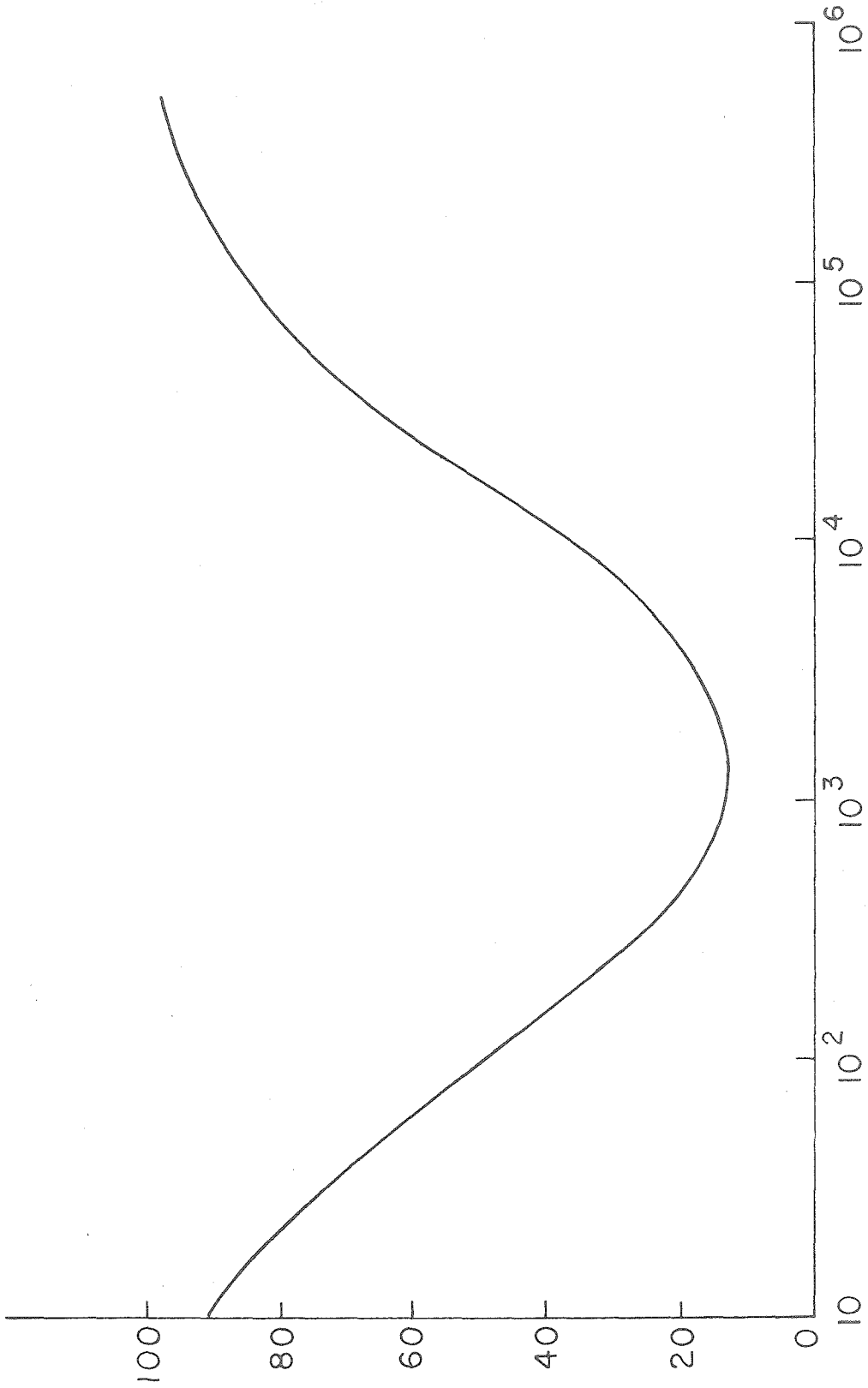

FIGURE 25. EFFICIENCY OF LOADED FULL-WAVE ANTENNA VS. LOADING IMPEDANCE Z_o.

$$\eta = \frac{\text{radiated power}}{\text{input power}} = \frac{V_o I^r(0) - 2 Z_o I(h/2)\, I^*(h/2)}{V_o I^r(0)} \qquad \text{(II-41)}$$

This value of efficiency is plotted in figure 25 as a function of Z_o. It is seen that the efficiency has a minimum in the vicinity of 1,000 ohms. It is apparent from figure 25 that the feedpoint resistance of the antenna represents the actual radiation resistance of the antenna for very large and very small values of Z_o. In the intermediate range, the feedpoint resistance is also determined by the power dissipated in the loading elements.

Having solved for the current distribution, it is a straightforward matter to solve for the free-space radiation pattern. Equation II-11 now becomes:

$$I(z) = \sum_{n\ \text{odd}} \left[I_n^r + j I_n^i \right] \cos \frac{n\pi z}{2h} \qquad \text{(II-42)}$$

From equation 8.7(3) on page 440 in reference 25, the radiation field from a linear antenna with an arbitrary current distribution is:

$$E_{n\theta} = \frac{+j\omega\mu_o}{4\pi} \frac{\sin\theta}{R} e^{-j(\beta_o R - \omega t)} \int_{-h}^{+h} e^{+j\beta_o z \cos\theta} i_n(z)\, dz \qquad \text{(II-43)}$$

Since

$$i_n(z) = \left[I_n^r + j I_n^i \right] \cos \frac{n\pi z}{2h} \qquad \text{(II-44a)}$$

$$E_\theta = \sum_{n\,odd} E_{n\theta} = \frac{\omega\mu_o h}{\pi^2} \frac{e^{-j(\beta_o R - \omega t)}}{R} \left\{ \sin\theta \cos(\pi\cos\theta) \right\}$$

$$\left\{ \sum_{n\,odd} \frac{I_n^r}{n\left[\left(\frac{2}{n}\cos\theta\right)^2 - 1\right]} + j \sum_{n\,odd} \frac{I_n^i}{n\left[\left(\frac{2}{n}\cos\theta\right)^2 - 1\right]} \right\} \qquad \text{(II-44b)}$$

The intensity of radiation at any angle θ is given by the complex Poynting vector

$$S = \frac{1}{2}\sqrt{\frac{\varepsilon_o}{\mu_o}}\, E_\theta \cdot E_\theta^* \qquad \text{(II-45a)}$$

or

$$S = \frac{60}{\pi R^2} \left\{ \sin\theta \cos(\pi\cos\theta) \right\}^2 \left\{ \left[\sum_{n\,odd} \frac{I_n^r}{n\left[\left(\frac{2}{n}\cos\theta\right)^2 - 1\right]} \right]^2 + \left[\sum_{n\,odd} \frac{I_n^i}{n\left[\left(\frac{2}{n}\cos\theta\right)^2 - 1\right]} \right]^2 \right\} \qquad \text{(II-45b)}$$

Using equation II-45b, radiation patterns have been calculated for different values of Z_o. These radiation patterns are plotted in figure 26 for constant values of power into the antenna $\left(P_{in} = V_o \sum_{n\,odd} I_n^r(0) \right)$. It is apparent that although figure 26 is plotted for constant input power, the total radiated power is not the same for each example. This is due to the fact that the amount of power dissipated is also a function of the

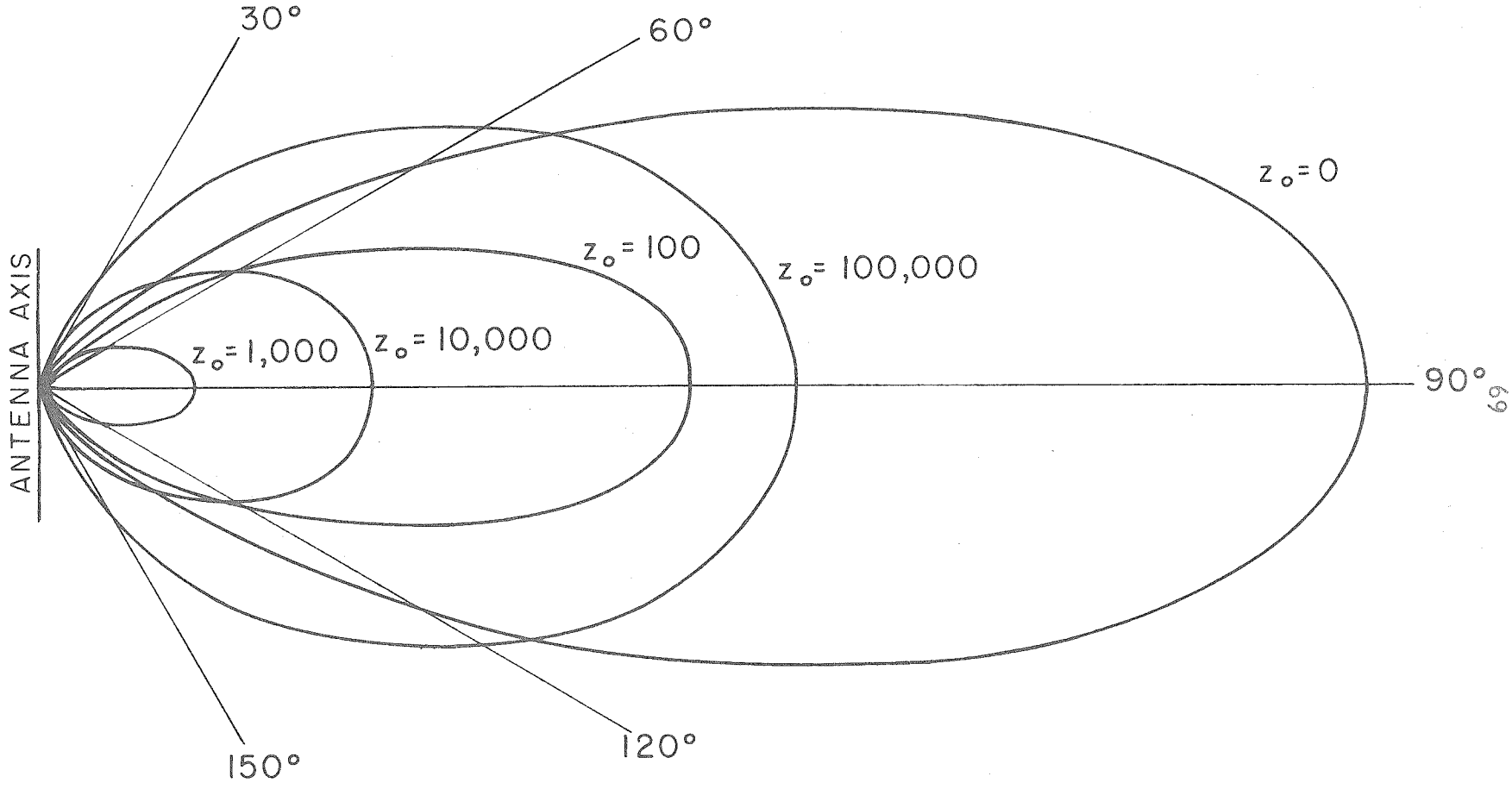

FIGURE 26. FREE-SPACE RADIATION PATTERN FROM LOADED FULL-WAVE ANTENNA FOR DIFFERENT VALUES OF LOADING IMPEDANCE Z_o WITH EQUAL INPUT POWER.

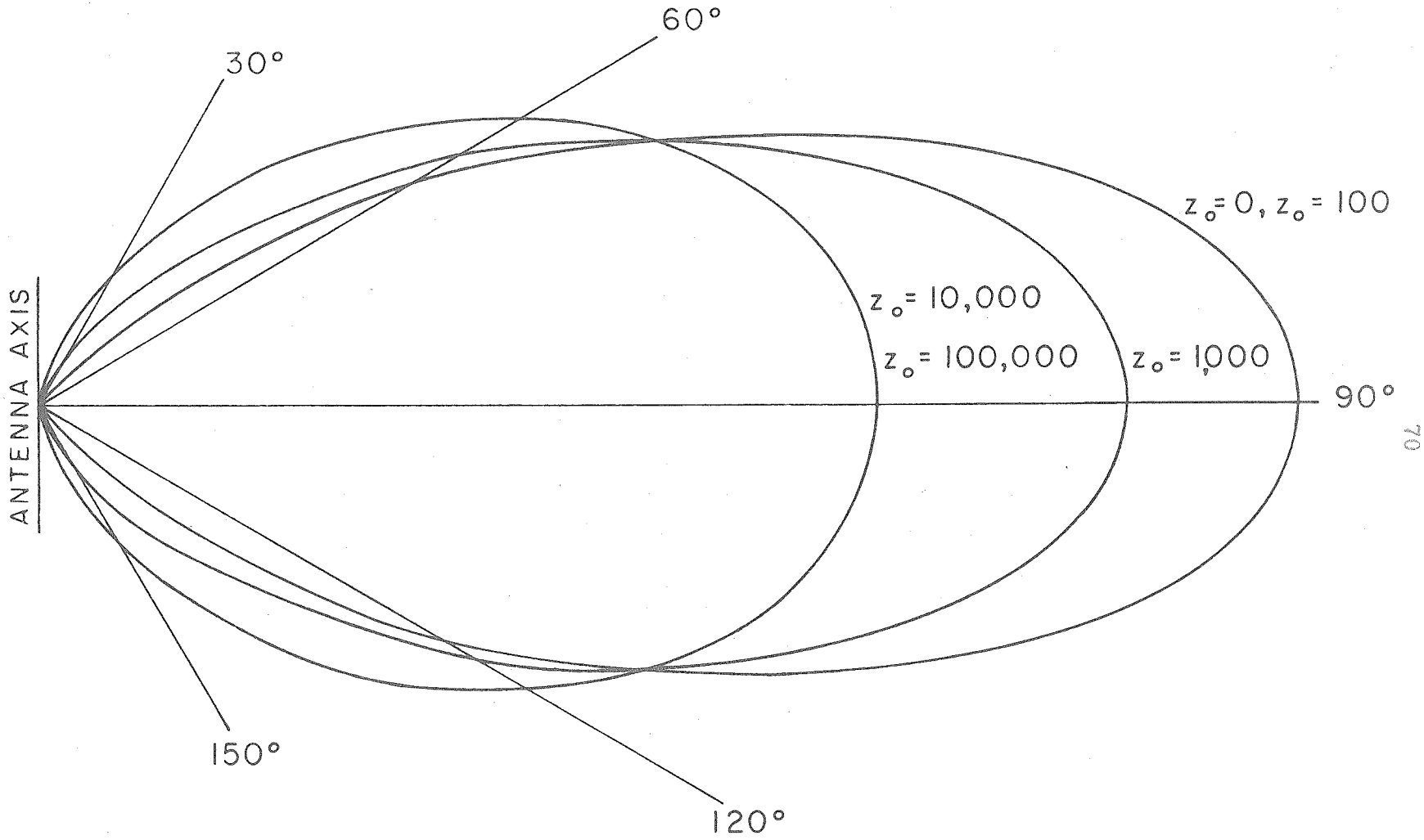

FIGURE 27. FREE-SPACE RADIATION PATTERN FROM LOADED FULL-WAVE ANTENNA FOR DIFFERENT VALUES OF LOADING IMPEDANCE Z_o WITH EQUAL RADIATED POWER.

impedance Z_o (cf. equation II-40). Therefore, the total radiated power for constant input power is minimum near $Z_o = 1,000$ ohms (minimum efficiency). The radiation patterns of figure 26 are normalized in figure 27 for constant values of radiated power. The patterns for large Z_o and small Z_o are similar, respectively, to the radiation patterns of half-wave and full-wave antennas in free space.

In general, it is not possible to compare the matrix method results with results obtained by other theories since the problem of a linear antenna loaded in this manner has not been considered previously in the literature. However, it is possible to compare the results for the unloaded antenna ($Z_o = 0$) and for the antenna loaded with very large Z_o.

The current distribution of figure 12 corresponds to the current distribution of a thin, unloaded, full-wave, center-fed linear antenna. This problem has been solved by King and others. The results of the King solution are plotted in figure 28 along with the current distribution calculated in this thesis. The comparison is not exact, however, since the King curve was calculated for an antenna with $h/a = 10^4$, whereas the antenna considered in this thesis had $h/a = 10^6$. The thinner antenna is nearer antiresonance and therefore the current at $z = 0$ is considerably smaller. When the difference in thinness of the two cases is taken into account, it will be seen that the two results are in agreement.

Tabulation of the feedpoint impedances of the unloaded, full-wave antenna is contained in table 3. Again, data are not available for the

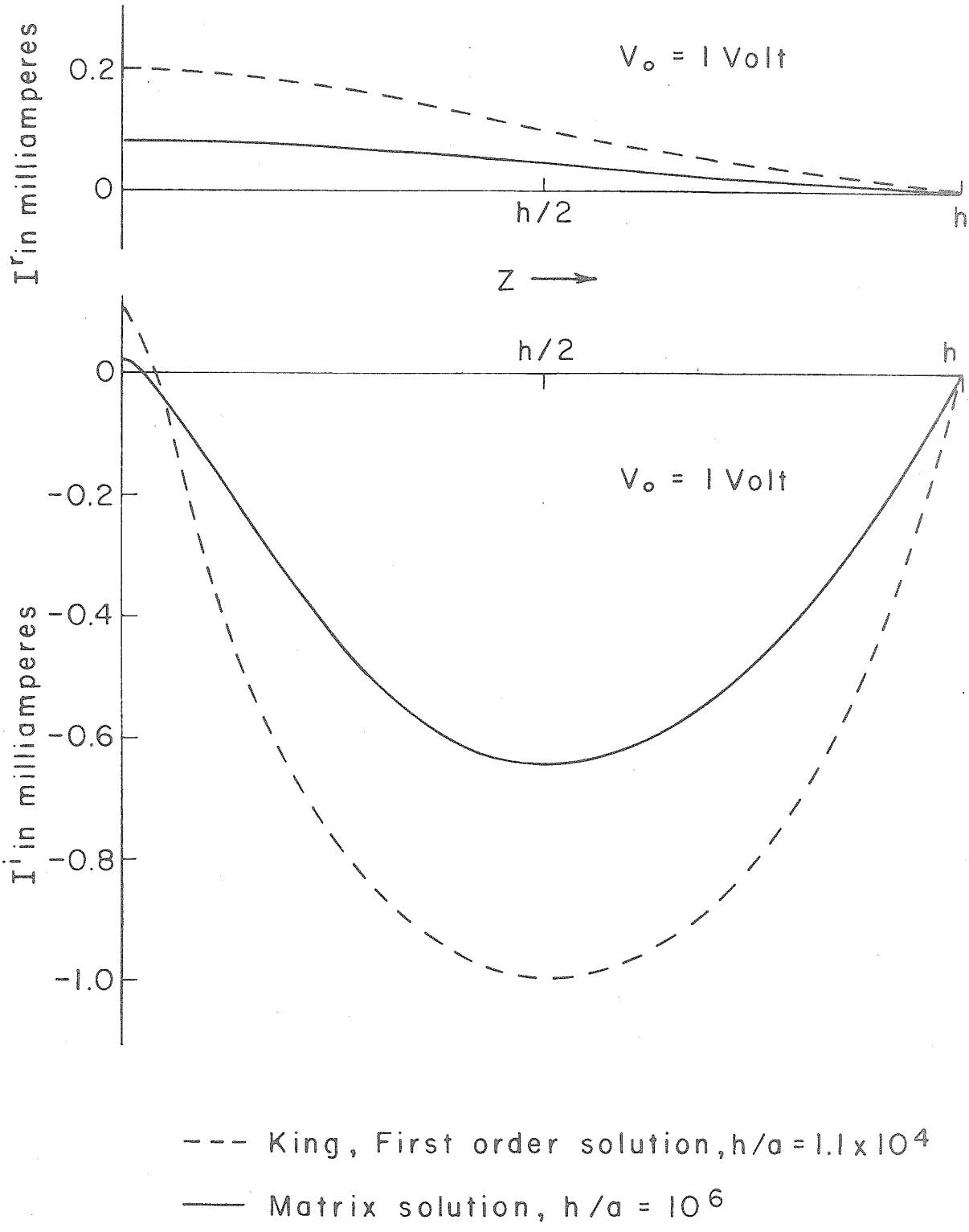

FIGURE 28. COMPARISON OF REAL AND IMAGINARY CURRENT DISTRIBUTIONS ON FULL-WAVE UNLOADED ANTENNA CALCULATED BY KING AND MATRIX METHODS.

very thin antenna, so it is necessary to extrapolate in order to obtain a comparison of the different results. Hence the results are plotted for a number of different thicknesses.

Method of Solution	h/a	R_{fp} ohms	X_{fp} ohms
King	75	270	- 440
King	259	650	- 810
King	904	1,150	-1,300
King	11,013	2,550	-2,600
Matrix	1,000,000	11,913	-2,126*

TABLE 3. COMPARISON OF FEEDPOINT IMPEDANCE OF THIN, UNLOADED, FULL-WAVE LINEAR ANTENNA CALCULATED BY KING AND MATRIX METHODS

It is apparent from figures 12 to 21 that as Z_o becomes very large, the effect of the sections of antenna beyond the loading elements becomes small. It is therefore probable that the highly-loaded full-wave antenna would have some properties similar to those of a half-wave antenna. From figure 21, the current distribution of the highly-loaded antenna is similar to that of a half-wave antenna. Table 4

* For a ten-term expansion, the value of the feedpoint reactance is not as accurate as the feedpoint resistance. At the feedpoint, all the cosinusoidal factors are unity; thus the reactive current series for $z = 0$ becomes a large positive term and nine rapidly converging but negative terms. The nine smaller negative terms nearly cancel the positive term, and more negative terms in the series are needed to evaluate the reactive current at $z = 0$ with accuracy. However, for values of z not near the origin, the cosinusoidal factors become more random in sign, and the reactive current distribution becomes more accurate over the rest of the antenna. The exceptional reactive current series of a large positive term and several smaller negative terms is not encountered for non-zero values of the loading impedance Z_o.

presents a comparison of the feedpoint impedance of a half-wave antenna (for different theories and different h/a) with the feedpoint impedance of the highly-loaded full-wave antenna.

Method of Solution	h/a	R_{fp}	X_{fp}
King	75	86.5	+j41.7
King	259	83.0	+j43.0
Nomura and Hatta	250	75.5	+j43.5
King	904	80.8	+j43.4
Storm	904	82.7	+j45
King	11,013	78.5	+j43.6
Matrix	1,000,000	70.3	-j18

TABLE 4. COMPARISON OF MATRIX METHOD CALCULATION OF FEEDPOINT IMPEDANCE OF THIN, HIGHLY-LOADED, FULL-WAVE ANTENNA WITH FEEDPOINT IMPEDANCE OF THIN, UNLOADED, HALF-WAVE ANTENNA CALCULATED BY OTHERS

The feedpoint resistances agree quite closely. However, the sign of the reactance of the highly-loaded full-wave antenna is opposite to the sign of the half-wave antenna reactances. Although there is no reason to expect all the properties of the two antennas to agree, this difference might be due to the fact that near resonance the reactance of a thin antenna changes rapidly with length while the resistance varies relatively slowly with length. Consequently the reactances of the two cases may not compare as closely.

In general, then, the matrix method gives results which are in agreement with other theories. Comparison is only possible in special limiting cases, however, since the loading problem has not been analyzed with the other theories.

D. Extension of Matrix Method to the General Antenna Problem

The matrix method for solving the problem of a loaded, linear antenna is well suited for nearly every type of loading condition, if a means is available to evaluate equation II-28 for a sufficient number of terms of the series. A computer with semi-automatic coding schemes and matrix subroutines facilitates an accurate determination of the current series. The problem of Sections II-B and II-C was a full-wave antenna symmetrically loaded with real impedance elements. However, the method can be extended to general loading conditions in which the impedances may be real, imaginary, or complex, and may be symmetrically or asymmetrically placed. The method is also valid for impedances with negative real parts, i.e., active circuits, amplifiers, etc. One need only evaluate F_{nm} from equation II-17 for the particular type of impedance.

The matrix method can also solve the general feeding problem for which there may be more than one feedpoint located at various places along the antenna conductor. The arrangement of feedpoints is evaluated in equation II-13. The antenna of Section II-C (cf. figure 10) was center-fed, which led to symmetry of the current about the origin. Consequently, the subsequent current expansion consisted only of odd cosine functions. The general problem with arbitrary location of the feedpoints will require both even and odd terms in the expansion when the symmetry does not exist.

No other method of analysis of the linear antenna has been able to solve the problem of an antenna with finite internal impedance (cf. equation II-16) without extreme complication of the mathematics. In the classical Hallén-King theory the integral on the right-hand side of equation II-6 is neglected. However, in the matrix method this term can easily be considered by a suitable choice of the impedance $Z^i(z)$ in equation II-13. No additional mathematics are introduced.

Although the completely general loaded, linear antenna can be analyzed with great facility, the series expansions for the general problem may converge only slowly. Nevertheless, for a desired accuracy, it is then necessary to evaluate a greater number of terms. If adequate computing facilities are available, convergence problems can be eliminated. Complication of the problem geometry introduces no new mathematical difficulties. As seen in Section II-B, however, the convergence problem is not serious for antennas with only a few loading elements; reasonable accuracy was obtained with only ten terms in the expansion. The Burroughs Datatron 205 computer can be coded for a series of 52 terms. The Burroughs Datatron 220 computer can be coded for 100 terms. The ultimate limitation of any computer in solving the antenna problem is the size of its memory and the nature of the round-off error.

Not only can the general antenna problem be evaluated with ease, but other properties of the antenna can also be determined without great difficulty using the matrix method of solution. The Q of the antenna can be evaluated by computing the feedpoint reactance for several different frequencies. This involves computation of the impedance

matrix $\left[Z_{nm}\right]$ for each frequency considered (cf. Appendix I). The relation of antenna impedance to antenna radius can be considered by re-evaluating only the diagonal terms X_{nn} of the reactance matrix for each radius. Many array problems can also be solved by appropriate evaluation of $A(\rho, z)$ in equation II-25. Thus radiation patterns and mutual impedances of arrays can also be determined using the matrix method.

E. Application of Theoretical Results to the Power-Line Antenna

The results described in Section II-C are valid for a free-space, full-wave linear antenna with passive circuit loading as shown in figure 10. The matrix method of analysis used for this particular antenna problem can easily be extended to most loaded, linear antenna problems (cf. Section II-D). This section will apply the results of the previous sections to the problem of the power-line transmitting antenna.

The power-line antenna (figure 8) consists of a section of single-phase power line which is isolated from the rest of the distribution system by two pairs of radio frequency line traps. Consequently, the actual antenna consists of <u>two</u> parallel conductors, separated by a small distance D. These two parallel antennas are fed in a balanced manner, so that, by symmetry, the current distributions are identical on each conductor. The presence of the second current-carrying conductor requires modification of equation II-25 for the mth partial vector potential:

$$A_m'(a,z) = \frac{\mu}{4\pi}\int_{-h}^{h} I_m \sin(k_m z' + \alpha_m)\,\frac{e^{-j\beta_o\sqrt{(z-z')^2+a^2}}}{\sqrt{(z-z')^2+a^2}}\,dz'$$

$$+ \frac{\mu}{4\pi}\int_{-h}^{h} I_m \sin(k_m z' + \alpha_m)\,\frac{e^{-j\beta_o\sqrt{(z-z')^2+(D-a)^2}}}{\sqrt{(z-z')^2+(D-a)^2}}\,dz' \qquad \text{(II-46)}$$

where $D << h$. Equation II-46 is then substituted into equation II-27 to evaluate the modified impedance matrix $\left[Z_{nm}'\right]$ for the two conductors. From equation A-23 in Appendix I it is apparent that the impedance matrix for the two-conductor problem is twice the matrix of a single conductor of radius $\sqrt{a(D-a)}$. Substitution of the matrix into equation II-28 yields, finally, that the current distribution on each of the two conductors is that of a single conductor of radius $\sqrt{a(D-a)}$ with $\frac{1}{2}V_o$ applied and $\frac{1}{2}Z_o$ loading impedance. For large Z_o the current distribution and feedpoint impedance become independent of Z_o so the current distribution is nearly the same for Z_o as for $\frac{1}{2}Z_o$ (figures 20 and 21). Since the effective radius $\sqrt{a(D-a)}$ of the two-conductor modification still corresponds to an extremely thin antenna, the current distributions of Section II-C should be accurate approximations to the distribution on the two-conductor antenna, for large Z_o . If the exact current distribution is required, equation II-46 should be substituted into equation II-28.

The length of the actual power-line antenna may be considerably different from the idealized antenna of figure 10. The general power-line antenna will have very long sections beyond the traps. The Dinkey Creek power-line antenna of this thesis had rather short sections beyond the traps (figure 32). However, for a large trap impedance Z_o the sections beyond the traps have only a small effect upon the current distribution and feedpoint impedance. Consequently, for a general length of antenna beyond the traps, the current distribution will be very similar to the problem of figure 10 for large Z_o. In order to solve the general length problem exactly, the correct value of s should be substituted into equations A-20, A-21, A-22, and A-23 in Appendix I to determine $[Z_{nm}]$.

However, if the sections beyond the traps were an integral number of half-wavelengths long, a resonance condition would be set up, allowing a large standing wave of current to exist beyond the traps. This special case would have to be analyzed as outlined above. To eliminate large currents from the sections of line beyond the traps, it would be necessary to locate a second set of traps at a position in the line where one of the resonant maxima would exist.

In addition to being of a different length than the idealized antenna of figure 10, the power-line antenna may not be exactly linear. Although many transmission and distribution lines are nearly straight, the Dinkey Creek power-line antenna did have a slight curvature. An exact solution for the current distribution on this antenna would involve a second coordinate to describe the two-dimensional geometry. Many

of the simplifying assumptions of the linearized matrix method would no longer be valid. In order to apply the results of the idealized linear antenna problem to the actual power-line antenna, slight deviations from perfect linearity will be neglected.

The loading elements on the power-line antenna, or line traps, are actually not coaxial cylinders of radius a, but are large (relative to a) rectangular elements, hung on crossarms a few feet below the antenna conductors (figure 42). However, if the maximum dimension of the traps is M, $\beta_o M \ll 1$, so that to a good first-order approximation, the effect of the trap size can be neglected. The actual loading network is shown in figure 29:

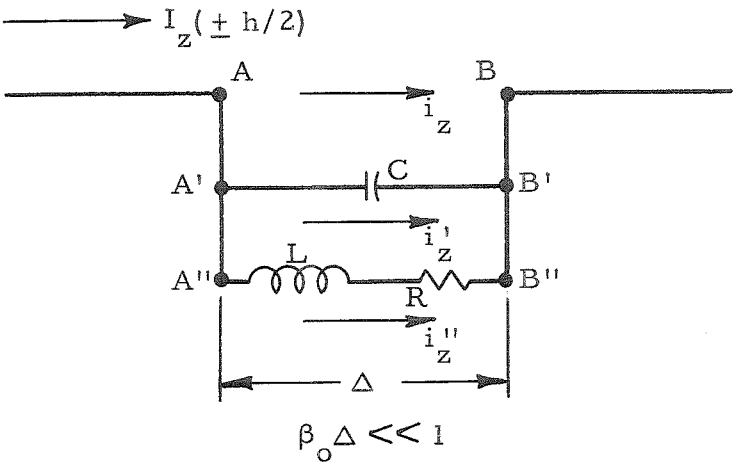

FIGURE 29. ACTUAL LOADING NETWORK

Neglecting flux linking path $AA'A''B''B'B$ and resistance of the leads, $\nabla \times \overline{E} = 0$, and

$$\oint_{AA'B'B} E \cdot d\ell = 0 \cong (E_{A'B'} - E_{AB})\Delta \qquad \text{(II-47a)}$$

and

$$\oint_{A'A''B''B'} E \cdot d\ell = 0 \cong (E_{A''B''} - E_{A'B'})\Delta \qquad \text{(II-47b)}$$

Then

$$E_{AB} = E_{A'B'} = E_{A''B''} = E_z(\pm h/2) \qquad \text{(II-48)}$$

From the definitions of lumped circuit elements (reference 28):

$$\int_{A'}^{B'} E_{A'B'} dz \triangleq \frac{1}{j\omega C} i_z' \cong E_z(\pm h/2)\Delta \qquad \text{(II-49a)}$$

and

$$\int_{A''}^{B''} E_{A''B''} dz \triangleq R i_z'' + j\omega L i_z'' \cong E_z(\pm h/2)\Delta \qquad \text{(II-49b)}$$

It is possible to define $Z' = 1/Y'$, where Z' represents distributed coupling effects across the loading gap, so that, with reference to figure 29:

$$\int_{A}^{B} E_{AB} dz \triangleq Z' i_z \cong E_z(\pm h/2)\Delta \qquad \text{(II-49c)}$$

Therefore

$$i_z + i_z' + i_z'' = I_z(\pm h/2) = E_z(\pm h/2)\Delta\left(Y' + j\omega C + \frac{1}{R + j\omega L}\right) \qquad \text{(II-50)}$$

Then, in terms of equations II-13 and II-15:

$$E_z(\pm h/2) = \frac{Z_o}{\Delta} I_z(\pm h/2) \qquad \text{(II-51a)}$$

where

$$Z_o = \frac{1}{Y' + (j\omega C + \frac{1}{R + j\omega L})} \qquad \text{(II-51b)}$$

It has been found experimentally that at the resonant frequency ω_o the effect of Y' is small so that

$$Z_o \cong Q\omega_o L \qquad \text{(II-52a)}$$

where

$$Q = \omega_o L/R \quad \text{and} \quad \omega_o \cong 1/\sqrt{LC} \qquad \text{(II-52b)}$$

In order to make Z_o of equation II-51b the purely real loading impedance of the idealized problem, it is necessary to tune the traps so that the entire impedance network, including the stray coupling Z', is resonant.

The effect of the conducting ground beneath the power-line antenna will not be considered in detail. However, the ground problem takes two forms: (1) calculating the fields of the antenna-earth combination for an assumed current distribution of the antenna, and (2) calculating the current distribution on the antenna in the presence of the earth. The former problem (1) has been solved by Sommerfeld and others (references 29 and 30). The radiation fields due to an assumed current on an antenna located over a conducting earth take on a form similar to the problem of the antenna with a quasi-image antenna located an equal

distance below the earth. However, the problem cannot be completely solved in terms of the antenna and its image alone, and a third component of the vector-potential (vertically-polarized) must be introduced to match boundary conditions. The radiation fields in three mutually-orthogonal planes have been calculated for a linear, half-wave antenna with an assumed cosinusoidal current distribution located over a plane earth of finite conductivity. These fields are given in equations I-2, I-3, and I-4.

The second form of the ground problem (2) has not been considered previously in the literature. If the effect of the conducting ground is to be considered in the calculation of the current distribution itself, the matrix method solution becomes extremely complicated. It is then necessary to include in equation II-26 a secondary component of the vector potential due to the conducting ground. Although the effect of the ground upon the current distribution will not be considered in detail, a number of qualitative remarks can be made concerning the problem.

Referring to the coordinate system of figure 30, the vector potential of a horizontal, infinitesimal dipole of length L carrying current I located at the surface* of a plane conducting earth is (reference 29):

$$A_z = \frac{j\mu I L}{4\pi} \int_0^\infty \frac{2 J_o(\lambda \rho)\, e^{-y\sqrt{\lambda^2 - k^2}}}{\sqrt{\lambda^2 - k^2} + \sqrt{\lambda^2 - k_E^2}}\, \lambda d\lambda \qquad \text{(II-53)}$$

---

* Actually the antenna is a few meters above the earth, but $\frac{H}{\lambda_o} \ll 1$.

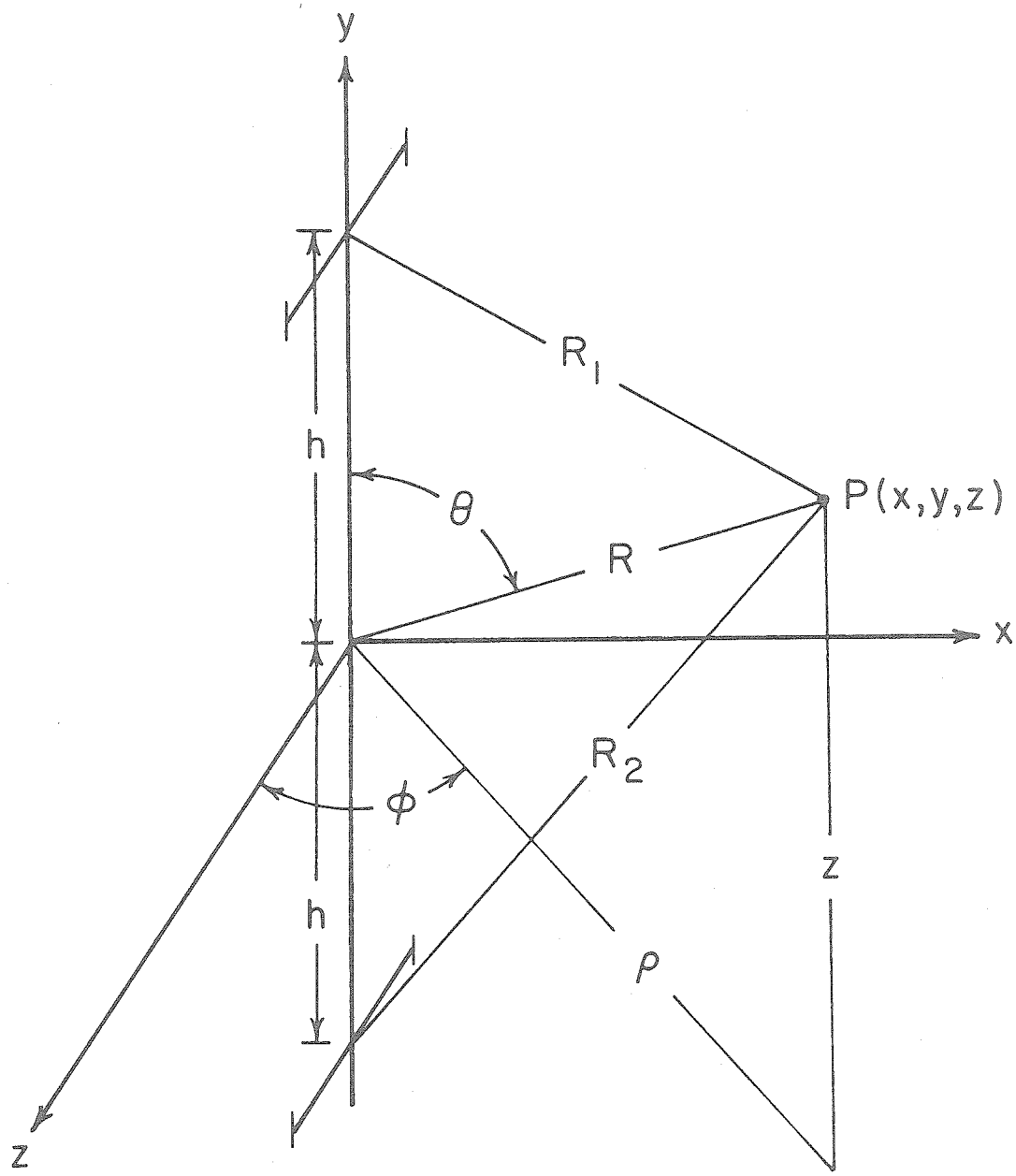

FIGURE 30. GEOMETRY OF THE SOMMERFELD ANTENNA PROBLEM.

where $k^2 = \omega^2 \mu_v \varepsilon_v$ and $k_E^2 = \omega^2 \mu \varepsilon - j\omega\mu\sigma$. (The y-component of the vector potential will not be considered since it does not contribute to a z-component of antenna current.) By manipulating the denominator of equation II-53 A_z can be rewritten as:

$$A_z = \frac{j\mu I L}{4\pi} \left\{ \int_0^\infty \frac{J_o(\lambda\rho)\, e^{-y\sqrt{\lambda^2 - k^2}}}{\sqrt{\lambda^2 - k^2}} \lambda d\lambda \right.$$

$$\left. + \int_0^\infty \frac{J_o(\lambda\rho) e^{-y\sqrt{\lambda^2 - k^2}}}{\sqrt{\lambda^2 - k^2}} \frac{\left[\sqrt{\lambda^2 - k^2} - \sqrt{\lambda^2 - k_E^2}\right]^2}{(k_E^2 - k^2)} \lambda d\lambda \right\} \qquad \text{(II-54)}$$

Using the Fourier-Bessel integral theorem (reference 25), the vector potential becomes:

$$A_z = \frac{j\mu I L}{4\pi} \left\{ \frac{e^{-jkR}}{R} + \int_0^\infty \frac{J_o(\lambda\rho) e^{-y\sqrt{\lambda^2 - k^2}}}{\sqrt{\lambda^2 - k^2}} \frac{\left[\sqrt{\lambda^2 - k^2} - \sqrt{\lambda^2 - k_E^2}\right]^2}{(k_E^2 - k^2)} \lambda d\lambda \right\} \qquad \text{(II-55)}$$

The first term of equation II-55 is the vector potential of the dipole located in free space (primary excitation); the second term is the perturbation effect of the conducting earth. For $y = 0$ and $\rho = 0$, the perturbation term can be shown to be finite. Consequently, in the immediate vicinity of the antenna, where the primary excitation becomes very large as $R \longrightarrow 0$, the relative effect of the conducting earth is small.

From the dipole results, then, it can be inferred that if any thin linear antenna is located over a conducting earth, the vector potential at a point on the antenna conductor is primarily due to the current there, and at that point the secondary excitation of the earth is relatively small. Since, from equation II-27, it is the vector potential at the surface of the antenna that determines the current distribution, for very thin antennas the current distribution is not strongly affected by the presence of the ground. Therefore, to a first order approximation, the current distributions calculated in Section II-C will be assumed to be relatively accurate expressions for the actual radio frequency current on the power-line antenna. This assumption has been verified experimentally for a number of models of the power-line antenna. For these models, the presence of the earth modified the current only a few percent from the expected distribution.

Having determined the current distribution, the problem of computing the radiation fields has been solved previously. The radiation fields are given by equations I-2, I-3, and I-4, and are plotted in figures 4, 5, and 6. Unlike the current distribution, these fields are strongly affected by the presence of the ground. The horizontally-polarized field is much less than that of an identical antenna in free space. A vertically-polarized field is introduced. With reference to equation II-55, the perturbation term is no longer small relative to the primary excitation term since R is not small in the radiation zone.

The radius-to-length ratio for a power-line antenna is extremely small. For the Dinkey Creek power-line antenna, $a/2h \cong 10^{-6}$.

Therefore assumption II-9 is valid, and the linearized theory can be applied. The excitation, however, is not maintained by an idealized generator, but by a two-dimensional coupling network (figure 8). A one-dimensional analysis cannot take such regions into account. Additional lumped capacitances in parallel with the antenna should be included to represent the effect of these regions. However, these junction effects have been neglected in determining the current distribution.

III. THE DINKEY CREEK POWER-LINE TRANSMITTING ANTENNA

The power-line antenna system described in this section was located along the Dinkey Creek Road near Shaver Lake, California, in the Sierra Nevada Mountains about fifty miles northeast of Fresno (figure 31). The antenna consisted of an eight-mile section of the Dinkey Creek 12 kv, single-phase distribution line, operated by the Southern California Edison Company. The single-phase line branched from two conductors of a three-phase distribution line at the west end of the antenna. The Sierra Nevada Mountain site was selected because the underlying substructure there was primarily unfractured granite, and hence the resistivity of the ground was relatively large (cf. Section I-B). A detailed map of the antenna is shown in figure 32, which indicates that the section was only approximately linear. The feedpoint was located near the center of the antenna section.

The radio frequency transmitter, consisting of a 20 kw power amplifier driven by a crystal oscillator, was located in a small cabin near the center of the antenna. A picture of the transmitting station, including the equipment for coupling from the transmitter into the power line, is shown in figure 43.

The resonant, radio frequency line traps played a fundamental role in the performance of the system. They are shown mounted in position in figure 42. The design and construction of the line traps are completely described in reference 31. However, a brief description of the line trap components is included below.

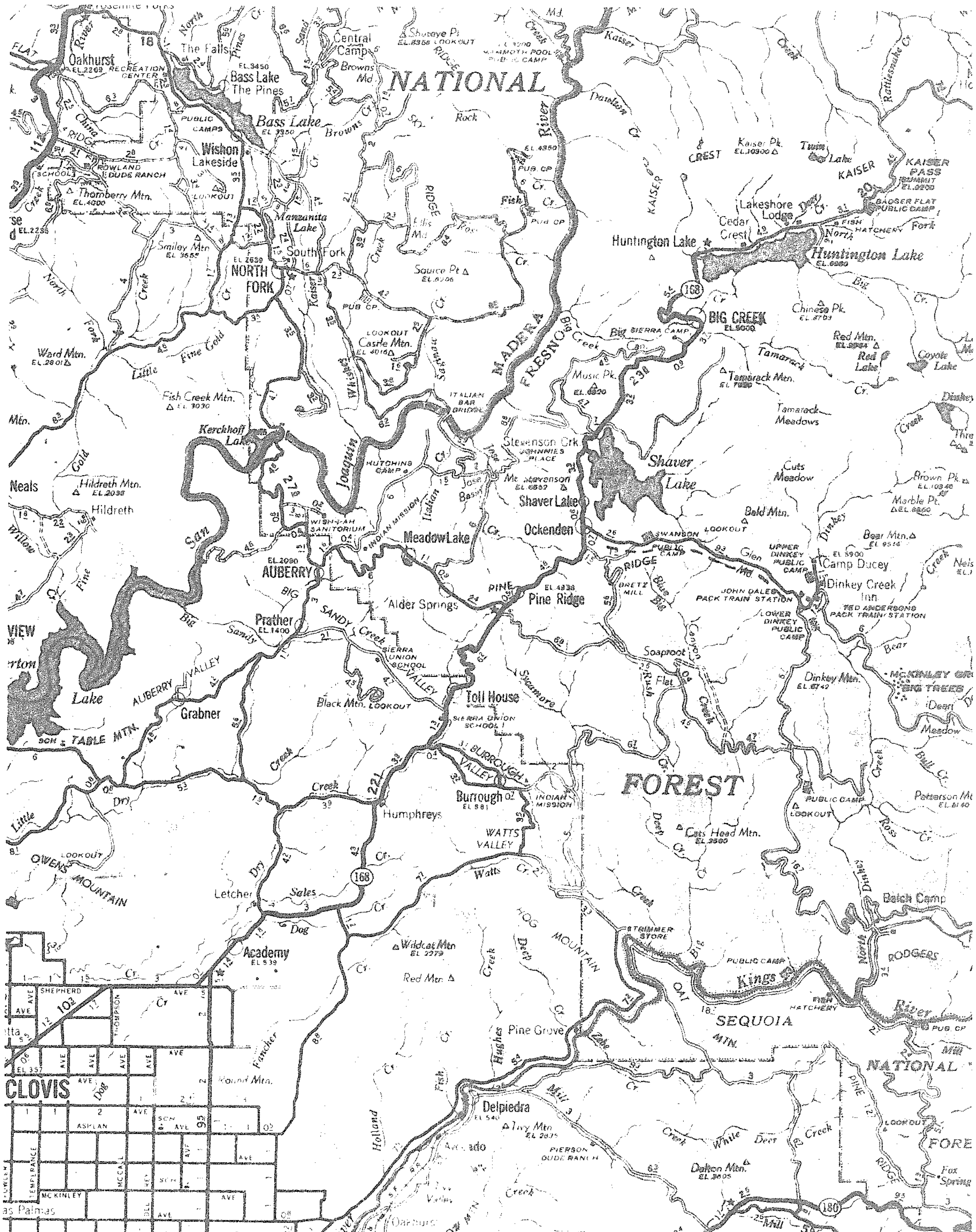

- - - - - Dinkey Creek Power-line Antenna

FIGURE 31. MAP OF SHAVER LAKE AREA.

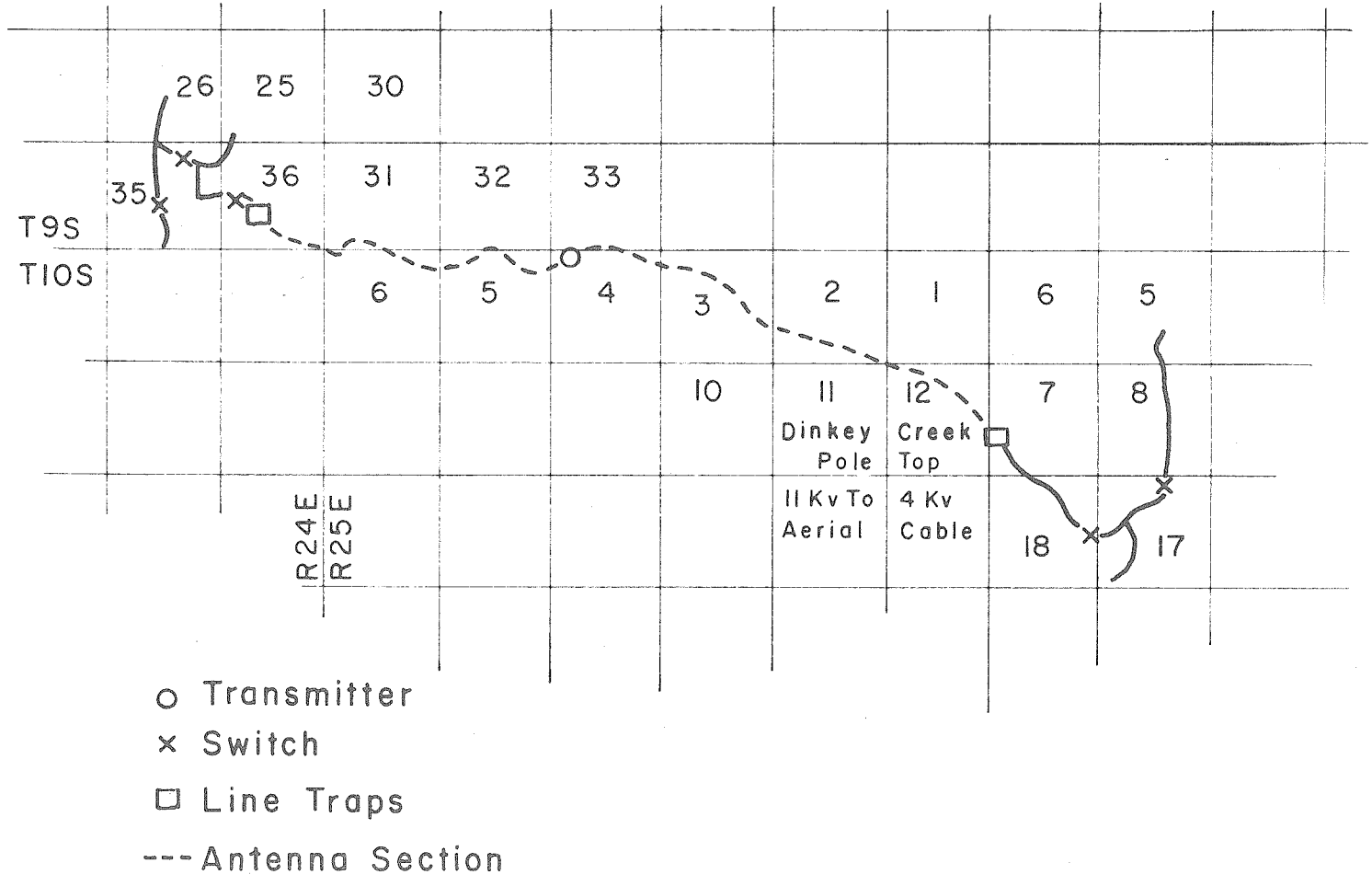

FIGURE 32. SECTION OF DINKEY CREEK 12 KV POWER LINE USED AS TRANSMITTING ANTENNA.

A. Construction of the Line Trap Inductors

If a magnetic core material had been used, the 60 cps power-line current also flowing through the trap inductor would have acted as a slowly varying "bias" current which might have saturated the core and detuned the trap from resonance. The permeability of magnetic core materials is frequently temperature sensitive; an extreme temperature change might also have detuned the traps. Consequently, the trap inductors were of an air core design.

In order to make the effective resonant impedance of the traps as large as possible (cf. equations II-52a and II-52b), it was necessary to minimize the losses in the inductors. Skin effect in the conductor, increasing the effective resistance of the coil, was reduced by using a cable of 420 strands of extremely fine AWG No. 34 wire. Sufficient oxide coating on the fine strands produced a Litz-type wire and reduced skin effect. Proximity effect between turns was reduced by making the cross-section of copper considerably less than the total coil cross-section. Dielectric loss was decreased by impregnating the wooden coil forms with a very low loss organic varnish. Eddy current losses in nearby conductors were eliminated by placing the coils in large cylindrical fiberglass tanks. The tanks were covered by impregnated plywood lids on which the bushings were mounted.

Since a large radio frequency potential difference was developed across the trap inductors (figure 23), it was necessary to increase the layer-to-layer dielectric strength with fish paper and bone fiber corrugated duct between alternate layers. In addition, the coils were

submersed in insulating oil to increase their general voltage reliability. The insulating oil also improved the heat rejection of the coils, preventing their temperature from becoming too large under full-load conditions. The corrugated duct allowed the oil to flow between layers, thereby cooling internal parts of the coil.

Fine tuning of the traps was accomplished by tapping the last 11 turns of the coil in 12 places, providing 11 increments of inductance. The taps were connected to a tap switch mounted inside the lid. The tap switch handle extended through the lid into the base of a non-rising gate valve stem and gland mounted on the outside of the lid, making it possible to vary the inductance externally.

The coils were made weather-tight with a heavy fiberglass covering on the lid and a cork gasket around the flange of the tank. Moisture which entered the inductor from "breathing" was absorbed by silica gel dryers mounted on the lid of the tank. Details of the trap inductor construction are shown in figure 44.

B. Construction of the Line Trap Capacitors

Commercial chlorinated hydrocarbon oil capacitors could not be used to resonate the high Q coils in the line traps because of their relatively high dissipation at 8.4 kc. Consequently mica transmitting capacitors, with an extremely low dissipation factor at radio frequencies, were chosen. The capacitors were mounted on insulators in a steel tank filled with insulating oil. The oil minimized corona losses, reduced the possibility of voltage flashover, and improved the cooling. Silica gel

was placed in the air space above the oil. The tanks were covered with aluminum lids through which passed the two bushings. Rectangular cork gaskets were used to seal the lids. A picture of the completed trap capacitors is shown in figure 45.

C. Construction of the Coupling Network

The network which coupled radio frequency energy from the transmitter into the antenna was designed to satisfy the following requirements:

1. Since both conductors of the single-phase power line were fed in phase, the coupling network was symmetrical with respect to the two lines. Because of the nature of a center-fed antenna, the coupling network was also symmetrical with respect to the east and west halves of the antenna (figure 8).

2. To avoid an excessively large 60 cps potential difference between the primary and secondary windings of the output transformer, and to provide safety for personnel, the secondary center tap of the output transformer was grounded (figure 8).

3. To prevent a short circuit of the power line to ground through the grounded transformer secondary, and to block the 60 cps line voltage from the transformer, large surge capacitors were placed in the branches from output transformer to power line. To minimize the radio frequency impedance of these branches, the blocking capacitors were resonated with series inductors. The resonating inductors were composed of two coils (figure 46), one of the approximate resonating inductance, and the

other an adjustable tuning coil. For safety, all high voltage components were mounted in a locked cabinet, 18 ft above the ground (figure 43).

4. Adequate disconnect switches were provided to completely disconnect the coupling network from the power line (figure 33). By placing a current transformer in the ground lead from the output transformer secondary, it was possible to provide a ground fault protection system (figure 34). In the event of excessive 60 cps ground current, a relay would be activated to open a circuit breaker in series with the output transformer leads, completely disconnecting the radio frequency transmitter from the antenna. Simultaneously, the 480 v input power to the transmitter would be disconnected.

D. Lightning Protection

Each of the end traps was protected from lightning surges by 18 kv lightning arresters which bypassed the traps, and 12 kv arresters connected from line to ground on the sides of the traps outside the antenna section. The coupling network was similarly protected.

E. 60 cps Ground Current

The antenna section consisted of the two conductors of a single-phase line. However, the third conductor of the balanced three-phase distribution line terminated at the west end of the antenna (figure 32). A capacitor was connected between the terminated third phase and ground, equal in capacitance to the capacitors connected between the other two conductors and ground at the center of the antenna. In this

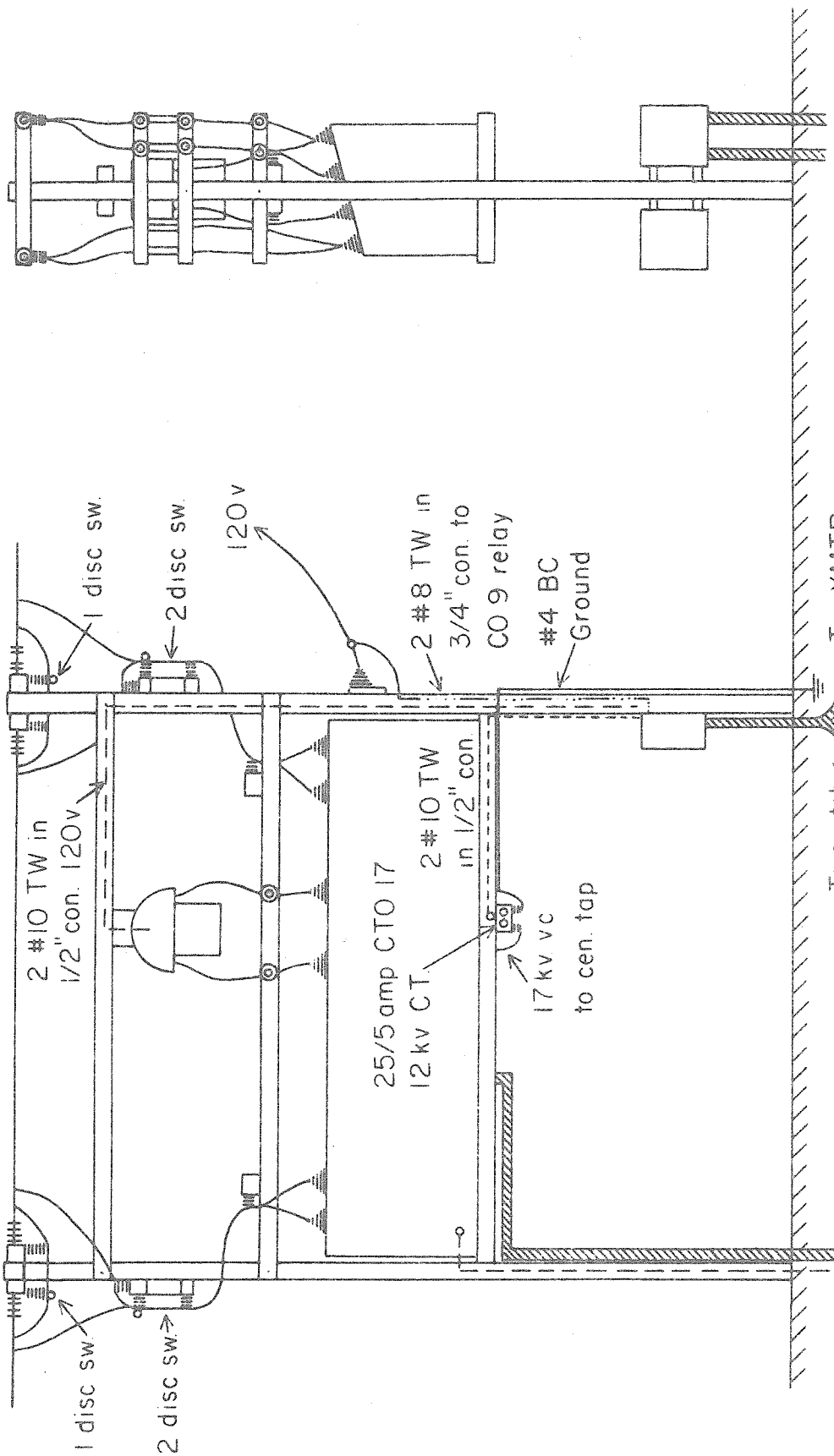

FIGURE 33. EXTERIOR WIRING FOR COUPLING NETWORK.

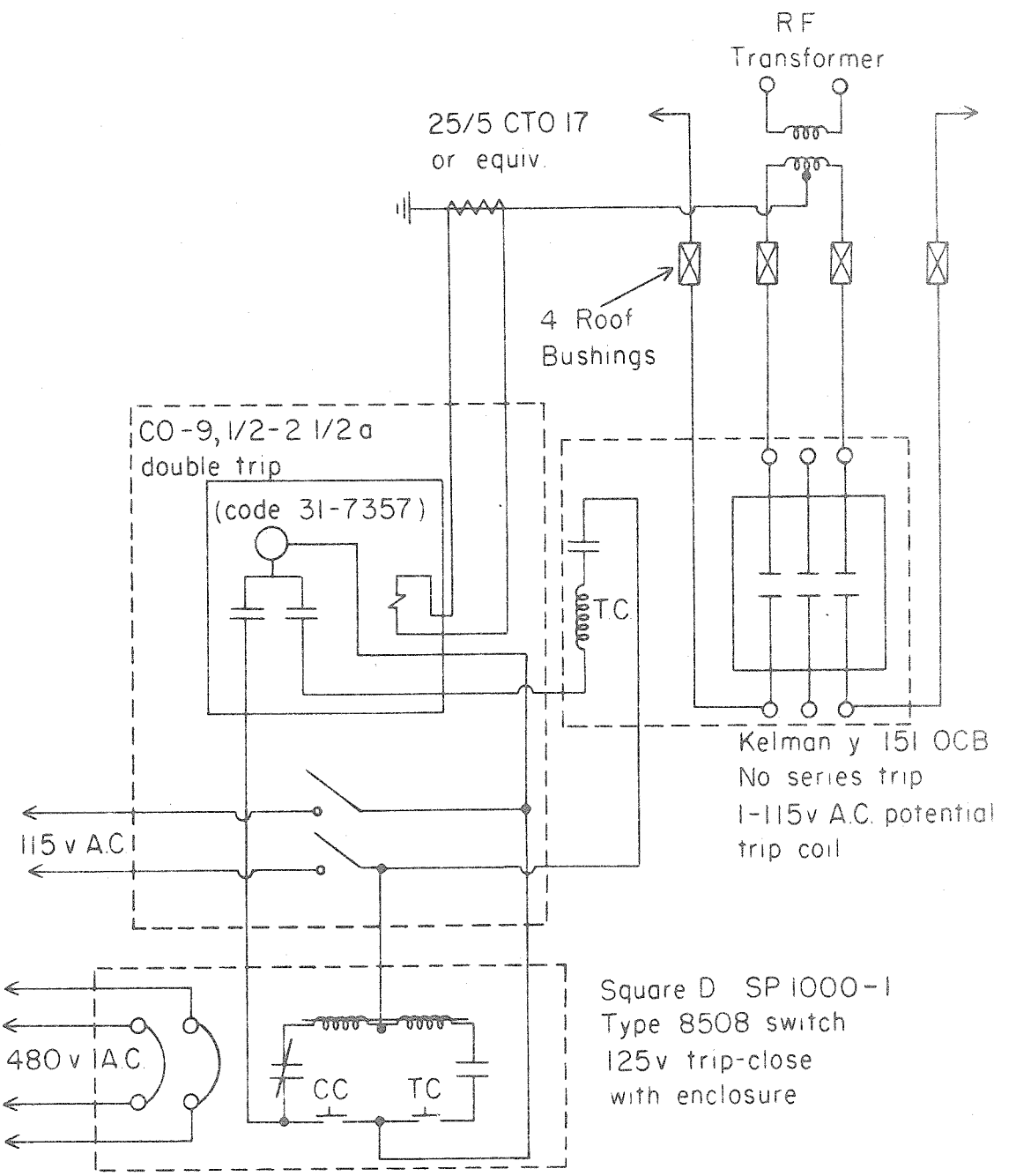

FIGURE 34. GROUND FAULT PROTECTION SYSTEM.

manner equal components of ground current flowed in each of the three conductors of the three-phase distribution line. The sum of these three phase-currents was the net ground current. Although they were nearly equal in magnitude, they were separated 120 degrees in phase, so the sum of the three was nearly zero. Consequently, by placing the capacitor in the third phase at the west end of the antenna, the total ground current was effectively eliminated.

F. Performance of the Antenna System

Before construction of the Dinkey Creek antenna system, a 10 mc scale model was used to obtain preliminary data on this type of antenna. The model, mounted horizontally, was 150 ft long, or approximately 1.5 wavelengths. Without loading, the antenna current was measured and found to be almost exactly sinusoidal. Tuned circuits, with a resonant impedance of 200,000 ohms, were then mounted in the antenna as shown in figure 10, on opposite sides of the center feed. When the tuned circuits were tuned for maximum impedance, the current in the antenna section beyond them was reduced to less than 0.5 percent of its value without loading. Location of the tuned circuits at other points on the antenna also nearly eliminated the current beyond them. The results of these preliminary experiments qualitatively verified the theoretical results of Section II-C.

A serious problem in the design of the power-line antenna was the coupling of radio frequency energy into the power distribution system. If

an appreciable fraction of the radio frequency energy passed beyond the ends of the antenna section, it would not only pass into consumer house wiring, but would also disrupt nearby audio-frequency communication systems. In the Shaver Lake - Big Creek area, the Southern California Edison Company operated a series of power stations, within a radius of 25 miles from the Dinkey Creek antenna. These stations were connected by an extensive system of audio-frequency control and telephone circuits on open wire lines near to and parallel to the distribution lines. These circuits were operated at a power level of about five watts. Table 5 presents a listing of these circuits, and figure 35 shows their locations in relation to the Dinkey Creek antenna. Since the radio frequency transmitter was to be operated at a power level of 10,000 - 20,000 watts, it was necessary to measure the amount of that power which was coupled into the Edison telephone circuits before radio frequency transmissions were permitted. Table 6 presents the amount of radio frequency (8.4 kc) signal coupled into the telephone circuits for different power levels of the transmitter. Although the signal was detectable on most of the lines, it was generally small enough not to cause appreciable interference. Consequently, the ability of the line traps to contain the radio frequency energy within the antenna section was demonstrated.

Evidence that nearby audio-frequency communication systems may be seriously affected by the radio frequency signal was vividly presented on one occasion when a trap inductor became defective during a series of high power transmissions. As a result, the 8.4 kc power was free to pass into the distribution system and thence into nearby communication

Big Creek No. 3 - Big Creek No. 1	
3.5 kc	(3.8 kc - 6.3 kc)
11.5 kc	(8.7 kc - 11.2 kc)
7.6 kc	
8.0 kc	

Big Creek No. 3 - Big Creek No. 2	
25.0 kc	(26.2 kc - 28.7 kc)
35.0 kc	(31.3 kc - 33.8 kc)

Big Creek No. 3 - Big Creek No. 4	
25.0 kc	(25.3 kc - 27.8 kc)
35.0 kc	(32.2 kc - 34.7 kc)

Big Creek No. 3 - Big Creek No. 8
4.4 kc
4.8 kc
5.2 kc
5.6 kc
6.0 kc
6.4 kc
7.6 kc
8.0 kc

Big Creek No. 3 - Alhambra	
5.90 kc	
6.25 kc	(6.5 kc - 9.1 kc)
9.45 kc	(9.7 kc - 12.3 kc)
12.85 kc	(13.1 kc - 15.7 kc)
17.70 kc	(17.95 kc - 20.55 kc)
21.45 kc	(21.7 kc - 24.3 kc)
25.35 kc	(25.6 kc - 28.2 kc)
29.6 kc	

Big Creek No. 3 - Piedra	
6.8 kc	
13.0 kc	
17.0 kc	(14.2 kc - 16.7 kc)
19.0 kc	(19.3 kc - 21.8 kc)
23.0 kc	

Big Creek No. 8 - Big Creek No. 1	
13.0 kc	(13.3 kc - 15.8 kc)
17.0 kc	
19.0 kc	
23.0 kc	(20.2 kc - 22.7 kc)
3.5 kc	(3.8 kc - 6.3 kc)
7.0 kc	
8.0 kc	
11.5 kc	(8.7 kc - 11.2 kc)

TABLE 5. TELEPHONE CARRIER FREQUENCIES IN THE SHAVER-BIG CREEK AREA

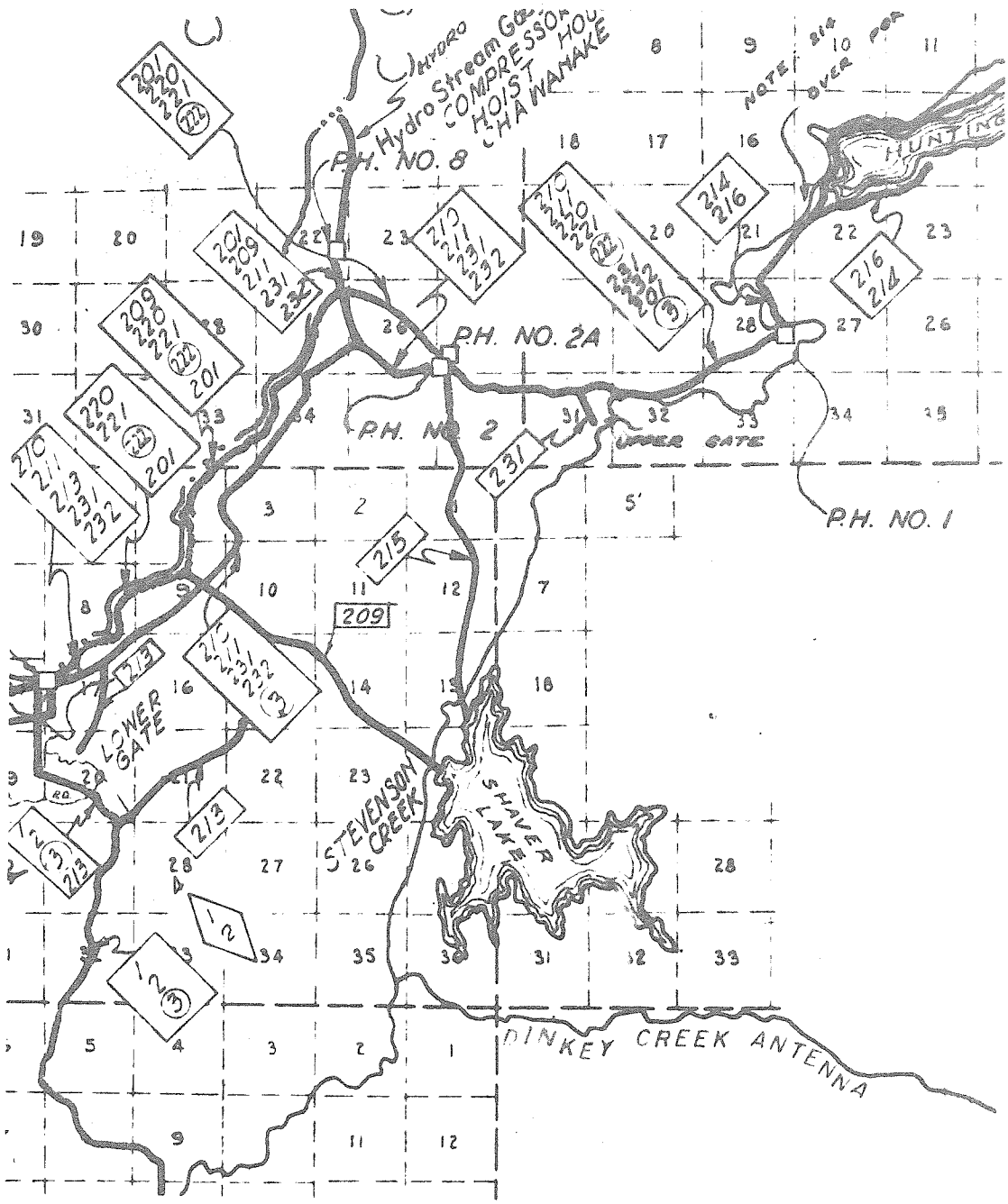

FIGURE 35. DETAIL OF SOUTHERN CALIFORNIA EDISON COMPANY MAP SHOWING COMMUNICATION CIRCUITS IN SHAVER LAKE-BIG CREEK AREA.

Line	Transmitter Power: Destination	0	1.28 kw	4.50kw	8.0kw	15.7kw
222	Bechtel-Fresno	-55dbm	-30dbm	-26dbm	-24dbm	-20dbm
221	301 CXR Ext.	-70	-31	-27	-25	-23
231	Canyon	-70	-46	-39	-27	-34
233	No. 3 Vincent Px.	-60	- 6	- 2	0	+ 3
232	Canyon	-70	-32	-23	-36	-35
211	Dispatcher	-70	-55	-51	-50	-43
7	Bigelow (Shaver)	-70	-44	-40	-40	-36
3	Bigelow (Huntington)	-50	-50	-44	-43	-40
220	303 CXR Ext.	-40	-35	-31	-30	-27
210	No. 33 Px. Ext.	-40	-18	-14	-12	-10
201	Radio - B.C. No. 3	-45	-46	-42	-40	-38

Measurements made with Sierra No. 103 Frequency Selective VTVM

TABLE 6. 8.4 KC NOISE MEASUREMENTS ON EDISON TELEPHONE CIRCUITS DURING RF TESTS 3 DECEMBER, 1958.

systems. Edison telephone circuits near 8.4 kc were immediately rendered inoperative. A number of ringing and alarm circuits were energized. The radio frequency power passed into the homes of a number of consumers, causing a loud acoustic tone which could be heard throughout the house. This breakdown demonstrated the importance of effective traps in the performance of the power-line antenna. When a trap does not operate effectively, not only is there the possibility of interference and danger to consumers, but also it becomes increasingly difficult to match power into the antenna, since a decrease in the impedance of the traps rapidly changes the feedpoint impedance of the antenna (figure 22).

A secondary effect considered in the performance of the antenna system was the amount of 60 cps voltage fed back into the transmitter through the output transformer. Inspection of the coupling network schematic diagram in figure 8 reveals that a small amount of 60 cps voltage will be coupled into the transmitter because of unbalances which exist. However, only about 25 v was measured across the primary side of the output transformer, which was not enough to affect the operation of the transmitter.

The feedpoint impedance of the power-line antenna has been measured to be approximately 90 - j60 ohms, 11 ohms of which represent the ohmic resistance of the power line itself. However, the remaining real component of the feedpoint impedance, about 79 ohms, does not represent the radiation resistance of the antenna. Although this value of resistance is nearly the value predicted in figure 22, it primarily represents power which is absorbed in the line traps and in

ground heating. Only a percent or two represents the actual power radiated into space.

The power-line antenna system of figure 8 operated satisfactorily for the requirements of the Dinkey Creek area. Had it been located elsewhere, the system might have had to be modified to meet different requirements. For example, if consumers had been obtaining 60 cps power from the antenna section, it would have been necessary to provide a pair of traps for each spur line. However, the basic principles of the Dinkey Creek system will apply to other locations and other requirements.

IV. 8.4 KC EXPERIMENTAL RESULTS

Although this thesis is intended primarily to describe the nature and operation of the power-line antenna, Section IV contains a description of the propagation experiments for which the antenna was used. Some of the experimental results are also presented.

A. Whistler-Mode Studies

As indicated in Section I, reproduction of the whistler mode of vlf propagation is expected to yield valuable information about the nature of the outer ionosphere. Initially, this author made a study of the nature of the radiation fields of whistling atmospherics (reference 32). The results of this study were used in the design of the radio frequency transmitting system. A brief outline of this calculation is presented below.

By analyzing the mechanism of a lightning discharge, and examining considerable experimental data, a simple approximation for the radiation field from a lightning discharge has been derived:

$$E_\theta(t) = - \frac{\mu_v I_o H \sin\theta}{\pi R \Delta t} \left(\frac{t}{\Delta t}\right) e^{-\left(\frac{t}{\Delta t}\right)^2} \qquad \text{(IV-1)}$$

where

I_o = peak lightning current, in amperes

H = height of the vertical discharge, in meters

θ = colatitude angle

Δt = a function of the duration and shape of the lightning pulse, in seconds

R = atmospheric distance from stroke to observation point, in meters

The frequency spectrum of the radiation field is then:

$$e(\omega) = \int_{-\infty}^{+\infty} E_\theta(t)\, e^{-i\omega t}\, dt = i A \omega e^{-\left(\frac{\omega}{\Delta\omega}\right)^2} \qquad \text{(IV-2)}$$

where $A = \mu_v I_o H \Delta t \sin\theta / 2\sqrt{\pi} R$ and $\Delta\omega = 2/\Delta t$.

By taking the inverse transform, it can be shown that the radiation field is equivalent to:

$$E_\theta(t) = \frac{iA}{2\pi} \sum_{n=-\infty}^{n=+\infty} \int_{\omega_n - \frac{\delta\omega}{2}}^{\omega_n + \frac{\delta\omega}{2}} \omega\, e^{-\left(\frac{\omega}{\Delta\omega}\right)^2} e^{i\omega t}\, d\omega \qquad \text{(IV-3)}$$

where $\omega_n = (n + \frac{1}{2})\delta\omega$ and $\delta\omega$ is a small bandwidth.

Thus the original function of time has been divided into a large number of wave "packets", each packet with a center frequency ω_n and a bandwidth $\delta\omega$. If no dispersion takes place, equation IV-3 reduces to the original function of time given in equation IV-1. When this radiation field enters the ionosphere, each packet will travel at a different velocity, since the ionosphere is a dispersive medium. Consequently, when the lightning pulse emerges from the ionosphere after traveling a distance D , it will have the following form:

$$E_\theta(t, D) = \frac{iA}{2\pi} \sum_{n=-\infty}^{n=+\infty} \int_{\omega_n - \frac{\delta\omega}{2}}^{\omega_n + \frac{\delta\omega}{2}} \omega\, e^{-\left(\frac{\omega}{\Delta\omega}\right)^2} e^{i\omega\left(t - \frac{D}{v_p(\omega)}\right)}\, d\omega \qquad \text{(IV-4)}$$

where $v_p(\omega)$ is the phase velocity, a function of frequency for the dispersive medium. From an experimental examination of $v_p(\omega)$ for the propagation of lightning pulses through the ionosphere, and subsequent integration of the terms of equation IV-4, the final expression for the dispersed lightning discharge becomes:

$$E_\theta(t, D) = \frac{-\mu_v I_o H \Delta t \sin\theta}{\pi\sqrt{\pi}\, R} \sum_{n=0}^{\infty} \omega_n e^{-\left(\frac{\omega_n}{\Delta\omega}\right)^2} \sin\omega_n(t - 2k/\sqrt{\omega_n}) \cdot$$

$$\cdot \frac{\sin\frac{\delta\omega}{2}(t - k/\sqrt{\omega_n})}{(t - k/\sqrt{\omega_n})} \qquad \text{(IV-5)}$$

where the experimentally-determined constant k is a function of D and the dispersion. It is then possible to compute the magnitude of the dispersed field for typical values of I_o, H, and Δt.

The natural whistler fields are detected by broadband receivers. The transmitted whistler-mode signal would be detected by a narrow-band receiver. For the signal-to-noise ratio of the transmitted signal to be comparable to the signal-to-noise ratio of the natural whistler (and hence detectable), the signal could be smaller by a factor η, where

$$\eta = \sqrt{\frac{\text{experimental receiver bandwidth}}{\text{whistler receiver bandwidth}}} \qquad \text{(IV-6)}$$

It has been assumed that the amplitude of the noise is proportional to the square root of the receiver bandwidth.

No account has been taken of the various effects which attenuate the whistler fields, nor has compensation been made for the focusing action of the earth's magnetic field in the ionosphere. However the whistler fields and the transmitted signal will undergo approximately the same focusing and dissipative effects. To detect the signal, it is only necessary that the ratio of the generated and natural fields be equal to IV-6. If both fields are reduced by the same attenuation factor, the ratio will remain constant, independent of the attenuation. Consequently the attenuation effects have not been included.

Equations IV-5 and IV-6 yield the magnitude of the experimentally radiated field necessary for a detectable whistler-mode echo. The current on a horizontal, half-wave antenna to produce this field can be calculated from equation I-2. From this value of current and the feedpoint resistance of the antenna, the power requirements of the antenna can be determined. The results of the calculation indicated that a transmitter capable of a full output of 20 kw would be necessary for the whistler-mode experiments.

In the actual whistler experiments, the transmitter was driven by an 8.4 kc crystal oscillator and keyed by a synchronous timer (figure 36). The transmitter was keyed <u>on</u> for 1/2 second and <u>off</u> for 4 1/2 seconds. Since the transit time of round-trip whistlers has been measured to be 1.5 - 2 seconds, the transmitter was off when the whistler-mode echo returned. However, after a number of transmissions conducted over a period of several months, no whistlers had been detected by direct examination of the receiver

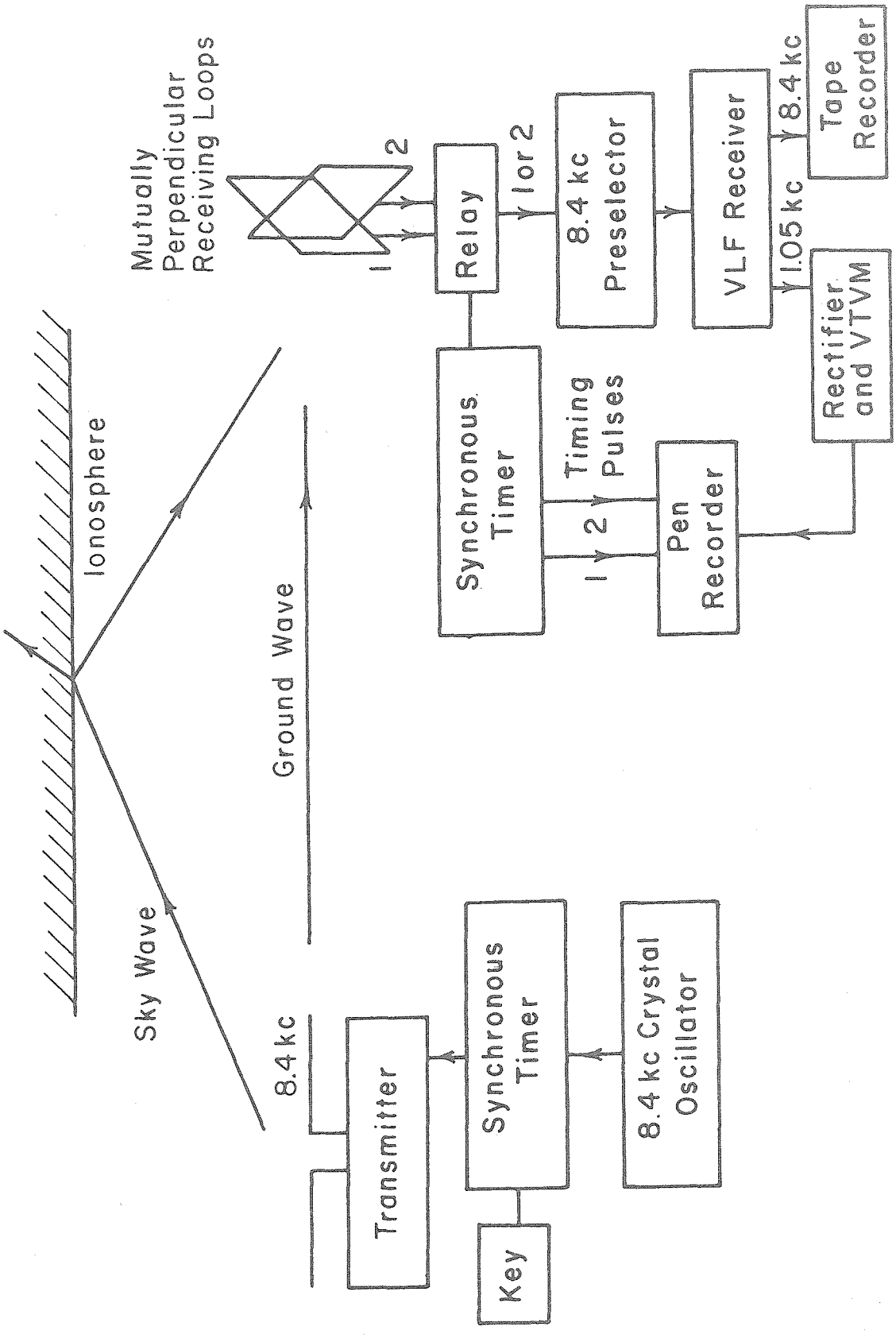

FIGURE 36. BLOCK DIAGRAM OF THE TRANSMITTING AND RECEIVING STATIONS.

output. The data have been retained on magnetic tape, and will be examined more carefully when refined detection techniques have been developed.

B. Ionospheric Sounding Experiments

The transmission scheme of figure 36 can also be used for ionospheric sounding experiments. Since the Dinkey Creek antenna was not perfectly straight (figure 32), the ground wave radiation pattern did not possess the sharp null of the idealized linear antenna (figure 6). However, at right angles to the antenna the ground wave was found to possess an appreciable minimum. By locating the receiver in this ground-wave minimum, the received signal consisted almost entirely of the sky wave reflected from the ionosphere. For a constant transmitter current, variations in the amplitude of the received signal were then caused by variations in the properties of the reflecting layer.

A considerable amount of ionospheric reflection information was obtained in this manner. By using two mutually perpendicular receiving loops, information was also obtained about the polarization of the reflected signal. Before the Dinkey Creek transmissions, no D-layer information had been obtained below 16 kc. It is expected that analysis of the data will yield valuable information about the hitherto unexplored regions of the lower ionosphere.

Examples of the data are plotted in figures 37A - 37F. The fading periods in the vicinity of local sunrise and local sunset are of special interest. At these particular times the D-layer, which exists only

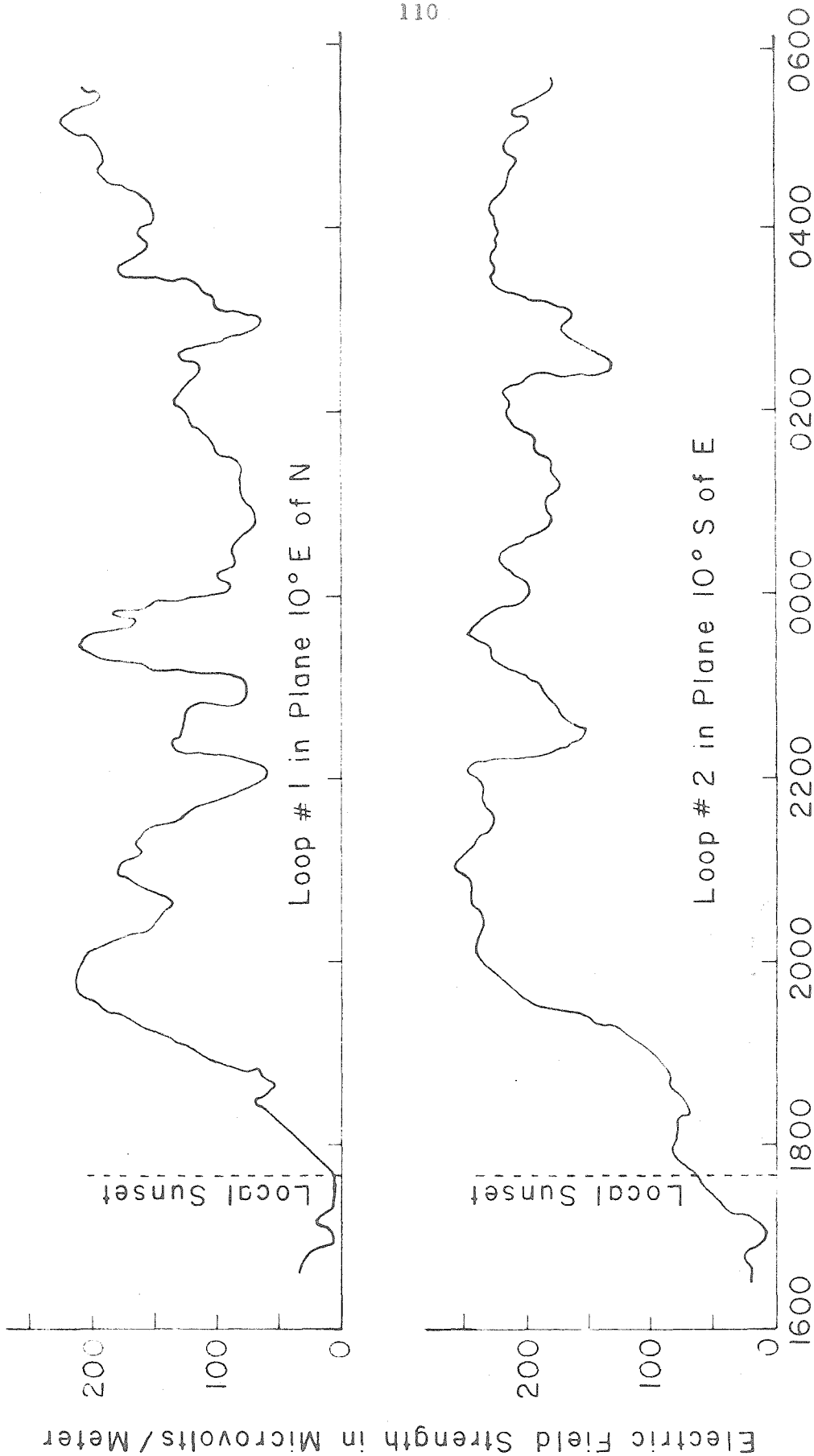

FIGURE 37A. ELECTRIC FIELD STRENGTH OF RECEIVED 8.4 KC SIGNAL RECORDED AT REEDLEY, CALIFORNIA, 20 FEBRUARY - 21 FEBRUARY 1959.

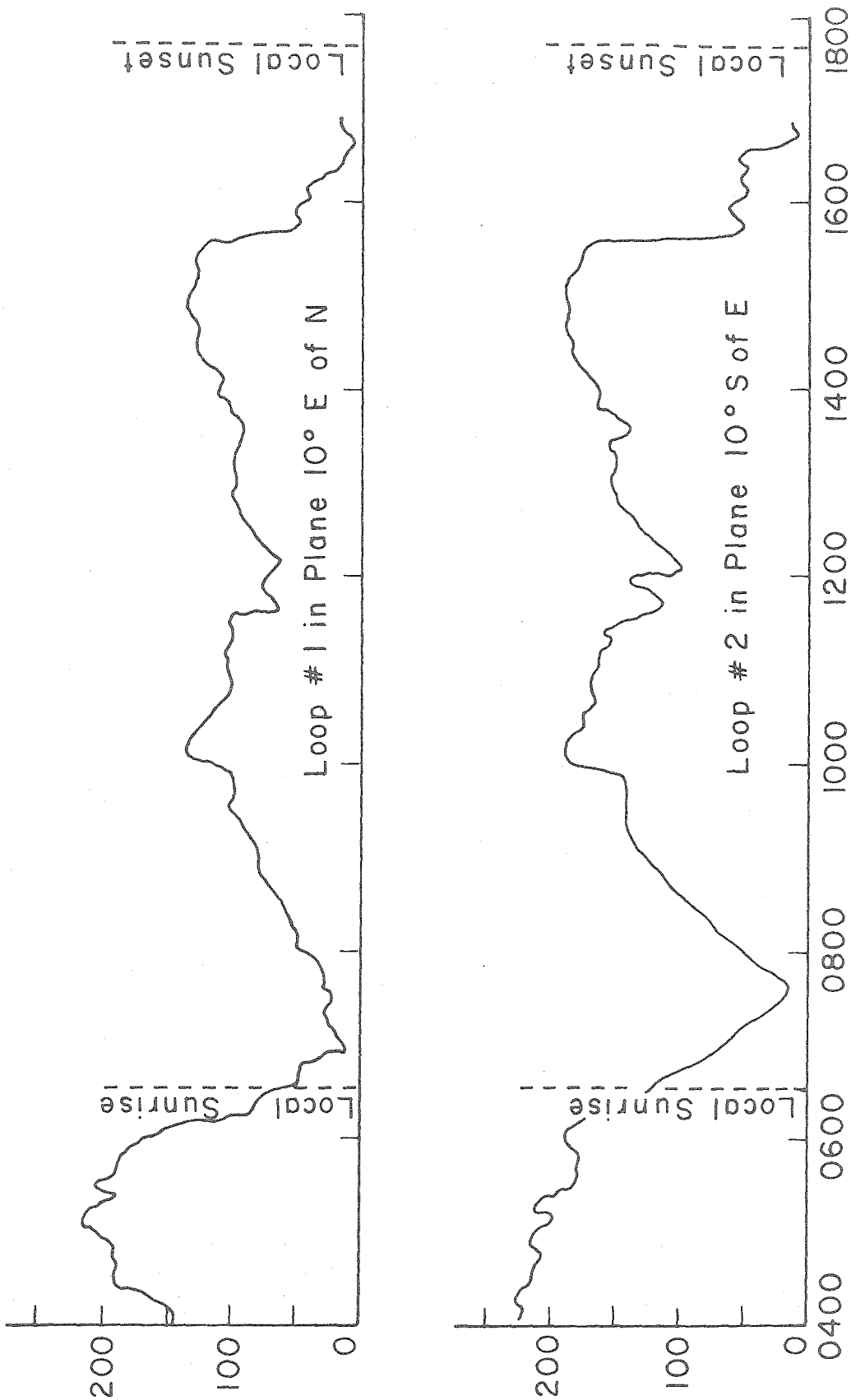

FIGURE 37B. ELECTRIC FIELD STRENGTH OF RECEIVED 8.4 KC SIGNAL RECORDED AT REEDLEY, CALIFORNIA, 21 FEBRUARY 1959.

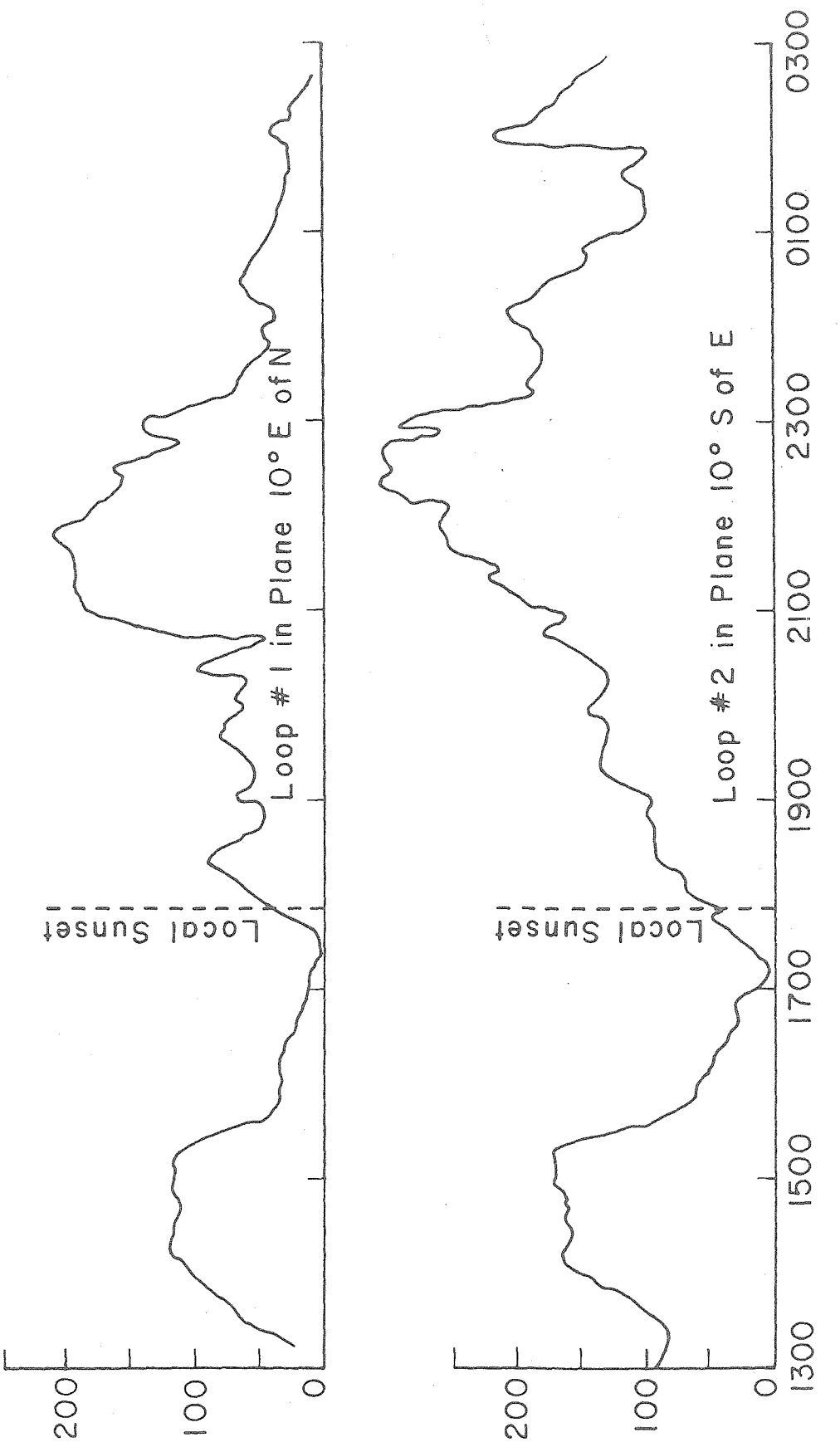

FIGURE 37C. ELECTRIC FIELD STRENGTH OF RECEIVED 8.4 KC SIGNAL RECORDED AT REEDLEY, CALIFORNIA, 6 MARCH - 7 MARCH 1959.

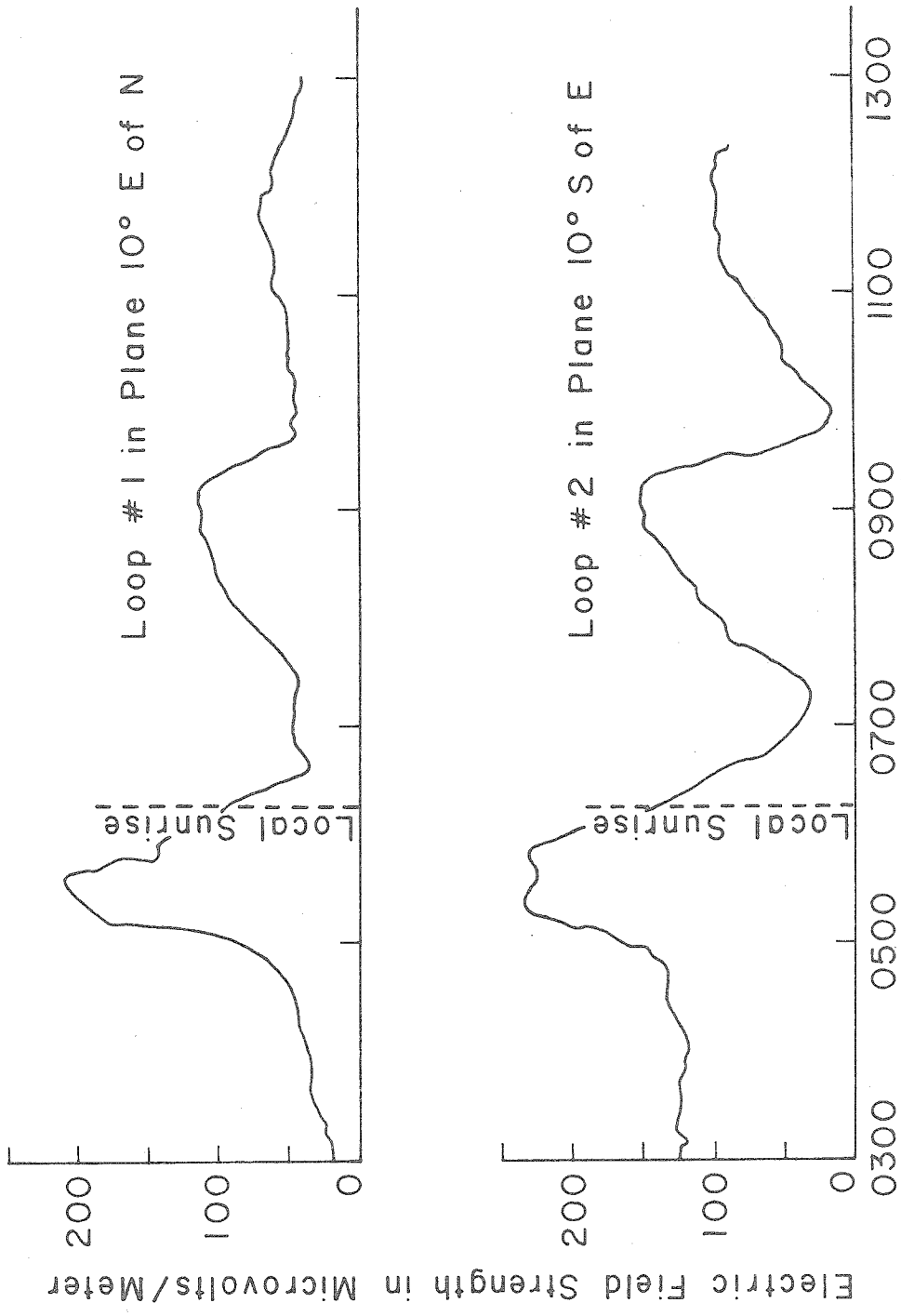

FIGURE 37D. ELECTRIC FIELD STRENGTH OF RECEIVED 8.4 KC SIGNAL RECORDED AT REEDLEY, CALIFORNIA, 7 MARCH 1959.

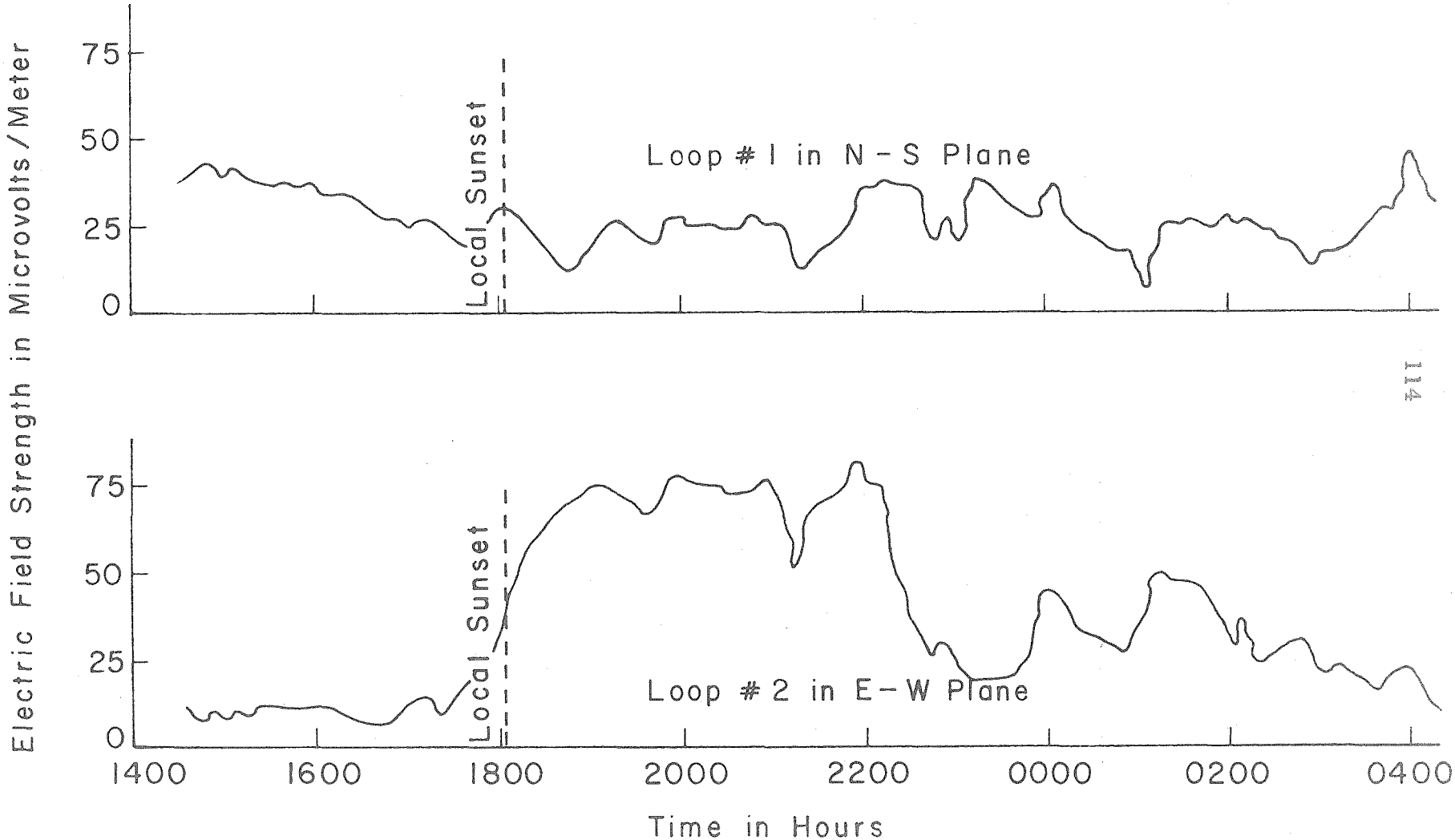

FIGURE 37E. ELECTRIC FIELD STRENGTH OF RECEIVED 8.4 KC SIGNAL RECORDED AT PASADENA, CALIFORNIA, 20 MARCH - 21 MARCH 1959.

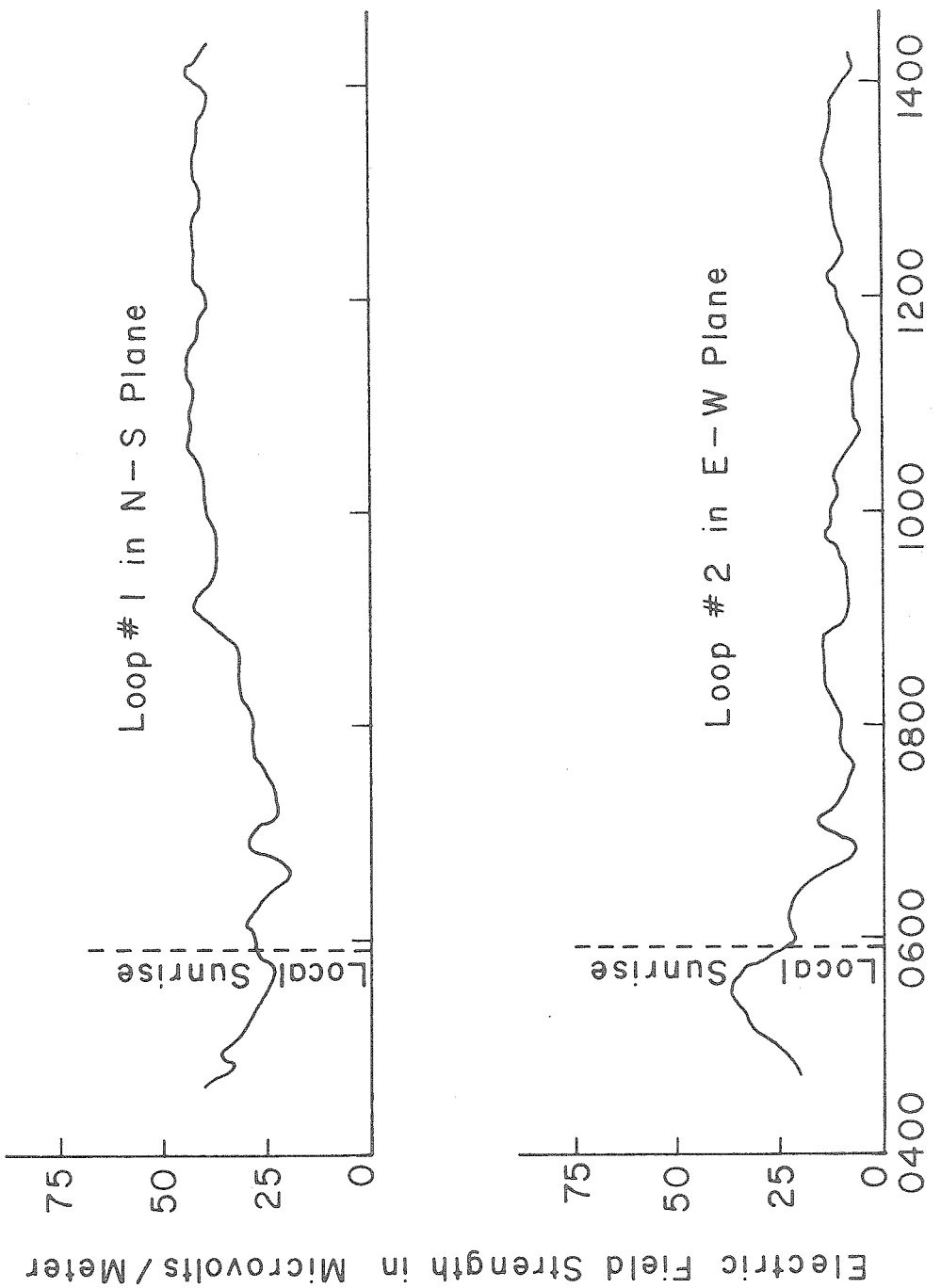

FIGURE 37F. ELECTRIC FIELD STRENGTH OF RECEIVED 8.4 KC SIGNAL RECORDED AT PASADENA, CALIFORNIA, 21 MARCH 1959.

during the daytime hours, undergoes its greatest change. It is generally accepted that the D-layer, extending from 60 to 90 km above the earth, is formed by the ionization of O_2. From the data it is apparent that during the formation and recombination processes at sunrise and sunset the absorption of vlf waves is greatest.

Since reflection coefficients are also functions of the angle of incidence, soundings were made at different locations. The various receiving locations are shown in figure 38 relative to the transmitting antenna near Shaver Lake.

C. Long-Range Propagation Experiments

Before the establishment of large scale navigation systems or world-wide standard frequency broadcasts at vlf, attenuation, fading, phase stability, etc., at these frequencies would first have to be examined. The Dinkey Creek station, being the lowest frequency high-power transmitting station in the world, should provide useful information about vlf propagation. The California receiving stations (figure 38) obtained data on relatively short-range vlf propagation. The distances from Shaver Lake to the various receiving sites were: Reedley, 35 miles; Stanford, 170 miles; Solvang, 178 miles; Pasadena, 220 miles.

In addition to the short-range receptions, a monitoring station was established at Harvard University in Cambridge, Massachusetts, 2,600 miles from the transmitter. Initial estimates indicated that the

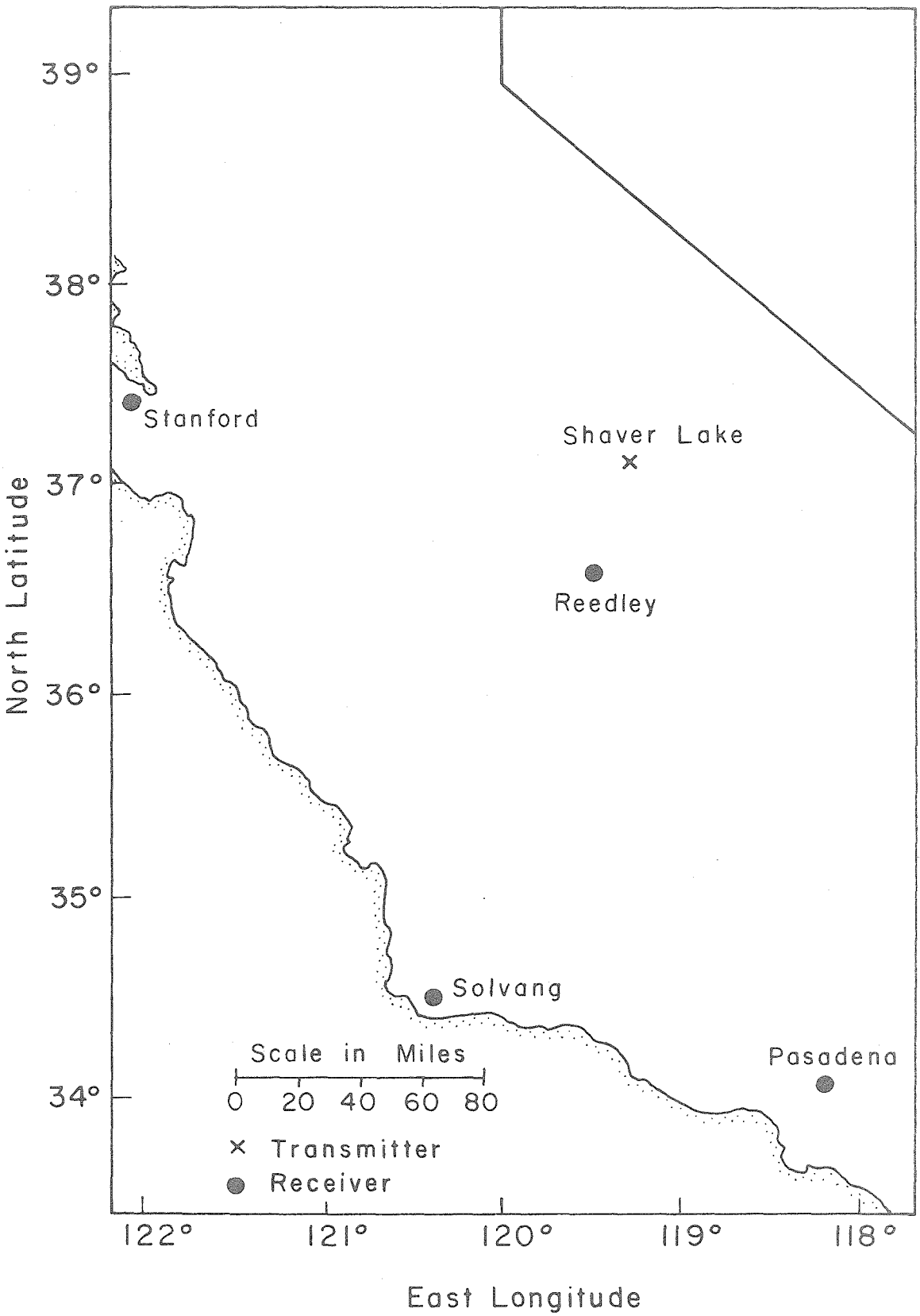

FIGURE 38. TRANSMITTING AND RECEIVING STATIONS LOCATED IN CALIFORNIA.

signal would not be detectable at this distance, since the relatively poor stability of the transmitter crystal would require a receiver bandwidth of at least 0.5 - 1.0 cycle. However, the signal was detected at Cambridge without great difficulty in two long-range experiments.

Since the signal-to-noise ratio at the Cambridge receiver was extremely small, however, conventional intensity modulation techniques were used to resolve the signal from the noise. Figure 39

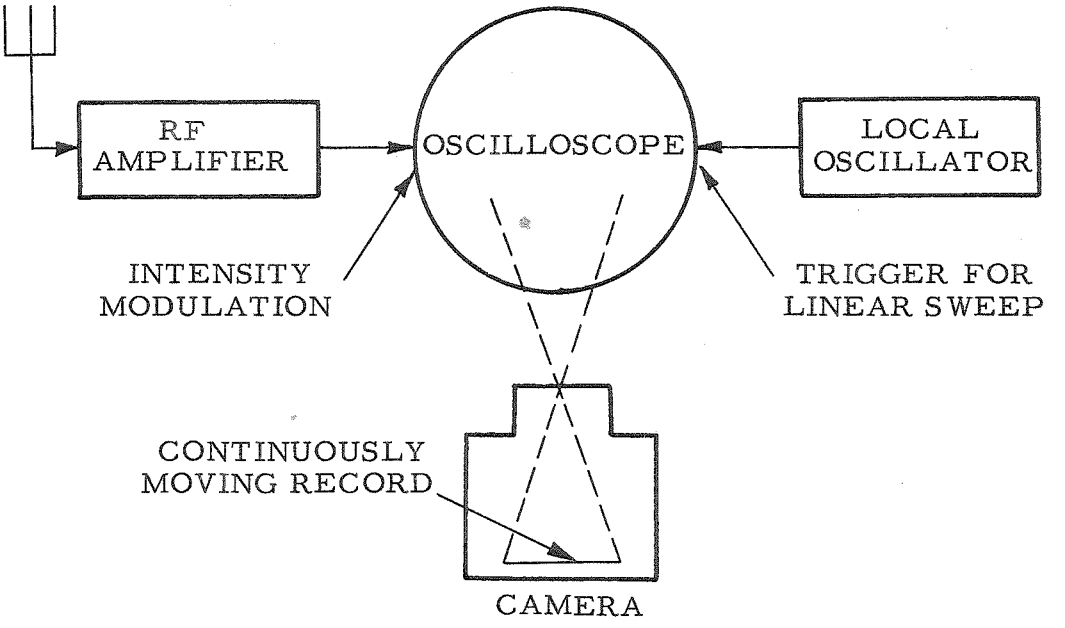

FIGURE 39. INTENSITY MODULATION SCHEME.

is a diagram of the intensity modulation method. The incoming signal is amplified and used to modulate the intensity grid of an oscilloscope. A local oscillator triggers a linear sweep of some convenient period. A camera then makes a continuous record of the scope trace. Since

the signal repeats periodically while the noise is random, the persistence of the scope face effectively integrates the signal to a detectable level. The scheme can be modified by mixing the incoming signal with a local oscillator to obtain a lower frequency for modulation of the scope intensity.

Figures 47A, 47B, and 47C contain photographic records of data from the two long-range experiments. Figure 47A is a sample of data taken about 0600 EST, 21 March 1959. The dark and light streaks indicate, respectively, the presence and absence of the signal. The transmitter was being keyed on and off at approximately a three minute - one minute rate. These data were obtained by mixing the 8.4 kc signal with a local oscillator to obtain 100 cps intensity modulation. The receiver bandwidth was 2 - 3 cps. Figures 47B and 47C are samples of the data from 28 March 1959. The dark streaks again indicate the presence of the signal. During this reception the 8.4 kc signal directly modulated the scope intensity. Individual 8.4 kc cycles can be identified on the record. However, inadequate transmitter stability caused abrupt changes in the record. A sufficiently stable source would have produced solid lines on the record instead of the "herringbone" pattern.

The 8.4 kc Dinkey Creek signal was also detected by the Radio Corporation of America at Rocky Point, New York.

It was only possible to detect the bare presence of the Cambridge and Rocky Point signals. Field strengths, stabilities, etc., could not be determined. The receiver bandwidth must be decreased to obtain

such information, which would necessitate an adequate phase-stable source at the transmitter. However, the unexpected detection of the signal over the 2,600-mile path indicates less attenuation than originally expected. The Navy transmitting antennas, for example, radiate several hundred kw. The estimated radiated power of the Dinkey Creek transmissions was only 100 watts. A more stable signal transmitted from the Dinkey Creek antenna could then be detected at greater distances, possibly on a world-wide basis.

V. SUMMARY

The power-line transmitting antenna system, described in this thesis, is well suited for many vlf propagation experiments. Being much lower in cost than conventional vlf transmitting antennas, it also possesses an unlimited prime source of power - the power line itself. When the line traps of the system isolate a half-wavelength section, the radiation pattern is ideal for ionospheric experiments: radiation is maximum in the vertical direction, and the signal detected by a receiver located in the ground-wave minimum consists almost entirely of the reflected sky wave. Well-designed line traps virtually eliminate radio frequency current from the power line beyond the antenna section.

The Dinkey Creek power-line antenna was used primarily for ionospheric experiments at 8.4 kc. Measurements of the amplitude variations of the reflected sky wave signal revealed information about the lower regions of the ionosphere. Although the initial whistler-mode experiments were unsuccessful, it was apparent that more refined detection techniques were needed to resolve the echoes from the atmospheric noise. Further whistler-mode experiments with the Dinkey Creek transmitter are planned when adequate circuitry has been developed to analyze the data.

Successful transcontinental detection of the 8.4 kc signal at Cambridge and Rocky Point indicates that the antenna system is also capable of long-range propagation. Before additional long-range experiments are conducted, however, the transmitted signal should

be stabilized to a greater degree. Transoceanic propagation experiments would also provide valuable information on the attenuation over a sea-water path.

The ionospheric sounding experiments could be refined with suitable phase-stable oscillators at both transmitter and receiver. The phase of the reflected sky wave signal could then be directly compared with the standard phase of a local oscillator. Direct high frequency links to provide a standard phase reference could be eliminated. Such phase measurements would provide information on the virtual height of the ionosphere, information previously unavailable at frequencies below 16 kc.

The usefulness of the Dinkey Creek antenna system was enhanced by the presence of the unfractured granitic substructure in the Sierras, which led to a higher radiation efficiency for the horizontal antenna. The success of the transcontinental propagation experiments was achieved by selecting ground with the highest possible resistivity. Antenna efficiency (cf. Section I-B) should be an important consideration in the design of power-line antennas. However, even under the most favorable ground conditions, horizontal antennas are limited to radiation efficiencies of only a few percent at very low frequencies. The power-line antenna would be unsuitable for long-range, high-power applications. Nevertheless, under favorable geological conditions, the power-line antenna provides an extremely useful experimental facility.

The Dinkey Creek transmissions were conducted entirely at 8.4 kc. The transmission frequency could have been varied over a small range

of about $\pm$ 50 cps. This range was limited by the narrow bandwidth of the high-Q line traps. Although a small class of narrowband variable-frequency transmissions was then possible, the power-line antenna is basically a fixed-frequency system.

However, by employing similar techniques, it would be possible to construct a multi-tuned antenna system. To make the system half-wave resonant at n different frequencies $f_1, f_2, \cdots f_n$, it would only be necessary to locate n sets of line traps in the line, each set being resonant at a different one of the n frequencies and located one half-wavelength apart at that frequency. When the system was excited at any one of the resonant frequencies f_n, the $n-1$ off-resonance line traps would present negligible impedance. At each resonant frequency f_n the feedpoint impedance would be equal to the value calculated in Section II (figure 22). In this manner the multi-tuned power-line antenna could transmit at any one of the n resonant frequencies, individually or simultaneously. (Other tuned vlf trans-mitting antennas are limited to operation at one frequency at a time.) Further investigation could be made into the operation of such a multi-tuned vlf transmitting system.

The matrix method, developed in this thesis for analyzing the power-line antenna, can be applied to the general loaded, linear antenna problem. When used with adequate machine computation facilities, the matrix method can be extended to the linear antenna with virtually any type of loading or feeding. Arrays of linear antennas can also be analyzed. The ultimate limitation of the matrix method lies in the

slowness of the convergence of the current series. For a certain desired accuracy, this limitation is determined by the size of the computer memory available and the nature of its round-off error. A useful ground for further research would be to examine the convergence in greater detail than the approximate relations II-35 and II-36. However, for simple loading geometries (e.g., figure 10), the matrix method provides an accurate solution for the current distribution with relatively few terms in the expansion.

REFERENCES

1. Collins, A.F.; Wireless Telegraphy. McGraw Publishing Co., New York, (1905) p. 127.

2. Espenshied, L., C.N. Anderson, and A. Bailey; "Transatlantic Radio Telephone Transmission," Proc. IRE, Vol. 14, (January 1926) pp. 7-56.

3. Terman, F.E.; Electronic and Radio Engineering. McGraw-Hill Book Co., Inc., New York, (1955) p. 850.

4. Budden, K.G., J.A. Ratcliffe, and M.V. Wilkes; "Further Investigations of Very Long Waves Reflected from the Ionosphere," Proc. Roy. Soc., Vol. A-171, (1939) pp. 188-214.

5. Storey, L.R.O.; "An Investigation of Whistling Atmospherics," Phil. Trans. Roy. Soc., Vol. 246-A, (1953) pp. 113-141.

6. Pierce, J.A.; "Intercontinental Frequency Comparison by Very Low Frequency Radio Transmission," Proc. IRE, Vol. 45, (June 1958) pp. 794-803.

7. George, W.D.; "Proposal for Standard Frequency Broadcast at Very Low Frequencies," Paper No. 41 at VLF Symposium, Boulder, Colorado, (January 1958).

8. Pierce, J.A., A.A. McKenzie, and R.H. Woodward; Loran. McGraw-Hill Book Co., Inc., New York, (1948) p. 108.

9. Laport, E.A.; Radio Antenna Engineering. McGraw-Hill Book Co., Inc., New York, (1952) pp. 18-76.

10. Terman, F.E.; Radio Engineers' Handbook. McGraw-Hill Book Co., Inc., New York, (1943) pp. 841-843.

11. Hobart, T.D.; "Navy VLF Transmitter Will Radiate 1000 KW," Electronics, (December 1952) pp. 98-101.

12. Bernstein, H.E.; private communication (May 1956).

13. Gustavson, W.E.; private communication (October 1958).

14. Stanesby, H.; private communication (February 1959).

15. Shaughnessy, E.H.; "The Rugby Radio Station of the British Post Office," Proc. Inst. Elec. Eng., Vol. 164, (June 1926) pp. 683-712.

16. Macmillan, R.S.; "Some Properties of the Ionosphere at Low Radio Frequencies," Ph.D. Thesis, California Institute of Technology, (1954).

17. Bergman, C.W., R.S. Macmillan, and W.H. Pickering; "A New Technique for Investigating the Ionosphere at Low and Very Low Frequencies," Rocket Exploration of the Upper Atmosphere. Interscience Publishers, Inc., New York, (1954) pp. 247-255.

18. Golden, R.M., R.S. Macmillan, W.V.T. Rusch; "A VLF Antenna for Generating a Horizontally Polarized Radiation Field," AFOSR-TN-57-9 ASTIA Doc. No. AD 115041, (February 1958).

19. Cheek, R.C.; "Power Line Carrier Application," Westinghouse Handbook of Transmission and Distribution. (1950) pp. 401-432.

20. Hallén, E.; "Theoretical Investigations into Transmitting and Receiving Antennae," Nova Acta Regiae Soc. Sci. Upsaliensis, Vol. 4, (1938), p. 1.

21. Smythe, W.R.; Static and Dynamic Electricity. McGraw-Hill Book Co., Inc., New York, (1950) pp. 441-442.

22. King, R.W.P.; The Theory of Linear Antennas. Harvard University Press, Cambridge, (1956) p. 16, pp. 69-262.

23. Storm, B.; "Cylindrical Aerials," Wireless Engineer, Vol. 29, (July 1952) pp. 174-176.

24. Nomura, Y. and T. Hatta; "The Theory of a Linear Antenna (I)," Technology Reports, Tohoku University, Vol. 17, (1952) pp. 1-18.

25. Stratton, J.A.; Electromagnetic Theory. McGraw-Hill Book Co., Inc., New York, (1941) pp. 440, 537, 575.

26. Hebert, K.J. and H. Fox; "Semi-automatic Coding (SAC) for the Datatron with Simulated Matrix Commands," Computing Center Technical Report, California Institute of Technology, Pasadena, (January 1958).

27. Franklin, J.N. and K.J. Hebert; "A Simple Compiler for Automatic Programming of a Digital Computer," Computing Center Technical Report, California Institute of Technology, Pasadena, (January 1959).

28. Ramo, S. and J.R. Whinnery; Fields and Waves in Modern Radio. John Wiley and Sons, Inc., New York, (1953) pp. 207-229.

29. Sommerfeld, A.; Partial Differential Equations in Physics. Academic Press, Inc., New York, (1949) pp. 257-265.

30. Norton, K.A.; "The Propagation of Radio Waves Over the Surface of the Earth and in the Upper Atmosphere," Proc. IRE, Vol. 25, (September 1937) pp. 1203-1236.

31. Golden, R.M., R.V. Langmuir, R.S. Macmillan, and W.V.T. Rusch; "Design and Construction of Equipment Used to Operate a Commercial Power Line as a Very Low Frequency Antenna," AFOSR-TN-58-908, ASTIA Doc. No. AD 204 514, (October 1958).

32. Golden, R.M., R.S. Macmillan, R. Nathan, and W.V.T. Rusch; "A Calculation of the Radiation Fields of Whistling Atmospherics," AFOSR-TN-57-10, ASTIA Doc. No. AD 115 042, (June 1956).

APPENDIX I

EVALUATION OF THE IMPEDANCE MATRIX

$$Z_{nm} = -\frac{(\beta_o^2 - k_n^2)}{I_m} \int_{-h}^{+h} \sin(k_n z + \alpha_n) \frac{(-j\omega)}{\beta_o^2} A_m(a, z)\,dz$$

$$+ \frac{k_n}{I_m}(-1)^n \frac{(-j\omega)}{\beta_o^2} A_m(a, h) - \frac{k_n}{I_m} \frac{(-j\omega)}{\beta_o^2} A_m(a, -h) \qquad \text{(II-27)}$$

From equation II-25

$$A_m(a, h) = \frac{\mu I_m}{4\pi} \int_{-h}^{+h} \left[\frac{e^{j(k_m z' + \alpha_m)} - e^{-j(k_m z' + \alpha_m)}}{2j} \right] \cdot$$

$$\cdot \frac{e^{-j\beta_o \sqrt{a^2 + (z' - h)^2}}}{\sqrt{a^2 + (z' - h)^2}}\,dz' \qquad \text{(A-1)}$$

Then define:

$$t \triangleq \frac{1}{2}(r - z' + h) \qquad \text{(A-2)}$$

so that

$$\frac{dt}{t} = -\frac{dz'}{r} \qquad \text{(A-3a)}$$

$$\beta_o r - k_m z' + k_m h = (\beta_o + k_m)t + (\beta_o - k_m)\frac{a^2}{4t} \qquad \text{(A-3b)}$$

$$\beta_o r + k_m z' - k_m h = (\beta_o - k_m)t + (\beta_o + k_m)\frac{a^2}{4t} \qquad \text{(A-3c)}$$

Substitution of equations A-3 into A-1 yields:

$$A_m(a,h) = \frac{\mu I_m}{4\pi}\left\{ e^{j(k_m h + \alpha_m)} \int_{\frac{a}{2}}^{\frac{\sqrt{a^2+4h^2}+2h}{2}} \cdot \left[e^{-j\left[(\beta_o+k_m)t+(\beta_o-k_m)\frac{a^2}{4t}\right]} - e^{-j\left[(\beta_o-k_m)t+(\beta_o+k_m)\frac{a^2}{4t}\right]} \right] \frac{dt}{t} \right\} \quad \text{(A-4)}$$

Neglecting the terms in a^2, and using the definitions of the sine and cosine integrals

$$Si(x) = \int_0^x \frac{\sin x}{x}\, dx \quad \text{(A-5a)}$$

$$Ci(x) = -\int_x^\infty \frac{\cos x}{x}\, dx \quad \text{(A-5b)}$$

Equation A-4 becomes

$$\frac{(-j\omega)}{\beta_o^2} A_m(a,h) = \frac{I_m}{8\pi\varepsilon\omega}(-1)^m \left\{ Ci\left[(\beta_o - k_m)2h\right] - Ci\left[(\beta_o + k_m)2h\right] + \log\frac{(\beta_o - k_m)}{|\beta_o - k_m|} + jSi\left[(\beta_o + k_m)2h\right] - jSi\left[(\beta_o - k_m)2h\right] \right\} \quad \text{(A-6)}$$

In a similar manner, it can be shown that

$$\frac{(-j\omega)}{\beta_o^2} A_m(a,-h) = \frac{I_m}{8\omega\varepsilon\pi}\left\{ C_i\left[(\beta_o + k_m)2h\right] - Ci\left[(\beta_o - k_m)2h\right] - \log\frac{(\beta_o + k_m)}{|\beta_o - k_m|} + jSi\left[(\beta_o - k_m)2h\right] - jSi\left[(\beta_o + k_m)2h\right]\right\} \quad (A\text{-}7)$$

It now remains to evaluate

$$-\frac{\beta_o^2 - k_n^2}{I_m}\int_{-h}^{h} \sin(k_n z + a_n)\frac{(-j\omega)}{\beta_o^2} A_m(a,z)dz = -j\frac{(\beta_o^2 - k_n^2)}{4\pi\varepsilon\omega} J \quad (A\text{-}8a)$$

where

$$J \triangleq \int_{-h}^{+h} \sin(k_n z + a_n)dz \int_{-h}^{+h} \sin(k_m z' + a_m)\frac{e^{-j\beta_o\sqrt{a^2 + (z'-z)^2}}}{\sqrt{a^2 + (z'-z)^2}} dz' \quad (A\text{-}8b)$$

It can be shown that $J=0$ unless n and m are both even or odd. Expanding the sine functions as the sum of two exponentials, equation A-8b becomes

$$J = -\frac{1}{2}\left\{ e^{j(m+n)\frac{\pi}{2}} \int_{-h}^{o} e^{j(k_m+k_n)z}\, dz \int_{-h}^{+h} e^{+jk_m z' - j\beta_o r - jk_m z} \frac{dz'}{r} \right.$$

$$- e^{-j(m-n)\frac{\pi}{2}} \int_{-h}^{o} e^{-j(k_m-k_n)z}\, dz \int_{-h}^{+h} e^{-jk_m z' - j\beta_o r + jk_m z} \frac{dz'}{r}$$

$$- e^{j(m-n)\frac{\pi}{2}} \int_{-h}^{o} e^{j(k_m-k_n)z}\, dz \int_{-h}^{+h} e^{jk_m z' - j\beta_o r - jk_m z} \frac{dz'}{r}$$

$$\left. + e^{-j(m+n)\frac{\pi}{2}} \int_{-h}^{o} e^{-j(k_m+k_n)z}\, dz \int_{-h}^{+h} e^{-jk_m z' - j\beta_o r + jk_m z} \frac{dz'}{r} \right\} \qquad \text{(A-9)}$$

where

$$r = \sqrt{a^2 + (z' - z)^2}$$

Now, define:

$$\delta_1 \triangleq (m + n) \qquad \delta_2 \triangleq (m - n) \qquad \text{(A-10a)}$$

$$\alpha_1 \triangleq (k_m + k_n) \qquad \alpha_2 \triangleq (k_m - k_n) \qquad \text{(A-10b)}$$

$$\beta \triangleq (\beta_o + k_m) \qquad \beta' \triangleq (\beta_o - k_m) \qquad \text{(A-10c)}$$

$$t \triangleq \frac{1}{2}(r + z' - z), \frac{dt}{t} = \frac{dz'}{r} \qquad \text{(A-10d)}$$

$$f(\beta', \beta, t) \triangleq \frac{e^{-j\left[\beta' t + \beta \frac{a^2}{4t}\right]}}{t} \qquad \text{(A-10e)}$$

$$t_1(z) \triangleq \frac{1}{2}\left[\sqrt{a^2 + (h+z)^2} - (h+z)\right] \qquad \text{(A-10f)}$$

$$t_2(z) \triangleq \frac{1}{2}\left[\sqrt{a^2 + (h-z)^2} + (h-z)\right] \qquad \text{(A-10g)}$$

Then

$$J = -\frac{1}{2} e^{j\delta_1 \frac{\pi}{2}} \int_{-h}^{0} e^{j\alpha_1 z}\, dz \int_{t_1(z)}^{t_2(z)} f(\beta', \beta, t)\, dt$$

$$+ \frac{1}{2} e^{-j\delta_2 \frac{\pi}{2}} \int_{-h}^{0} e^{-j\alpha_2 z}\, dz \int_{t_1(z)}^{t_2(z)} f(\beta', \beta, t)\, dt$$

$$+ \frac{1}{2} e^{j\delta_2 \frac{\pi}{2}} \int_{-h}^{0} e^{+j\alpha_2 z}\, dz \int_{t_1(z)}^{t_2(z)} f(\beta', \beta, t)\, dt$$

$$- \frac{1}{2} e^{-j\delta_1 \frac{\pi}{2}} \int_{-h}^{0} e^{-j\alpha_1 z}\, dz \int_{t_1(z)}^{t_2(z)} f(\beta', \beta, t)\, dt \qquad \text{(A-11)}$$

$$= J_1 + J_2 + J_3 + J_4$$

Since all four integrals have the same form, only the first will be integrated as an example. Changing the order of integration of the first integral of equation A-11:

$$J_1 = -\frac{1}{2} e^{j\delta_1 \frac{\pi}{2}} \left\{ \int_{\frac{a^2}{4h}}^{\frac{a}{2}} f(\beta', \beta, t)dt \int_{z_1(t)}^{o} e^{j\alpha_1 z} dz \right.$$

$$+ \int_{\frac{a}{2}}^{h} f(\beta', \beta, t)dt \int_{-h}^{o} e^{j\alpha_1 z} dz$$

$$\left. + \int_{h}^{2h} f(\beta', \beta, t)dt \int_{-h}^{z_2(t)} e^{j\alpha_1 z} dz \right\} \qquad \text{(A-12)}$$

where

$$z_1(t) = -t - h + \frac{a^2}{4t} \qquad \text{(A-13a)}$$

and

$$z_2(t) = -t + h + \frac{a^2}{4t} \qquad \text{(A-13b)}$$

Carrying out the integration over z and substituting in the limits $z_1(t)$ and $z_2(t)$, for $\alpha_1 \neq 0$:

$$J_1 = \frac{-\frac{1}{2} e^{j\delta_1 \frac{\pi}{2}}}{j\alpha_1} \left\{ e^{j\alpha_1 h} \int_h^{2h} f(\beta', \beta, t)\, e^{-j\alpha_1 t + j\alpha_1 \frac{a^2}{4t}}\, dt \right.$$

$$- e^{-j\alpha_1 h} \int_{\frac{a}{2}}^{2h} f(\beta', \beta, t)\, dt + \int_{\frac{a}{2}}^{h} f(\beta', \beta, t) dt + \int_{\frac{a^2}{4h}}^{\frac{a}{2}} f(\beta', \beta, t) dt$$

$$\left. - e^{-j\alpha_1 h} \int_{\frac{a^2}{4h}}^{\frac{a}{2}} f(\beta', \beta, t)\, e^{-j\alpha_1 t + j\alpha_1 \frac{a^2}{4t}}\, dt \right\} \qquad \text{(A-14)}$$

Finally, making a substitution $t' = \frac{a^2}{4t}$ in the last two integrals of equation A-14, and neglecting terms in a^2 :

$$J_1 = \frac{-e^{j\delta_1 \frac{\pi}{2}}}{j\alpha} \left\{ e^{j\alpha_1 h} \int_h^{2h} e^{-j(\beta' + \alpha_1)t} \frac{dt}{t} - e^{-j\alpha_1 h} \int_{\frac{a}{2}}^{2h} d^{-j\beta' t} \frac{dt}{t} \right.$$

$$+ \int_{\frac{a}{2}}^{h} e^{-j\beta' t} \frac{dt}{t} + \int_{\frac{a}{2}}^{h} e^{-j\beta t} \frac{dt}{t}$$

$$\left. - e^{-j\alpha_1 h} \int_{\frac{a}{2}}^{h} e^{-j(\beta - \alpha_1)t} \frac{dt}{t} \right\} \qquad \text{(A-15)}$$

Evaluation of J_2 , J_3 , and J_4 results in forms similar to A-15. Substitution then into equation A-11 produces:

$$J = j\frac{k_n}{k_m^2 - k_n^2}\left\{ Ci\left[(\beta_o - k_m)2h\right] - jSi\left[(\beta_o - k_m)2h\right] - Ci\left[(\beta_o + k_m)2h\right] \right.$$

$$\left. - jSi\left[(\beta_o + k_m)2h\right] + \log\frac{\beta_o + k_m}{|\beta_o - k_m|} \right\}$$

$$+ j\frac{k_m}{k_m^2 - k_n^2}\left\{ Ci\left[(\beta_o + k_n)2h\right] - jSi\left[(\beta_o + k_n)2h\right] - Ci\left[(\beta_o - k_n)2h\right] \right.$$

$$\left. + jSi\left[(\beta_o - k_n)2h\right] - \log\frac{\beta_o - k_n}{|\beta_o - k_n|} \right\} \qquad \text{(A-16)}$$

Then, from equations II-27, A-6, A-7, A-8a, A-16, when $m \neq n$ and both m and n are even or odd:

$$Z_{mn} = -\frac{k_m}{4\pi\varepsilon_o\omega}\frac{\beta_o^2 - k_n^2}{k_n^2 - k_m^2}\left\{ Ci\left[(\beta_o - k_n)2h\right] - Ci\left[(\beta_o + k_n)2h\right] \right.$$

$$\left. + jSi\left[(\beta_o + k_n)2h\right] - jSi\left[(\beta_o - k_n)2h\right] + \log\frac{\beta_o + k_n}{|\beta_o - k_n|} \right\}$$

$$+\frac{k_n}{4\pi\varepsilon_o\omega}\frac{\beta_o^2 - k_m^2}{k_n^2 - k_m^2}\left\{ Ci\left[(\beta_o - k_m)2h\right] - Ci\left[(\beta_o + k_m)2h\right] \right.$$

$$\left. + jSi\left[(\beta_o + k_m)2h\right] - jSi\left[(\beta_o - k_m)2h\right] + \log\frac{\beta_o + k_m}{|\beta_o - k_m|} \right\}$$

(A-17)

From equation A-12, when $a = 0$ or $n = m$, it can be shown that

$$J = -\frac{j}{2k_n}\left\{\int_{\frac{a}{2}}^{2h} e^{-j(\beta_o - k_n)t}\,\frac{dt}{t} - \int_{\frac{a}{2}}^{h} e^{-j(\beta_o + k_n)t}\,\frac{dt}{t}\right\}$$

$$-\frac{j}{2(\beta_o - k_n)}\left\{e^{-j(\beta_o - k_n)t} - 1\right\} - \frac{j}{2(\beta_o + k_n)}\left\{e^{-j(\beta_o + k_n)t} - 1\right\}$$

$$+ h\left\{\int_{\frac{a}{2}}^{2h} e^{-j(\beta_o + k_n)t}\,\frac{dt}{t} + \int_{\frac{a}{2}}^{2h} e^{-j(\beta_o - k_n)t}\,\frac{dt}{t}\right\} \qquad \text{(A-18)}$$

so that

$$Z_{nn} = \frac{1}{8\pi\epsilon_o\omega}\left[\frac{(\beta_o^2 + k_n^2)}{k_n}\left\{Ci\left[(\beta_o - k_n)2h\right] - Ci\left[(\beta_o + k_n)2h\right] + \log\frac{\beta_o + k_n}{|\beta_o - k_n|}\right\}\right.$$

$$+ (\beta_o + k_n)\cos\left[(\beta_o - k_n)2h\right] + (\beta_o - k_n)\cos\left[(\beta_o + k_n)2h\right] - 2\beta_o$$

$$+ (\beta_o^2 - k_n^2)2h\left\{Si\left[(\beta_o - k_n)2h\right] + Si\left[(\beta_o + k_n)2h\right]\right\}$$

$$- j\frac{(\beta_o^2 + k_n^2)}{\beta_o}\left\{Si\left[(\beta_o - k_n)2h\right] - Si\left[(\beta_o + k_n)2h\right]\right\}$$

$$- j(\beta_o + k_n)\sin\left[(\beta_o - k_n)2h\right] - j(\beta_o - k_n)\sin\left[(\beta_o + k_n)2h\right]$$

$$+ j(\beta_o^2 - k_n^2)2h\left\{Ci\left[(\beta_o - k_n)2h\right] + Ci\left[(\beta_o + k_n)2h\right]\right.$$

$$\left.\left. - 2\log\gamma - \log\left|\beta_o^2 - k_n^2\right| - 2\log\frac{a}{2}\right\}\right] \qquad \text{(A-19)}$$

where $\gamma \cong 1.781$.

Finally, if $\frac{4h}{\lambda_o} \triangleq s$ (not necessarily an integer), i.e., the antenna is s half-wavelengths long:

$$R_{mn} = -30\frac{m}{s}\left[\frac{s^2-n^2}{n^2-m^2}\right]\left\{Ci(s-n)\pi - Ci(s+n)\pi + \log\frac{s+n}{|s-n|}\right\} + 30\frac{n}{s}\left[\frac{s^2-m^2}{n^2-m^2}\right]\left\{Ci(s-m)\pi - Ci(s+m)\pi + \log\frac{s+m}{|s-m|}\right\} \quad (A-20)$$

$$X_{mn} = 30\frac{m}{s}\left[\frac{s^2-n^2}{n^2-m^2}\right]\left\{Si(s-n)\pi - Si(s+n)\pi\right\} - 30\frac{n}{s}\left[\frac{s^2-m^2}{n^2-m^2}\right]\left\{Si(s-m)\pi - Si(s+m)\pi\right\} \quad (A-21)$$

$$R_{nn} = 15\frac{(s^2+n^2)}{sn}\left\{Ci(s-n)\pi - Ci(s+n)\pi + \log\frac{s+n}{|s-n|}\right\} + 15\frac{1}{s}\left\{(s+n)\cos(s-n)\pi + (s-n)\cos(s+n)\pi - 2s\right\} + 15\frac{(s^2-n^2)}{s}\pi\left\{Si(s+n)\pi + Si(s-n)\pi\right\} \quad (A-22)$$

$$X_{nn} = -15\frac{(s^2+n^2)}{sn}\left\{Si(s-n)\pi - Si(s+n)\pi\right\} - 15\frac{1}{s}\left\{(s+n)\sin(s-n)\pi + (s-n)\sin(s+n)\pi\right\} + 15\frac{(s^2-n^2)}{s}\pi\left\{Ci(s+n)\pi + Ci(s-n)\pi - \log(s+n) - \log|s-n| - 2\log\frac{a\pi}{4h} - 2\log\gamma\right\} \quad (A-23)$$

APPENDIX II

The following computer program was used to evaluate $\left[I_m^i\right]$ and $\left[I_m^r\right]$ from equations II-32a and II-32b. The calculation was carried out on the Burroughs Datatron 205 digital computer, using the semi-automatic coding scheme (SAC) with simulated matrix commands .

Sign	Spare	Command	Address	Remarks
4	0000	00	7000	Read Input
0	0020	42	0017	Bring SAC off of magnetic tape
0	4320	40	2600	
0	0000	28	7001	
0	0000	30	2600	
6	0000	20	7000	
4	0000	00	3460	
0	0000	02	0749	Number of routine
6	0000	30	2691	
0	0000	00	0001	
6	0000	30	2700	
0	0000	31	8502	Define Dictionary
0	0000	00	1500	
0	0000	31	8501	Matrix
0	0000	00	8507	Transfer A to C
0	0200	05	0000	$M_2 = M_5 = \left[X_{nm}\right]$
0	0000	31	8501	Matrix
0	0000	00	8510	C = A + B
0	0103	03	0000	$M_3 = \left[R_{nm}\right] + \left[F\right]$
0	0000	31	8501	Matrix
0	0000	00	8507	Transfer A to C
0	0300	06	0000	$M_3 = M_6 = \left[R_{nm}\right] + \left[F_{nm}\right]$
0	0000	31	8501	Matrix

Sign	Spare	Command	Address	Remarks
0	0000	00	8513	B = AC
0	0503	03	0000	$M_3 = [X_{nm}]^{-1}([R_{nm}] + [F_{nm}])$
0	0000	31	8501	Matrix
0	0000	00	8512	AB = C
0	0603	03	0000	$M_3 = ([R_{nm}] + [F_{nm}])[X_{nm}]^{-1} \cdot ([R_{nm}] + [F_{nm}])$
0	0000	31	8501	Matrix
0	0000	00	8510	C = A + B
0	0302	03	0000	$M_3 = ([R_{nm}] + [F_{nm}])[X_{nm}]^{-1} \cdot ([R_{nm}] + [F_{nm}]) + [X_{nm}]$
0	0000	31	8501	Matrix
0	0000	00	8513	B = AC
0	0304	08	0000	$M_8 = \left\{([R_{nm}] + [F_{nm}])[X_{nm}]^{-1} \cdot ([R_{nm}] + [F_{nm}]) + [X_{nm}]\right\}^{-1}$
0	0000	31	8501	Matrix
0	0000	00	8513	B = AC
0	0304	08	0000	$M_8 = -[I^i_m]$
0	0000	31	8501	Matrix
0	0000	00	8512	AB = C
0	0608	03	0000	$M_3 = ([R_{nm}] + [F_{nm}])[-I^i_m]$
0	0000	31	8501	Matrix
0	0000	00	8507	Transfer A to C
0	0200	05	0000	$M_2 = M_5 = [X_{nm}]$
0	0000	31	8501	Matrix
0	0000	00	8513	B = AC

Sign	Spare	Command	Address	Remarks
0	0503	07	0000	$M_7 = [X_{nm}]^{-1}([R_{nm}] + [F_{nm}]) \cdot [-I_m^i] = [I_m^r]$
0	0000	31	8501	Matrix
0	0000	00	8585	Print A
0	0000	07	0000	Print $[I_m^r]$
0	0000	31	8501	Matrix
0	0000	00	8585	Print A
0	0000	08	0000	Print $-[I_m^i]$
0	0000	08	0000	Stop
6	0000	30	2633	
6	0000	30	3025	

Dictionary:

4	0000	00	1500	Read Input
0	0000	00	0000	$[M_o] = 0$
0	1919	00	3600	$[M_1] = [R_{nm}]$
0	1919	00	3200	$[M_2] = [X_{nm}]$
0	1919	00	2800	$[M_3] = [F_{nm}]$
0	1900	00	2400	$[M_4] = [V_n]$
0	1919	00	2000	$[M_5]$
0	1919	00	1600	$[M_6]$
0	1900	00	1580	$[M_7] = [I_m^r]$
0	1900	00	1560	$[M_8] = -[I_m^i]$
0	0000	08	0000	Stop

APPENDIX III

Solutions of equations II-32a and II-32b are tabulated below for different values of Z_o .

Z_o	0	1 ohm	10 ohms
I_1^r	$+7.4256830 \times 10^{-5}$	$+7.4749945 \times 10^{-5}$	$+7.9185041 \times 10^{-5}$
I_3^r	$-8.1024515 \times 10^{-6}$	$-8.4111455 \times 10^{-6}$	-1.1187682
I_5^r	-1.1396308	-1.0622593	$-3.6633598 \times 10^{-7}$
I_7^r	$-3.6595385 \times 10^{-7}$	$-3.2864678 \times 10^{-7}$	$+6.9136800 \times 10^{-9}$
I_9^r	-1.5900994	-1.8137679	$-3.8255702 \times 10^{-7}$
I_{11}^r	$-8.1210660 \times 10^{-8}$	$-9.6211540 \times 10^{-8}$	-2.3113699
I_{13}^r	-4.5957377	-3.5184284	$+6.1714587 \times 10^{-8}$
I_{15}^r	-2.7858495	-1.9707945	+5.3602383
I_{17}^r	-1.7735855	-2.4155870	-8.1900720
I_{19}^r	-1.1692102	-1.6872595	-6.3468573
I_1^i	$+5.3319559 \times 10^{-4}$	$+5.3310065 \times 10^{-4}$	$+5.3224433 \times 10^{-4}$
I_3^i	+3.5164344	+3.5166988	+3.5190794
I_5^i	$-7.9613167 \times 10^{-5}$	$-7.9618325 \times 10^{-5}$	$-7.9664833 \times 10^{-5}$
I_7^i	+4.3209276	+4.3206693	+4.3183400
I_9^i	-2.2855354	-2.2853648	-2.2838269
I_{11}^i	+1.7375385	+1.7376516	+1.7386706
I_{13}^i	-1.1017304	-1.1018084	-1.1025103
I_{15}^i	$+9.4815771 \times 10^{-6}$	$+9.4809835 \times 10^{-6}$	$+9.4756401 \times 10^{-6}$
I_{17}^i	-6.5354011	-6.5349260	-6.5306487
I_{19}^i	+6.0077038	+6.0080861	+6.0115242

Z_o	100 ohms	500 ohms	1000 ohms
I_1^r	$+1.2326653 \times 10^{-4}$	$+3.1343170 \times 10^{-4}$	$+5.3868403 \times 10^{-4}$
I_3^r	$-3.8786215 \times 10^{-5}$	-1.5788405	-2.9903904
I_5^r	$+6.5511702 \times 10^{-6}$	$+3.6404478 \times 10^{-5}$	$+7.1790317 \times 10^{-5}$
I_7^r	$+3.3423926$	$+1.7736929$	$+3.4798875$
I_9^r	-2.3822824	-1.1012077	-2.1240644
I_{11}^r	-1.5722937	$-7.3600588 \times 10^{-6}$	-1.4220111
I_{13}^r	$+1.0248895$	$+5.1815126$	$+1.0108306$
I_{15}^r	$+7.8230694 \times 10^{-7}$	$+3.9270587$	$+7.6544848 \times 10^{-6}$
I_{17}^r	-6.5588403	-3.1329216	-6.0688979
I_{19}^r	-5.2663223	-2.5254265	-4.8945559
I_1^i	$+5.2370509 \times 10^{-4}$	$+4.8626195 \times 10^{-4}$	$+4.4063646 \times 10^{-4}$
I_3^i	$+3.5429097$	$+3.6494281$	$+3.7834159$
I_5^i	$-8.0131721 \times 10^{-5}$	$-8.2238426 \times 10^{-5}$	$-8.4929102 \times 10^{-5}$
I_7^i	$+4.2949684$	$+4.1896751$	$+4.0555375$
I_9^i	-2.2684149	-2.1992408	-2.1116508
I_{11}^i	$+1.7488842$	$+1.7947456$	$+1.8528602$
I_{13}^i	-1.1095484	-1.1412023	-1.1814181
I_{15}^i	$+9.4220533 \times 10^{-6}$	$+9.1811050 \times 10^{-6}$	$+8.8751109 \times 10^{-6}$
I_{17}^i	-6.4877698	-6.2950890	-6.0506359
I_{19}^i	$+6.0459953$	$+6.2009184$	$+6.3975137$

Z_o	2500 ohms	5000 ohms	7500 ohms
I_1^r	$+1.1419900 \times 10^{-3}$	$+1.9570274 \times 10^{-3}$	$+2.5991523 \times 10^{-3}$
I_3^r	$-6.7754578 \times 10^{-4}$	-1.1899253	-1.5944504
I_5^r	$+1.6669684$	$+2.9521599 \times 10^{-4}$	$+3.9671948 \times 10^{-4}$
I_7^r	$+8.0558561 \times 10^{-5}$	$+1.4252174$	$+1.9145736$
I_9^r	-4.8671297	$-8.5810256 \times 10^{-5}$	-1.1513688
I_{11}^r	-3.2617373	-5.7526246	$-7.7195787 \times 10^{-5}$
I_{13}^r	$+2.3321406$	$+4.1212255$	$+5.5340783$
I_{15}^r	$+1.7650963$	$+3.1186314$	$+4.1875181$
I_{17}^r	-1.3942709	-2.4603711	-3.3022509
I_{19}^r	-1.1248196	-1.9850956	-2.6644437
I_1^i	$+3.1159093$	$+1.2128074 \times 10^{-4}$	$-4.1751040 \times 10^{-5}$
I_3^i	$+4.1842706$	$+4.8238233$	$+5.4080463 \times 10^{-4}$
I_5^i	$-9.3184264 \times 10^{-5}$	-1.0678454	-1.1950626
I_7^i	$+3.6456803$	$+2.9738886 \times 10^{-5}$	$+2.3478084 \times 10^{-5}$
I_9^i	-1.8466831	-1.4178285	-1.0218385
I_{11}^i	$+2.0288755$	$+2.3142034$	$+2.5779696$
I_{13}^i	-1.3037459	-1.5031266	-1.6881796
I_{15}^i	$+7.9449594 \times 10^{-6}$	$+6.4301991 \times 10^{-6}$	$+5.0251530 \times 10^{-6}$
I_{17}^i	-5.3087737	-4.1031516	-2.9865680
I_{19}^i	$+6.9943719$	$+7.9648184$	$+8.8639263$

Z_o	10,000 ohms	25,000 ohms	50,000 ohms
I_1^r	$+3.1178940 \times 10^{-3}$	$+4.9002263 \times 10^{-3}$	$+6.0664413 \times 10^{-3}$
I_3^r	-1.9218001	-3.0503852	-3.7921682
I_5^r	$+4.7888229 \times 10^{-4}$	$+7.6231860 \times 10^{-4}$	$+9.4875708 \times 10^{-4}$
I_7^r	+2.3106711	+3.6769748	+4.5756059
I_9^r	-1.3887201	-2.2072614	-2.7454687
I_{11}^r	$-9.3115293 \times 10^{-5}$	-1.4801773	-1.8411855
I_{13}^r	+6.6776241	+1.0621810	+1.3215621
I_{15}^r	+5.0526556	$+8.0365449 \times 10^{-5}$	$+9.9987972 \times 10^{-5}$
I_{17}^r	-3.9836412	-6.3336931	-7.8790496
I_{19}^r	-3.2142880	-5.1106674	-6.3577105
I_1^i	$-1.8199729 \times 10^{-4}$	$-7.2331969 \times 10^{-4}$	$-1.1288729 \times 10^{-3}$
I_3^i	+5.9324167	+8.0988414	$+9.8312068 \times 10^{-4}$
I_5^i	-1.3109251	-1.8001122	-2.1988168
I_7^i	$+1.7788934 \times 10^{-5}$	$-6.1530650 \times 10^{-6}$	$-2.5614690 \times 10^{-5}$
I_9^i	$-6.6403720 \times 10^{-6}$	+8.2917180	+2.0337699
I_{11}^i	$+2.8164722 \times 10^{-5}$	$+3.8128580 \times 10^{-5}$	+4.6173658
I_{13}^i	-1.8559177	-2.5592287	-3.1290769
I_{15}^i	$+3.7520450 \times 10^{-6}$	$-1.5829720 \times 10^{-6}$	$-5.9035490 \times 10^{-6}$
I_{17}^i	-1.9757930	+2.2541120	+5.6747060
I_{19}^i	+9.6780094	$+1.3085906 \times 10^{-5}$	$+1.5842701 \times 10^{-5}$

Z_o	75,000 ohms	100,000 ohms	250,000 ohms
I_1^r	$+6.5899856 \times 10^{-3}$	$+6.8890941 \times 10^{-3}$	$+7.4996068 \times 10^{-3}$
I_3^r	-4.1260580	-4.3170447	-4.7074711
I_5^r	+1.0327151	+1.0807505	+1.1789695
I_7^r	$+4.9802559 \times 10^{-4}$	$+5.2117617 \times 10^{-4}$	$+5.6851127 \times 10^{-4}$
I_9^r	-2.9877801	-3.1263998	-3.4098040
I_{11}^r	-2.0037218	-2.0967063	-2.2868125
I_{13}^r	+1.4383517	+1.5051655	+1.6417755
I_{15}^r	+1.0882315	+1.1387779	+1.2421222
I_{17}^r	$-8.5748385 \times 10^{-5}$	$-8.9728944 \times 10^{-5}$	$-9.7867380 \times 10^{-5}$
I_{19}^r	-6.9191898	-7.2404087	-7.8971507
I_1^i	$-1.3246001 \times 10^{-3}$	$-1.4400929 \times 10^{-3}$	$-1.6848135 \times 10^{-3}$
I_3^i	+1.0692397	+1.1208682	+1.2315689
I_5^i	$-2.3986546 \times 10^{-4}$	$-2.5189046 \times 10^{-4}$	$-2.7771725 \times 10^{-4}$
I_7^i	$-3.5360220 \times 10^{-5}$	$-4.1210100 \times 10^{-5}$	$-5.3804050 \times 10^{-5}$
I_9^i	+2.6356285	+2.9958306	+3.7728077
I_{11}^i	+5.0194259	+5.2600012	+5.7780080
I_{13}^i	-3.4140803	-3.5851841	-3.9534084
I_{15}^i	$-8.0637210 \times 10^{-6}$	$-9.3591270 \times 10^{-6}$	-1.2132438
I_{17}^i	+7.3843660	+8.4101120	+1.0619423
I_{19}^i	$+1.7221303 \times 10^{-5}$	$+1.8048483 \times 10^{-5}$	+1.9819394

Z_o	500,000 ohms	750,000 ohms	1,000,000 ohms
I_1^r	$+7.7659281 \times 10^{-3}$	$+7.7156352 \times 10^{-3}$	$+7.8644367 \times 10^{-3}$
I_3^r	-4.8775530	-4.8469610	-4.9409080
I_5^r	+1.2217349	+1.2141381	+1.2377081
I_7^r	$+5.8912307 \times 10^{-4}$	$+5.8545418 \times 10^{-4}$	$+5.9681645 \times 10^{-4}$
I_9^r	-3.5332313	-3.5111666	-3.5792309
I_{11}^r	-2.3696068	-2.3548119	-2.4004906
I_{13}^r	+1.7012630	+1.6906583	+1.7234626
I_{15}^r	+1.2871244	+1.2790924	+1.3039078
I_{17}^r	-1.0141166	-1.0077836	-1.0273401
I_{19}^r	$-8.1831584 \times 10^{-5}$	$-8.1321173 \times 10^{-5}$	$-8.2897933 \times 10^{-5}$
I_1^i	$-1.7884757 \times 10^{-3}$	$-1.7916604 \times 10^{-3}$	$-1.8333161 \times 10^{-3}$
I_3^i	+1.2827644	+1.2758008	+1.2994924
I_5^i	$-2.8762576 \times 10^{-4}$	$-2.8781641 \times 10^{-4}$	$-2.9537046 \times 10^{-4}$
I_7^i	$-5.9478660 \times 10^{-5}$	$-5.9361700 \times 10^{-5}$	$-6.0861480 \times 10^{-5}$
I_9^i	+4.0934664	+4.1138019	+4.2797381
I_{11}^i	+6.0178985	+6.0102656	+6.1366476
I_{13}^i	-4.0950537	-4.1119078	-4.1708562
I_{15}^i	-1.3426196	-1.3370035	-1.3725136
I_{17}^i	+1.1509520	+1.1503265	+1.1766360
I_{19}^i	+2.0564303	+2.0632896	+2.0895325

APPENDIX IV

ELECTRONIC CIRCUIT DIAGRAMS

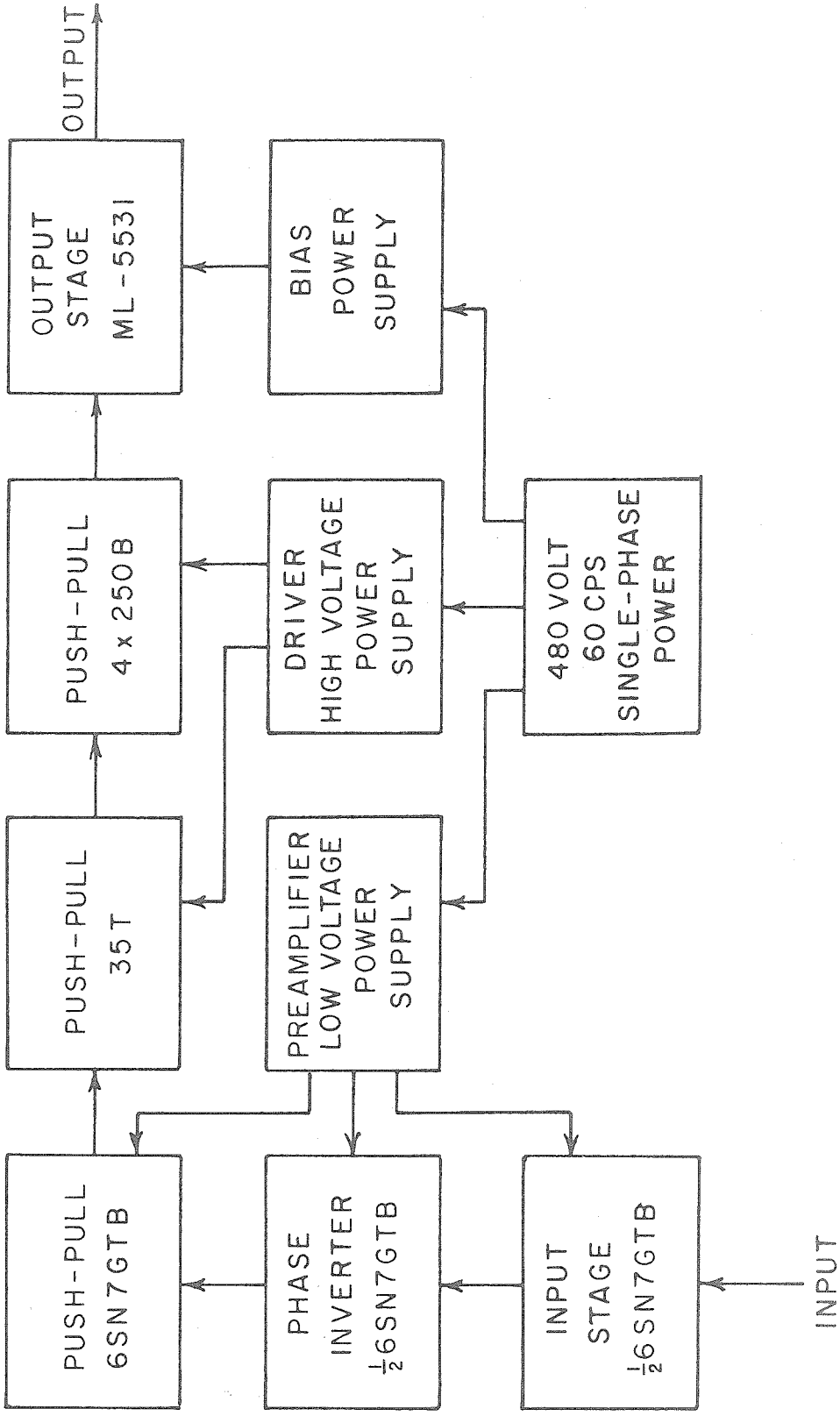

FIGURE 40. BLOCK DIAGRAM OF TRANSMITTER.

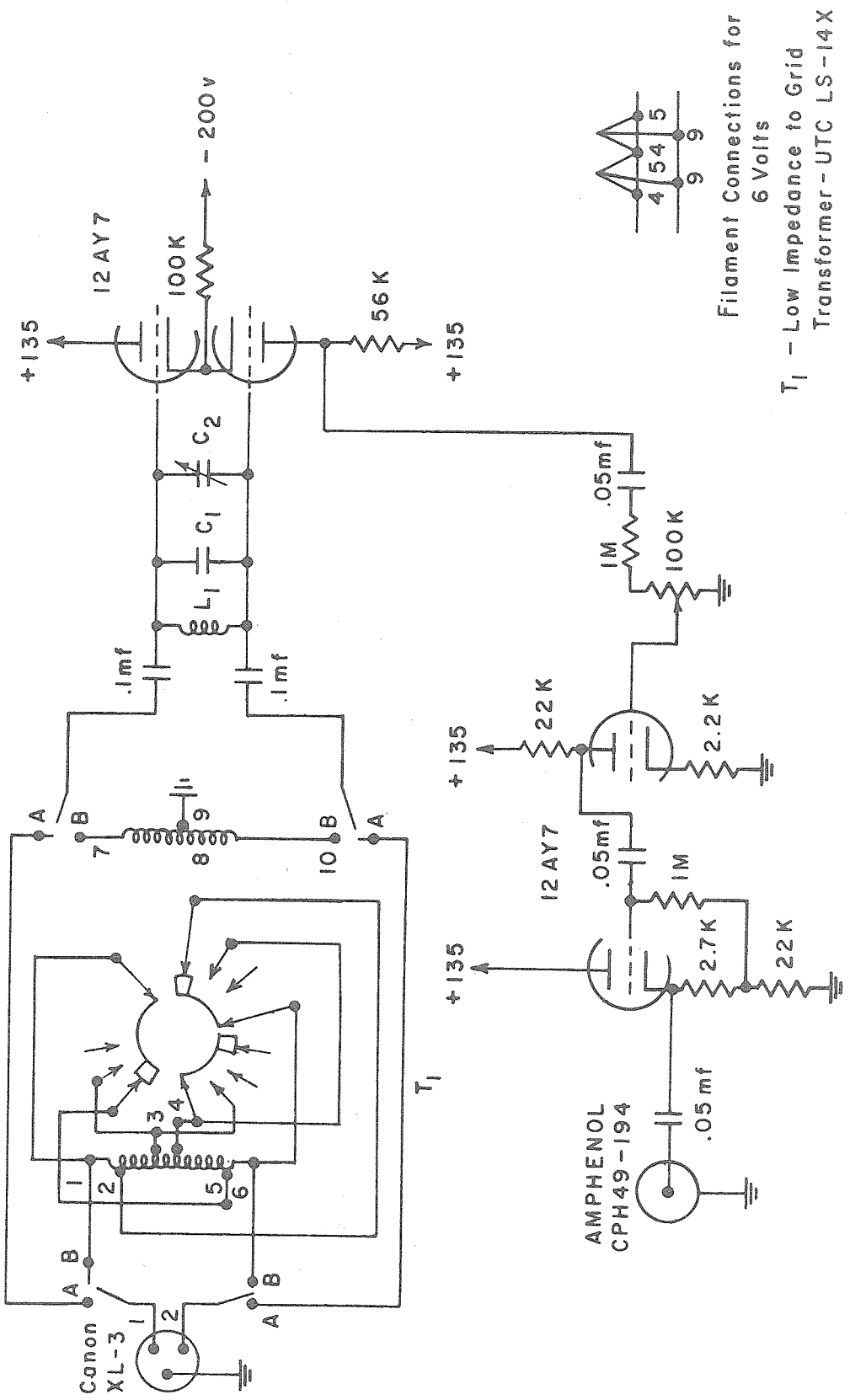

FIGURE 41A. PORTABLE 8.4 KC PRESELECTOR.

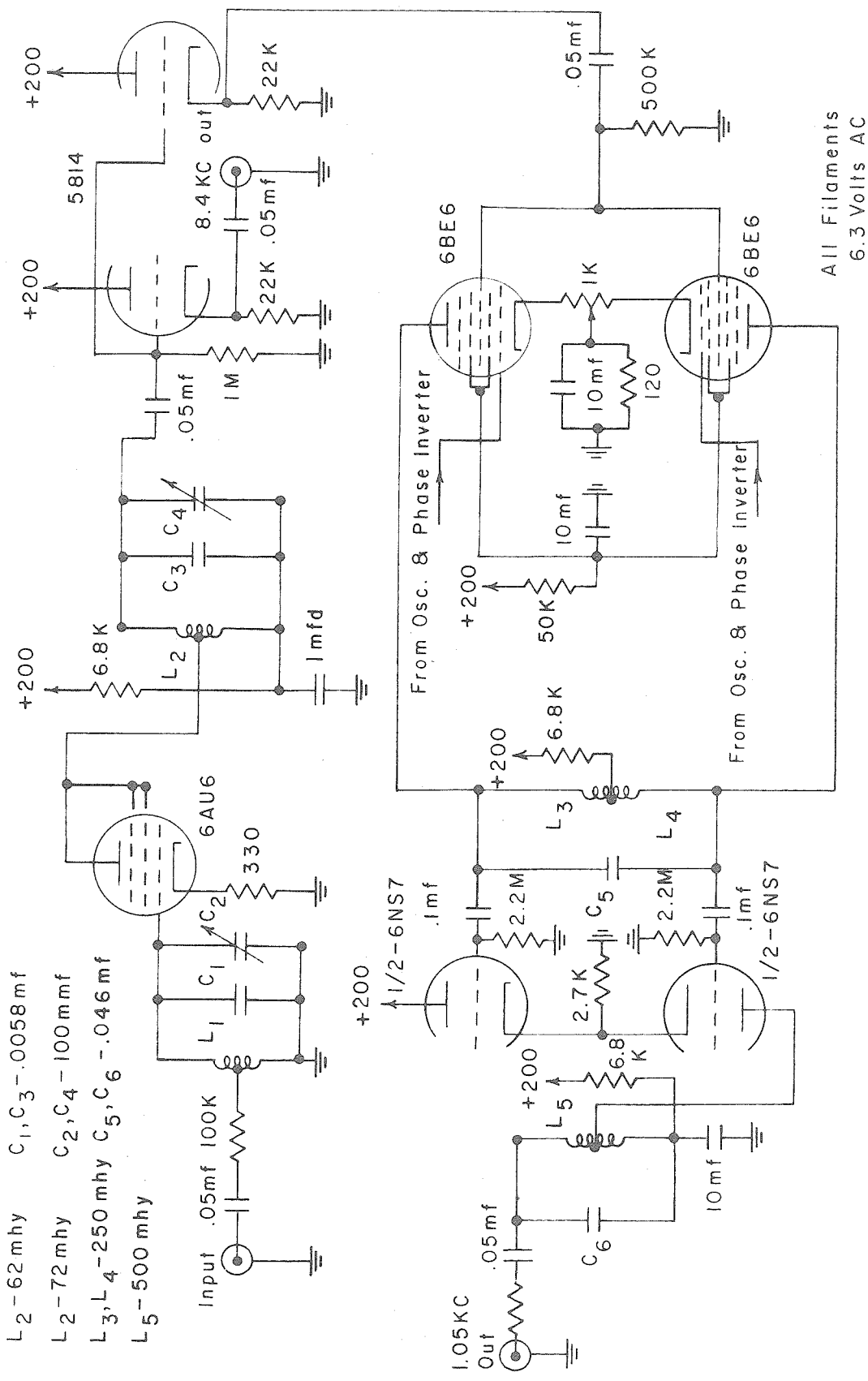

FIGURE 41B. VLF RECEIVER: 8.4 KC AMPLIFIER AND FIRST IF STAGE.

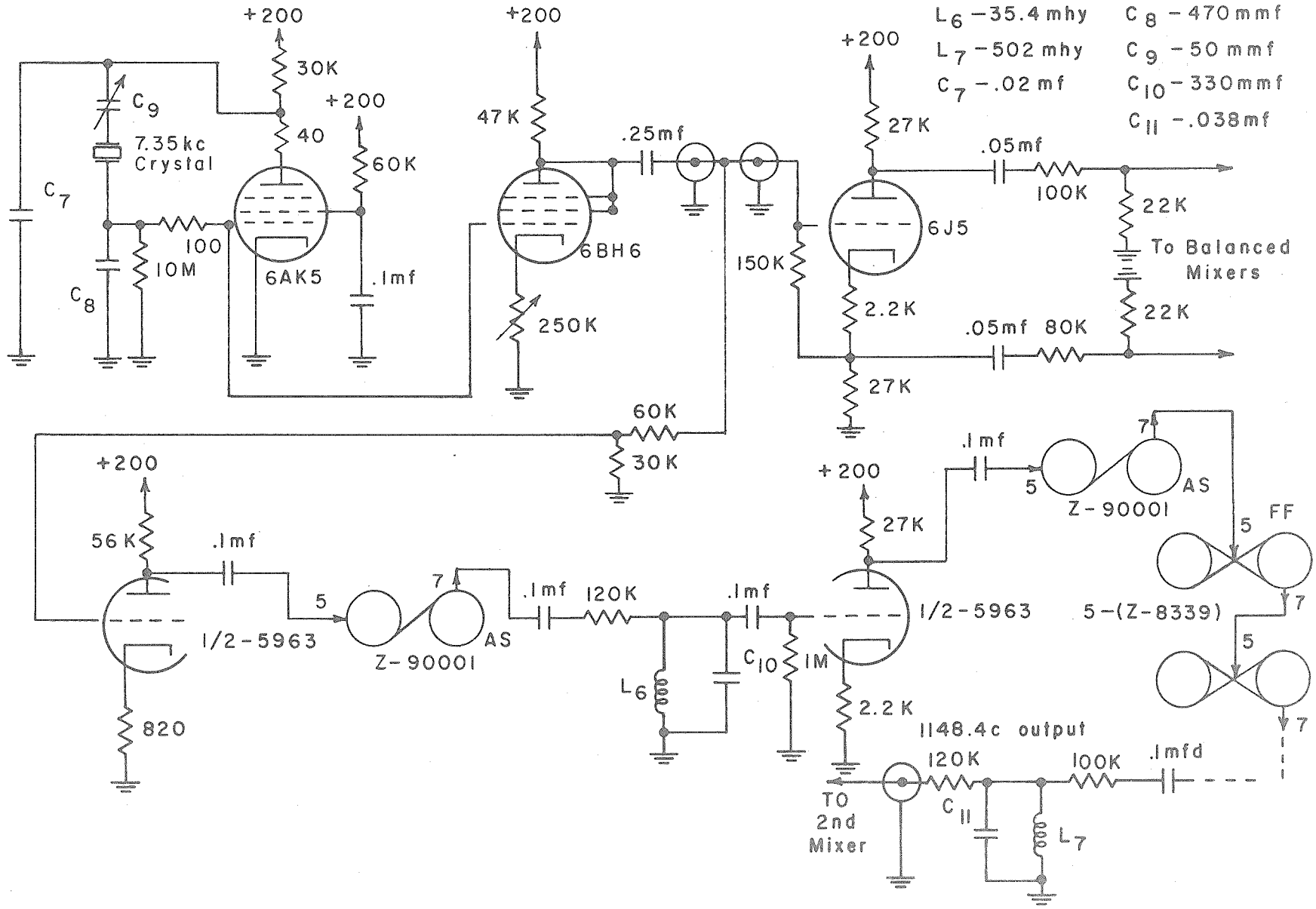

FIGURE 41C. VLF RECEIVER: CRYSTAL OSCILLATOR, PHASE INVERTER, AND SCALING CIRCUITS.

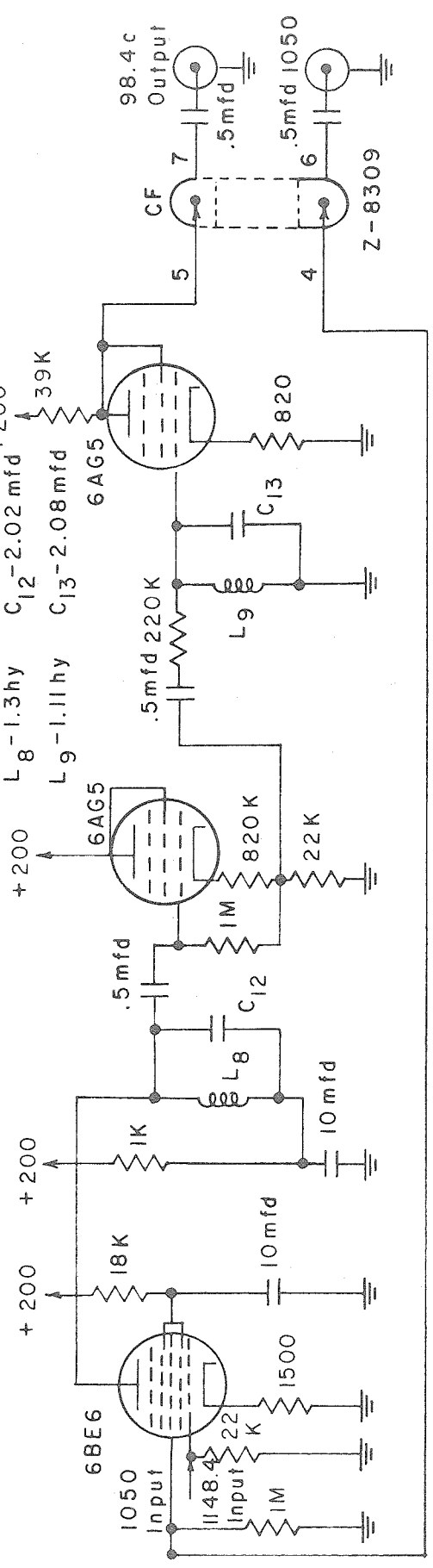

FIGURE 41D. VLF RECEIVER: SECOND IF STAGE AND CATHODE FOLLOWER OUTPUT.

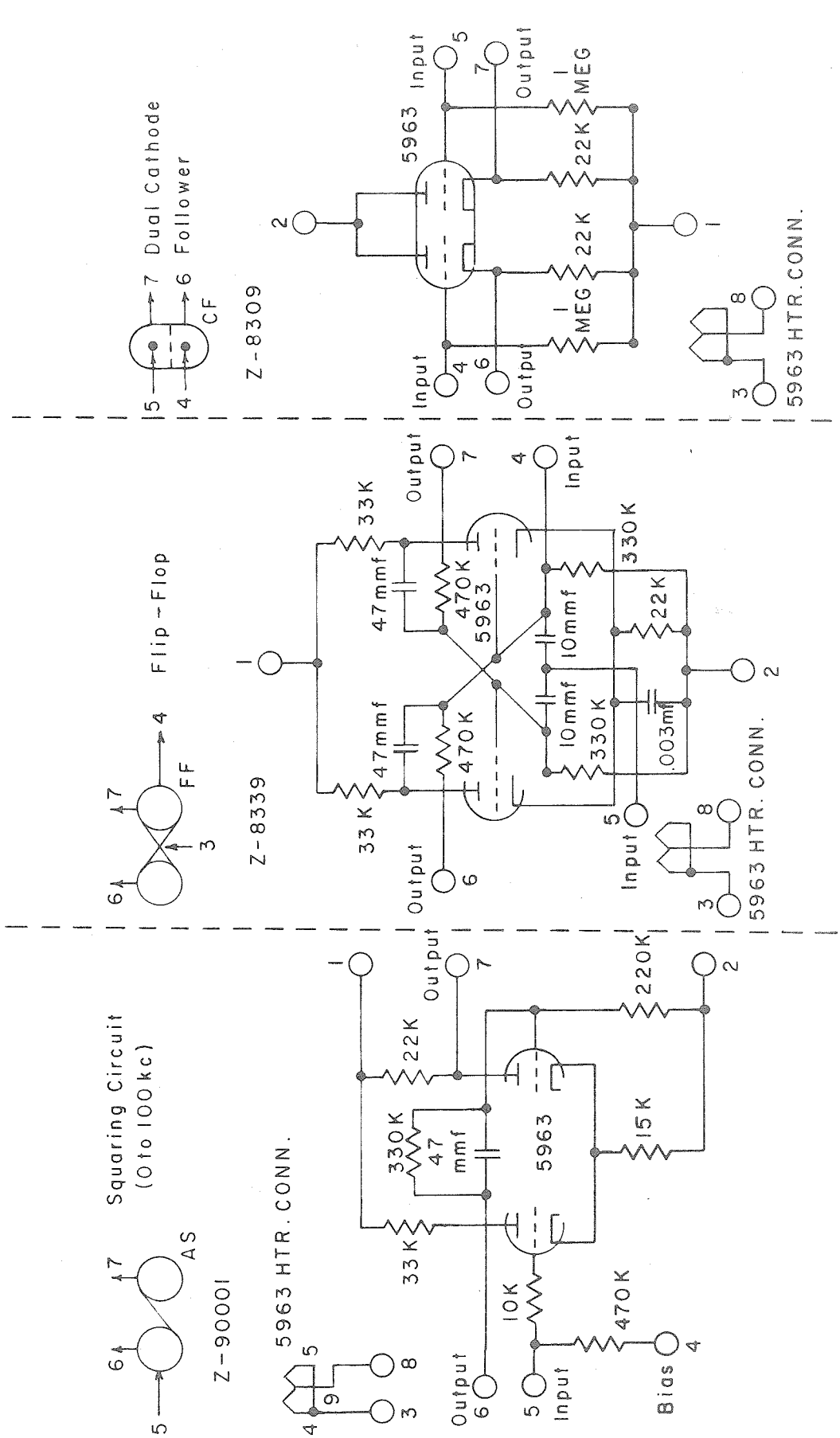

FIGURE 41E. VLF RECEIVER: PLUG-IN UNITS.

APPENDIX V

PHOTOGRAPHS

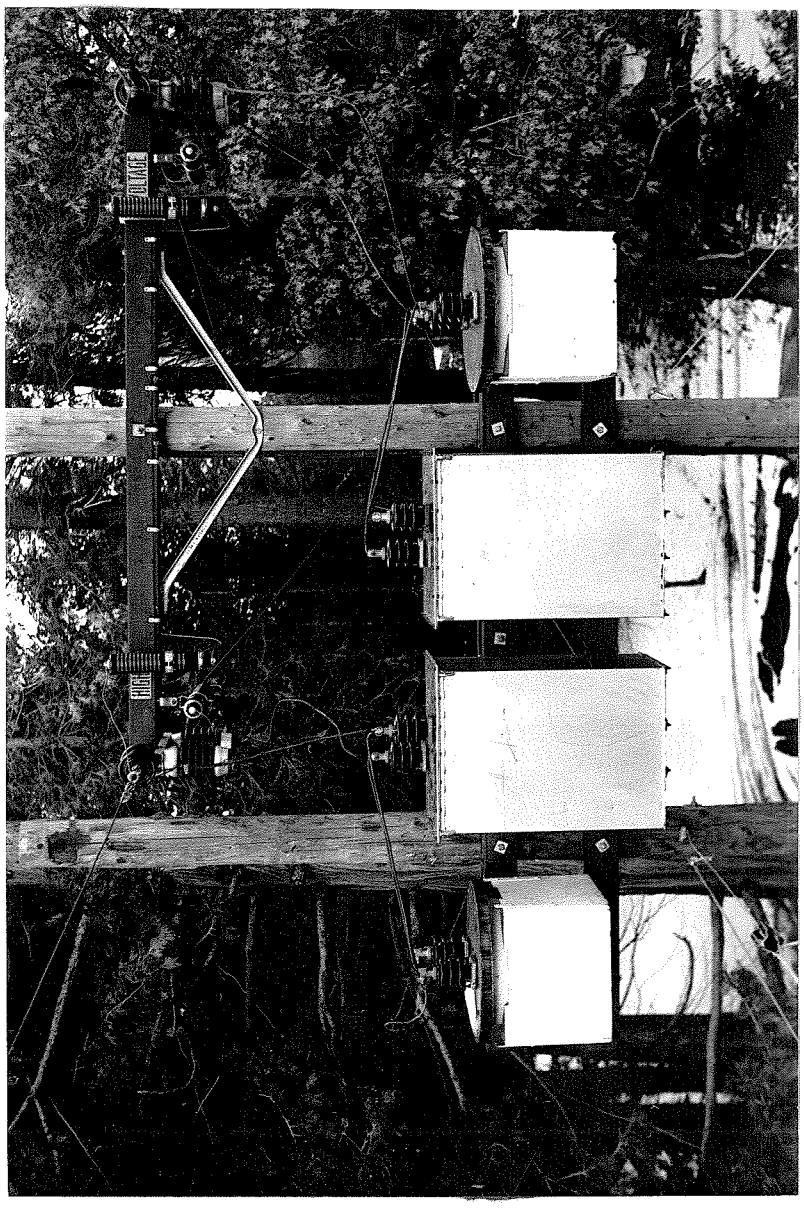

FIGURE 42. LINE TRAPS MOUNTED IN POSITION.

FIGURE 43. TRANSMITTING STATION.

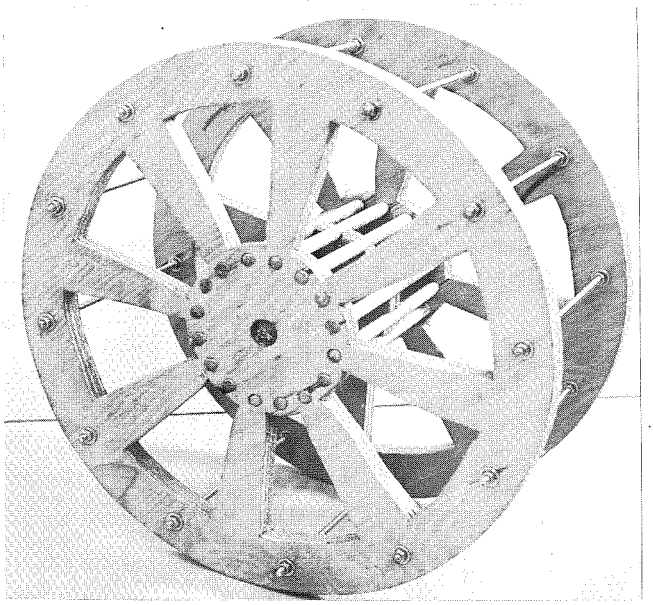

A. COIL FORMS.

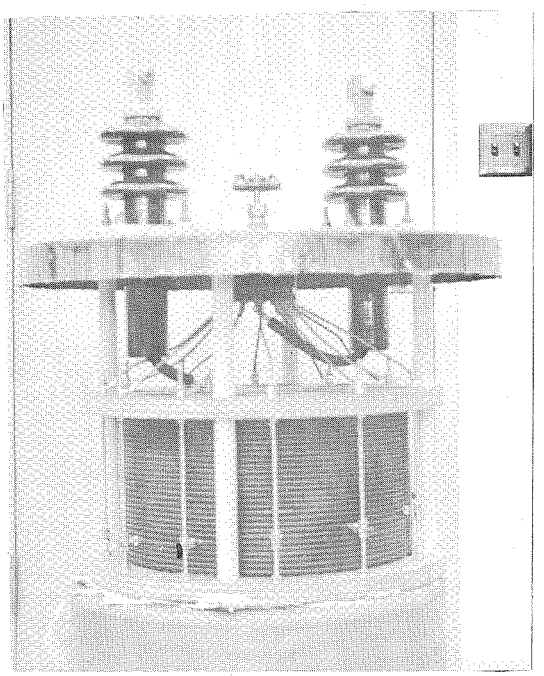

B. DETAIL OF TAP SWITCH.

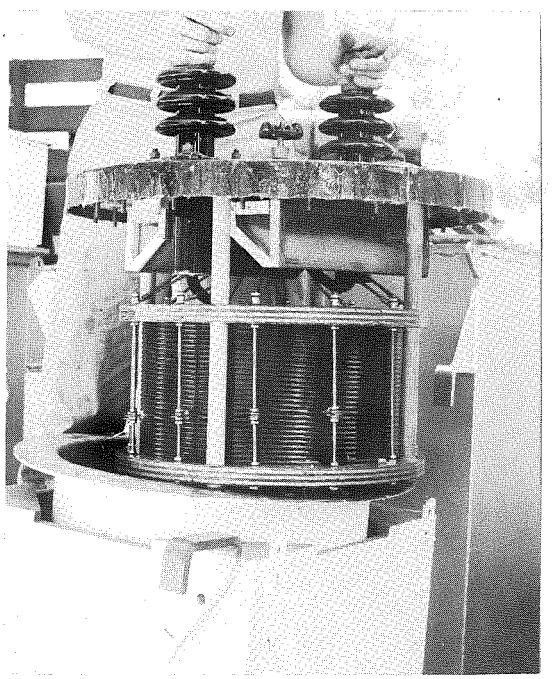

C. SILICA GEL DRYERS.

FIGURE 44. DETAILS OF LINE TRAP INDUCTOR CONSTRUCTION.

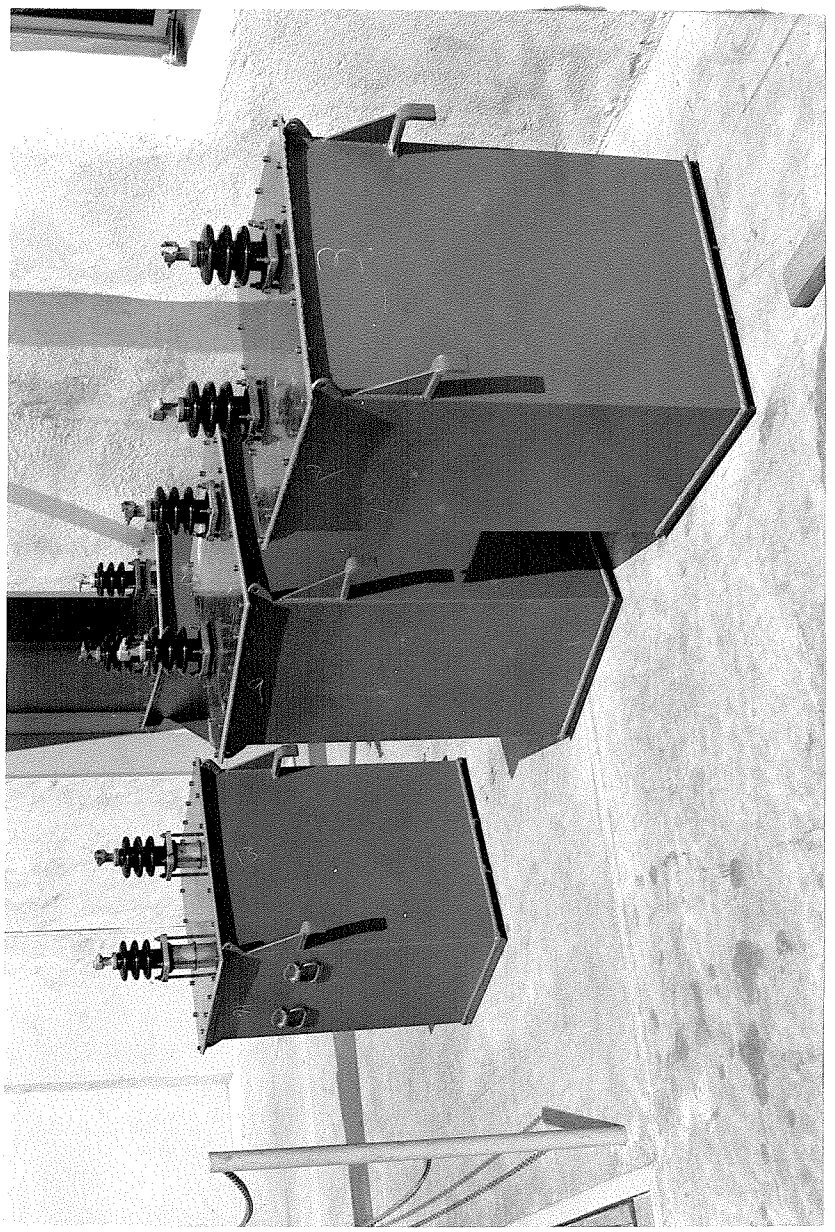

FIGURE 45. LINE TRAP CAPACITORS.

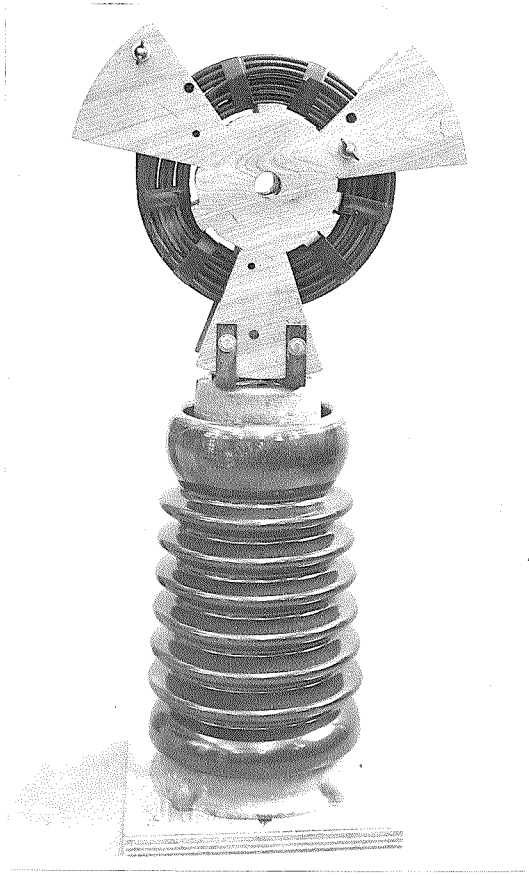

FIGURE 46A. LARGE COUPLING-NETWORK COIL.

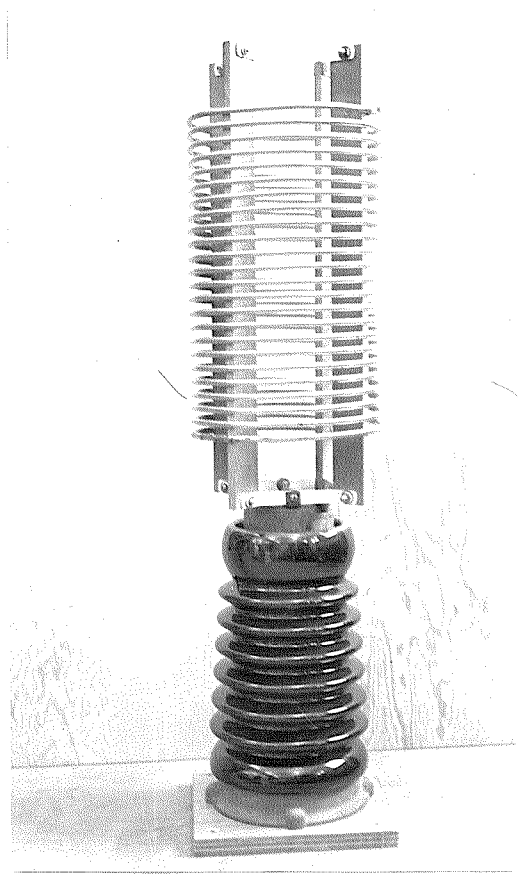

FIGURE 46B. COUPLING-NETWORK TUNING COIL.

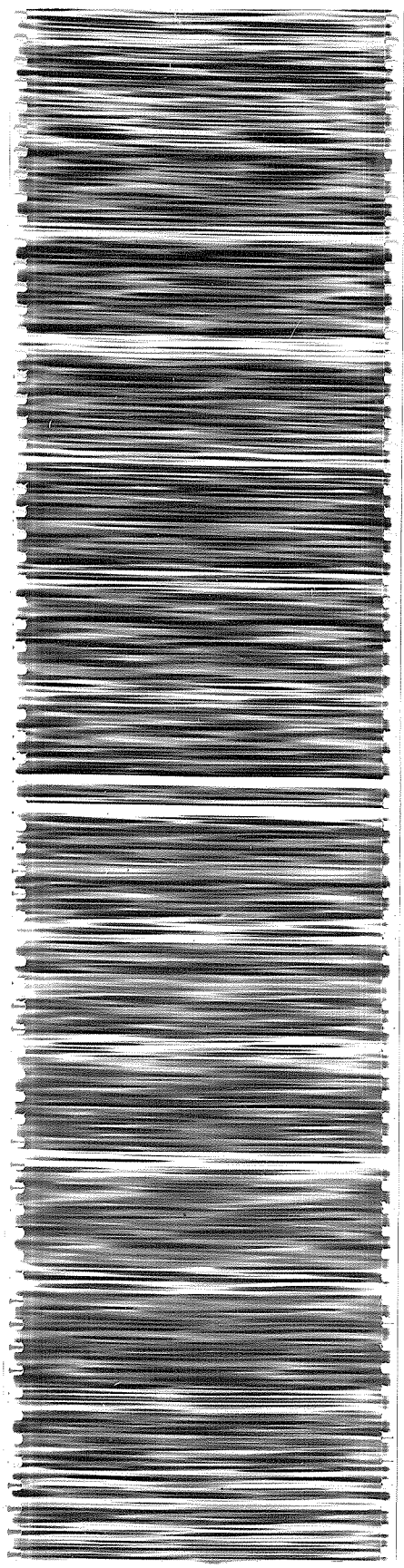

FIGURE 47A. SAMPLE OF CAMBRIDGE RECEIVING DATA TAKEN 21 MARCH 1959.

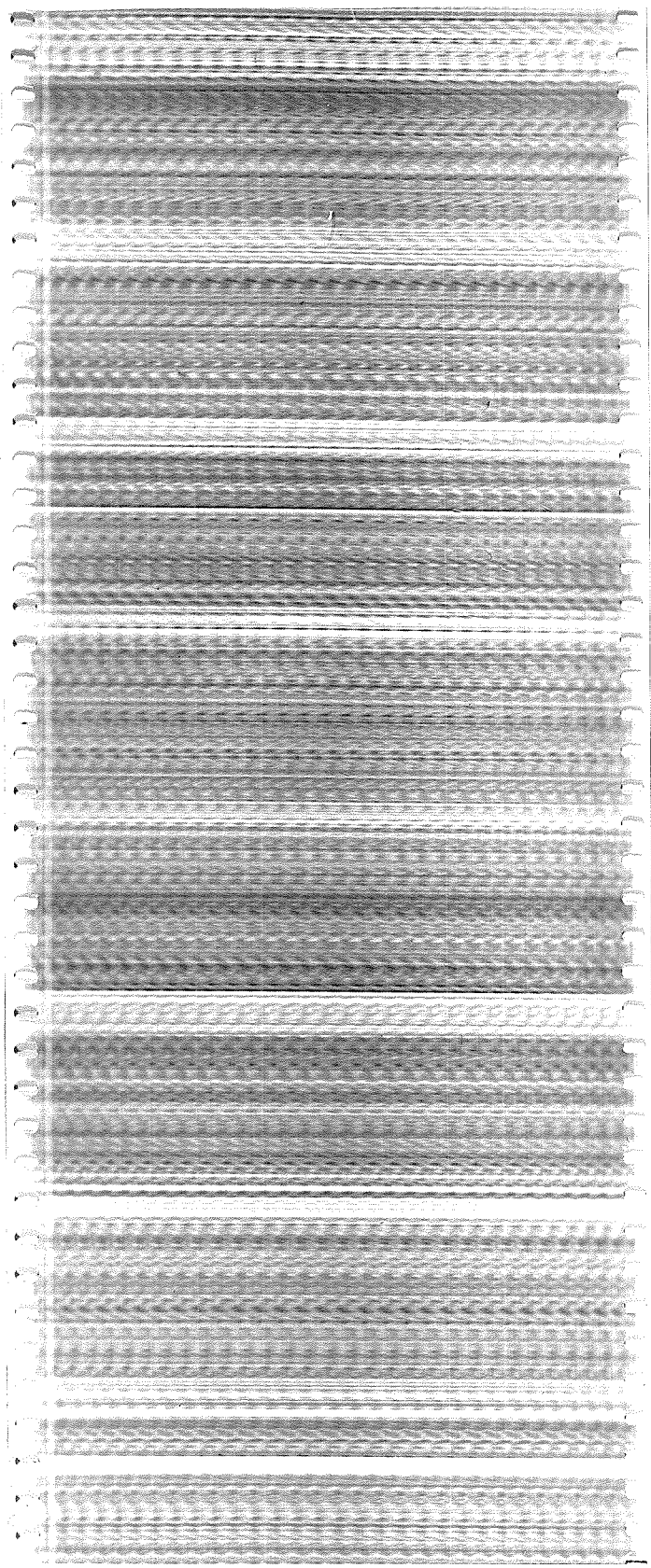

Scale: 3.736 minutes/inch

FIGURE 47B. SAMPLE OF CAMBRIDGE RECEIVING DATA TAKEN 28 MARCH 1959.

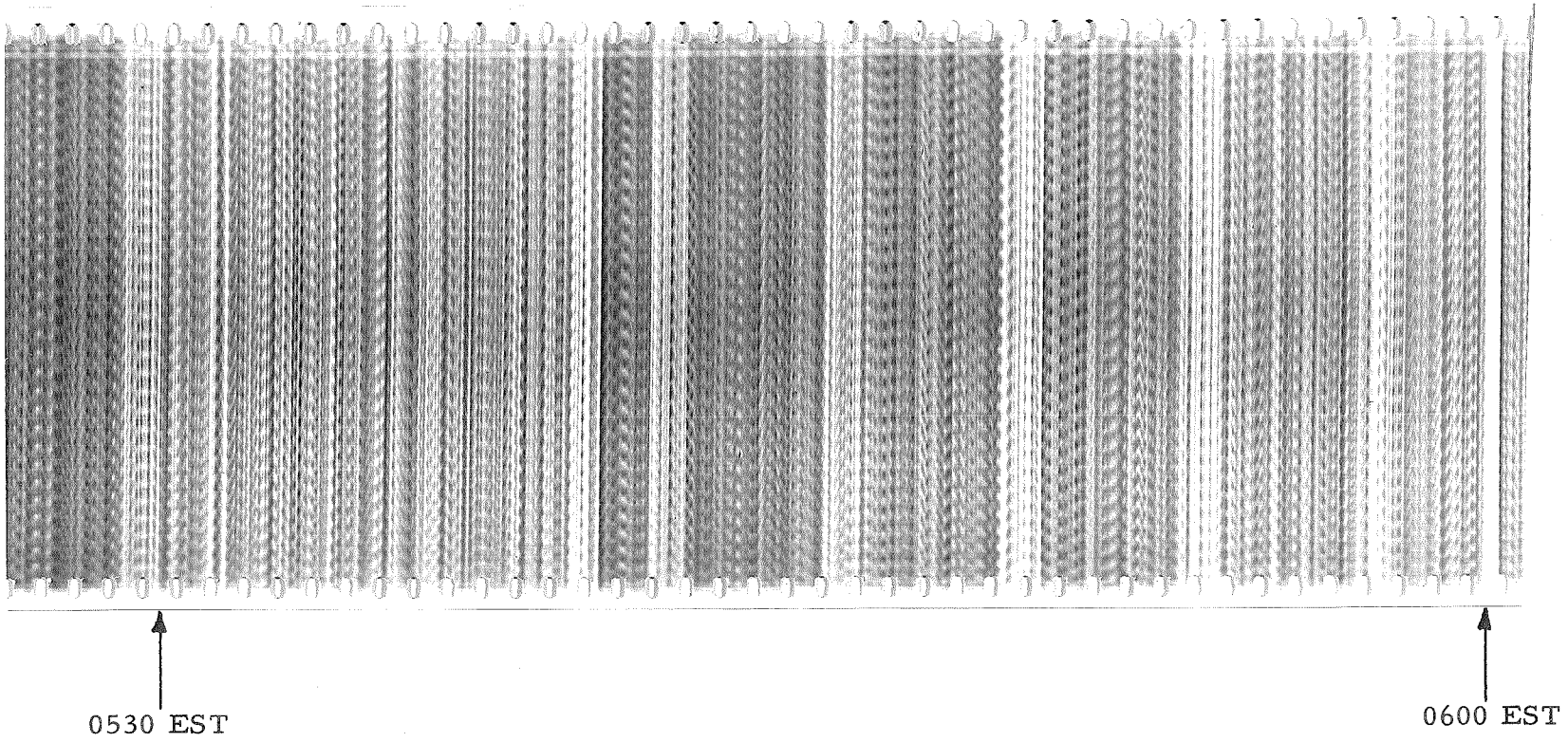

Scale: 4.142 minutes/inch

FIGURE 47C. SAMPLE OF CAMBRIDGE RECEIVING DATA TAKEN 28 MARCH 1959.